

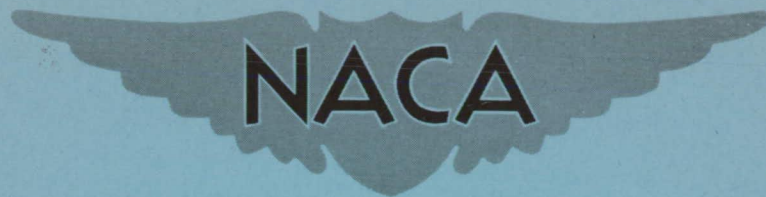
UNCLASSIFIED

CONFIDENTIAL

RML54-119

Copy
RM L54I19

141



RESEARCH MEMORANDUM

FLUTTER INVESTIGATION OF A TRUE-SPEED DYNAMIC MODEL WITH
VARIOUS TIP-TANK CONFIGURATIONS

By John L. Sewall, Robert W. Herr, and William B. Igoe

Langley Aeronautical Laboratory
Langley Field, Va.

Classification
CANCELLED
CHANGED TO UNCLASSIFIED
By authority of Naca Res No. 120 10-3-55
Chang by DFC Date 6-26-62

TECHNICAL LIBRARY
AIRESEARCH MANUFACTURING CO.
9851 SEPULVEDA BLVD.
LOS ANGELES 45, CALIF.
CALIFORNIA

CLASSIFIED DOCUMENT

This material contains information affecting the National Defense of the United States within the meaning of the espionage laws, Title 18, U.S.C., Secs. 793 and 794, the transmission or revelation of which in any manner to an unauthorized person is prohibited by law.

NATIONAL ADVISORY COMMITTEE
FOR AERONAUTICS

WASHINGTON

March 30, 1955

CONFIDENTIAL

UNCLASSIFIED

NATIONAL ADVISORY COMMITTEE FOR AERONAUTICS

RESEARCH MEMORANDUM

FLUTTER INVESTIGATION OF A TRUE-SPEED DYNAMIC MODEL WITH
VARIOUS TIP-TANK CONFIGURATIONS

By John L. Sewall, Robert W. Herr, and William B. Igoe

SUMMARY

A 1/6-scale dynamic model, equipped with wing tip tanks and representative of current unswept fighter-type airplanes of conventional planform, was tested for flutter. The model was dynamically scaled to flutter at the same speed as a typical full-scale configuration. The parameters important to flutter were satisfactorily approximated by the use of a spar-balsa segment-type wing construction.

A flutter-arresting device was located within each tip tank which would provide for a sudden shift in the tip-tank center of gravity. This device was very effective in stopping symmetric flutter for cases where the tip-tank center of gravity was shifted forward of the elastic axis of the wing.

The flutter investigation was concerned with the effects of external stores whose inertial and geometric properties were systematically varied. In general, the results obtained concur with those found in previous researches in that symmetric flutter speeds were increased for tip-tank centers of gravity forward of the wing elastic axis, and tended to decrease as the ratio of uncoupled wing bending frequency to torsion frequency approached unity. Increasing the volume of the tip tanks by a factor of 3 tended to decrease the flutter speed. The addition of a horizontal fin at the rear end of each tank may have been beneficial for the smaller tank and slightly detrimental for the larger tank.

Flutter speeds were calculated by means of a conventional Rayleigh-Ritz type of flutter analysis employing uncoupled modes. The effects of various assumptions in the calculations involving structural damping, higher structural modes, compressible aerodynamic coefficients, and sting-mount flexibility were explored. The calculations were, in general, excessively conservative for tip-tank centers of gravity near the elastic axis; however, the introduction of structural damping materially improved the agreement between experimental and calculated flutter speeds for ratios of uncoupled wing bending frequency to torsion frequency near unity. The introduction of sting-mount flexibility showed that this could have a

CONFIDENTIAL

strong effect on flutter speed particularly in those cases where the natural frequency of the sting system was near the flutter frequency, and further work in this regard is warranted in future flutter studies of sting-mounted models. Also indicated as desirable is the need for continued research on the oscillating aerodynamic coefficients for flutter calculations on wings equipped with large external stores or nacelles.

INTRODUCTION

Within the past several years a number of cases of flutter are known to have occurred on fighter and light bomber airplanes (at least in their development stages) carrying large external stores. Considerable interest has, therefore, developed in flutter problems for wings carrying such stores. References 1 to 10 are representative of both the theoretical and experimental investigations of problems of this kind. The calculations of flutter instabilities for these cases have, in general, been unsatisfactory where two-dimensional aerodynamic forces and moments together with a limited number of structural modes have been employed, and where aerodynamic forces and moments on the tip tank have been ignored. Because of weaknesses inherent in many of the more complete analyses available at present, greater emphasis has come to be placed on wind-tunnel testing of dynamically scaled models with external stores.

Although valuable experience has been obtained from flutter tests with scaled speed models (see, for example, refs. 11 to 13), these tests cannot provide needed information on the effects of Mach number. The extrapolations from low-speed model results to full-scale high Mach number conditions have proved troublesome and ambiguous, particularly where the margins of safety from flutter may have been small. In order to circumvent this difficulty, it is necessary to scale the model so that its Mach number at flutter will be the same as that of the prototype, or, in other words, to design and test a true-speed model. Accordingly, two principal objectives of the investigation reported in this paper were (1) to determine the feasibility of designing and building a true-speed dynamically similar model with tip tanks to meet a given set of elastic and inertial specifications, and (2) to locate the experimental flutter boundaries of this model for a variety of tip-tank conditions. Another objective was to evaluate a flutter-arresting device involving a rapid shift of the tip-tank center of gravity and having application to full-scale-flight flutter-testing techniques.

For the design of the model, in addition to keeping its flutter speed the same as that of the prototype, the principles followed in the scaling required that nondimensional parameters important in flutter, such as mass ratio, frequency ratio, and reduced frequency, remain the same on the model as on the full-scale counterpart. No attempt was made

to scale the stiffnesses in the tip-tank or wing-tip-tank attachment. Recent investigations reported in references 14 and 15 have dealt with the inertial and damping properties of sloshing fuel; however, in the present investigation fuel was simulated by means of solid weights, and no effort was made to account for the effects of fuel sloshing.

The main effort of the wind-tunnel test program was directed toward location of the flutter boundaries for a wide range of tip-tank inertial conditions corresponding to ratios of uncoupled wing bending frequency to torsion frequency near unity. Variations in these tip-tank conditions were accomplished by the use of fixed, solid weights. Also investigated were the aerodynamic effects of tip-tank size and the effects of a horizontal fin mounted at the rear portion of each tip tank. In order to study asymmetric flutter, the model was provided with one degree of freedom in roll.

The results of the flutter experiments are compared with the results of flutter calculations performed by utilizing a Rayleigh-Ritz type of analysis employing two-dimensional aerodynamic forces and moments together with a combination of uncoupled vibration modes to represent the flutter mode. No aerodynamic forces and moments were assumed to act on the tip tank.

The scaled wing stiffnesses and inertial properties specified in the design of the model were chosen to be fairly representative of present-day fighter-type airplanes. Scaled wing stiffnesses and inertial properties of an actual fighter airplane (the Lockheed F-94B) are included as a comparison. Also included for purposes of comparison are the results of a flight flutter experience on a related fighter airplane (the Lockheed F-80A) involving special tip-tank inertial loading conditions.

SYMBOLS

- a nondimensional wing elastic axis location relative to half-chord, positive for elastic axis rearward of midchord
- b half-chord of wing, ft
- b_F flange width on wing spar, in. (see fig. 9)
- b_r reference half-chord of wing (taken at the station at three-fourths of the semispan), ft
- b_w web spacing on wing spar, in. (see fig. 9)

c_r	root chord of wing along fuselage center line, in. (see fig. 3(a))
c_t	tip chord of wing at $y = l_w = 36$, in. (see fig. 3(a))
e	distance between wing elastic axis and center of gravity, in.; positive for center of gravity rearward
e_t	distance between wing elastic axis and tip-tank center of gravity, in.; positive for center of gravity rearward
f	frequency, $\omega/2\pi$, cps
f_{b1}	natural first bending frequency (experimental), cps
f_{b2}	natural second bending frequency (experimental), cps
f_f	flutter frequency, cps
f_{h1}	uncoupled first bending frequency (calculated), cps
f_{h2}	uncoupled second bending frequency (calculated), cps
f_s	uncoupled frequency of effective sting-fuselage combination, cps (see appendix)
f_{t1}	natural first torsional frequency (experimental), cps
f_{a1}	uncoupled first torsional frequency (calculated), cps
f_{a2}	uncoupled second torsional frequency (calculated), cps
g	coefficient of structural damping based on logarithmic decrement $\left(g = \frac{1}{n\pi} \log_e \frac{a_0}{a_n} \text{ where } a_0 \text{ is the initial amplitude and } a_n \text{ the nth amplitude in n cycles of freely decaying oscillation} \right)$
h_w	flange spacing on wing spar, in. (see fig. 9)
k	reduced frequency, $b\omega/v$

k_s	spring constant of equivalent sting support system, lb/in. (see the appendix)
l	general dimension of length (see text on selection of scale factors)
l_w	wing semispan from center line of fuselage to center of wing-tip-tank attachments, in.
m	mass of wing per unit length, slugs/ft
r_s	distance from effective pitch axis of rotation of sting to wing elastic axis at fuselage center line (see the appendix)
r_a	nondimensional radius of gyration of wing section about elastic axis, $\sqrt{I_a/m b^2}$
t_F	flange thickness on wing spar, in. (see fig. 9)
t_w	web thickness on wing spar, in. (see fig. 9)
v_f	flutter speed, fps
w	weight of wing per unit length, lb/in.
x_a	nondimensional center-of-gravity location of wing section relative to half-chord, e/b ; positive for center of gravity rearward of wing elastic axis
y	spanwise coordinate of wing as measured from fuselage center line, in.
EI	wing bending stiffness, lb-in. ²
$F + iG$	oscillating aerodynamic functions for two-dimensional incompressible flow (see ref. 16)
GJ	wing torsional stiffness, lb-in. ²
I_{f_r}	mass rolling moment of inertia of one-half fuselage about fuselage center line, ft-lb-sec ²
I_{f_s}	mass pitching moment of inertia of one-half fuselage and effective sting combination about effective axis of rotation in sting, ft-lb-sec ² (see the appendix)

I_{tr}	mass rolling moment of inertia of tip tank about wing tip, ft-lb-sec ²
I_a	mass pitching moment of inertia of wing per unit length about wing elastic axis, lb-sec ²
I_{at}	mass pitching moment of inertia of tip tank about wing elastic axis, in-lb-sec ²
M	Mach number
R	Reynolds number
W	weight, lb
w_t	weight of tip tank, lb
w_w	weight of each wing panel, lb
η_{asym}	nondimensional span coordinate used in antisymmetric flutter calculations, y/l_w
η_{sym}	nondimensional span coordinate used in symmetric flutter calculations, $\frac{y - 3}{l_w - 3}$
κ	wing mass ratio, $\pi \rho b^2/m$
λ	scale factor for length, l_M/l_F or b_M/b_F
μ	tip-tank weight ratio, w_t/w_w
ρ	density of test medium, slugs/cu ft
ω	angular frequency, $2\pi f$, radians/sec
Subscripts:	
f	flutter except as noted
h	bending degree of freedom
r	reference station at three-fourths semispan
t	tip tank

w	wing
F	full-scale airplane except as noted
M	model
S	sting support system
W	spar web
α	torsional degree of freedom
asym	antisymmetric fuselage boundary condition (fuselage free to roll) considered in flutter calculations
sym	symmetric fuselage boundary condition (cantilever and fuselage pitch) considered in flutter calculations

DESCRIPTION OF MODEL

The model (see fig. 1) was sting-mounted in the Langley 16-foot transonic tunnel (fig. 1(a)) and was representative of current unswept-wing fighter-type airplanes equipped with wing-tip fuel tanks. The aspect ratio of the wings without tip tanks was 6.0, the taper ratio was 0.381, and the airfoil shape was an NACA 65A013 section. The wing was untwisted, and the 52-percent-chord line was normal to the longitudinal center line of the airplane; although the elastic axis was swept back $3\frac{1}{2}$ ^o, the wing

was considered unswept.

The model was tested with two different-size tip tanks (shown in fig. 2) which were mounted so that the longitudinal axis of the tank fell in the plane of the wing. Tests were conducted with and without horizontal fins located at the rear of the tip tank as shown in figure 2. Some wing details may be seen in figure 3. Each wing panel was mounted as a cantilever (see fig. 3(a)) to a cylindrical body simulating the fuselage as a rigid structure that provided freedom of the model in roll.

Selection of Scale Factors

Scaling of the model was based on the simplified model construction discussed in reference 17. The quantities scaled were linear dimensions, mass, mass unbalance, moments of inertia, frequencies, and stiffnesses of the prototype. The wind tunnel used had an octagonal, slotted throat and was capable of attaining Mach numbers up to 1.05.

The following table lists the flutter parameters considered significant in this investigation in terms of the geometric scale factor λ . The model was chosen to be 1/6 the scale of a representative fighter-type airplane, and, therefore,

$$\lambda = \frac{b_M}{b_F} = \frac{1}{6} \quad \text{or} \quad \lambda = \frac{l_M}{l_F} = \frac{1}{6}$$

where the subscripts M and F refer to model and full scale, respectively. The choice of this particular value of λ was influenced by the desire to obtain Reynolds numbers that would be as realistic as possible with respect to the full-scale airplane within the restriction imposed by available wind-tunnel size. The density factor ρ_M/ρ_F was assumed to be unity.

Parameter	Symbol	Scale factor
Mass per unit length	$\frac{m_M}{m_F}$	$\lambda^2 = \frac{1}{36}$
Mass	$\frac{m_M l_M}{m_F l_F}$	$\lambda^3 = \frac{1}{216}$
Mass moment of inertia per unit length	$\frac{I_{\alpha_M}}{I_{\alpha_F}}$	$\lambda^4 = \frac{1}{1296}$
Mass moment of inertia	$\frac{I_{\alpha_M} l_M}{I_{\alpha_F} l_F}$	$\lambda^5 = \frac{1}{7776}$
Frequency	$\frac{\omega_M}{\omega_F}$	$\frac{1}{\lambda} = 6$
Bending stiffness	$\frac{(EI)_M}{(EI)_F}$	$\lambda^4 = \frac{1}{1296}$
Torsional stiffness	$\frac{(GJ)_M}{(GJ)_F}$	$\lambda^4 = \frac{1}{1296}$
Structural damping	$\frac{(g_h)_M}{(g_h)_F}$ or $\frac{(g_a)_M}{(g_a)_F}$	1
Mach number	$\frac{M_M}{M_F}$	1

It should be noted that $M_M = M_F$ is not precisely true because of differences which may exist between the stagnation temperature in the tunnel and that in free air for an airplane. No attempt was made to design a given value of structural damping (g_h, g_a) into the model.

Accurate measurements of the bending and torsional damping coefficients, as determined from logarithmic decrements during the test program, were difficult. The coefficients measured varied from 0.01 to 0.10. The mean value appeared to be approximately 0.035 for both bending and torsion degrees of freedom. This compares favorably with a structural damping value of 0.044 obtained from a current fighter airplane, the Lockheed F-94B.

Model-Construction Details

Wings.- The solid curves shown in figures 4 to 8 give the scaled stiffness and inertial properties typical of current fighter-type airplanes, and the model was designed to meet these specifications.

The wings were of spar-segment construction as shown in figure 3. The spar, the main structural member, was essentially a built-up box section made from thin sheet steel and welded at all four corners as shown in section A-A of figure 3(a). This type of spar construction was chosen because of the relative ease with which the bending and torsional stiffnesses could be varied essentially independent of one another. Dimensions of the spar are given in figure 9.

The wing plan form and airfoil shape were obtained by assembling a series of adjacent wing segments to the spar in the manner shown in figure 3(b) for a typical segment. Ballast weights of the kind indicated in the figure were added to each segment to adjust the wing mass, mass unbalance, and mass moment of inertia to the design values. The segments were built-up hollow sections made from sheet balsa and were coated inside and out with fiber glass and Paraplex to provide extra rigidity for the segment to withstand better the forces encountered during violent flutter. Each segment was fastened to the spar flanges by means of four screws, each screw bearing on a small metal-backed strip of hardwood glued to the inside of the segment.

The measured inertial properties of the completed model are indicated in figures 4, 5, and 6, and the spanwise distributions of wing stiffnesses in bending and torsion are given in figures 7 and 8, respectively. The attachment of the balsa segments to the spar caused no measurable increases in bending and torsional stiffnesses. The gaps between the balsa segments were covered with stiffened paper for most of the flutter runs, and later this material was replaced with silk for the remaining runs. Although the stiffness contribution of the silk was more noticeable than that of

the paper, the measured stiffnesses of the assembled model were not significantly altered because of the use of either material. However, the measured stiffnesses which are presented in figures 7 and 8 were obtained prior to the flutter tests without either paper or silk seals attached.

Stiffness measurements made at different times during the construction of the model and the flutter test program revealed some weakening of the wing due to flutter violence; however, on the basis of frequency checks made during the flutter program, it appeared that such changes had little effect on the vibration characteristics of the wing. The dashed-line curves in figures 7 and 8 were considered most representative of the stiffness properties of the wing and were used in the flutter calculations.

Scaled stiffness and inertia parameters of a current fighter airplane, the Lockheed F-94B, are included in figures 4 to 8 for comparison purposes. For the inertial parameters (figs. 4 to 6), these curves correspond to full fuel load in the integral wing fuel tanks.

Tip tanks.- Figure 2 shows the two tip tanks that were used in this investigation. The smaller of these two tanks (hereinafter referred to as tank A) was a geometrically scaled reproduction of a full-sized Fletcher 230-gallon tip tank, whereas the larger tank (tank B) was designed to have the same shape but three times the internal volume of the smaller tip tank. No attempt was made to scale the stiffness of the tip tank or its attachment to the wing.

Construction of the model tip tanks consisted of a duralumin cylindrical center section with hollow plastic nose and tail cones made of fiber glass and Paraplex. Tank B was assembled by replacing the smaller nose and tail cones with larger ones and mounting a thin duralumin cover (shown removed in fig. 2) over the center section. For each tank, two tail cones were provided, one with a horizontal fin and one without a fin, in order to explore the effects of the fin on flutter. For tank A the fin was scaled geometrically from the full-sized configuration. Each tip tank housed a flutter-arresting device which is described in detail later in the paper. This device involved the use of one of three different shifting weights to achieve a rapid change in the mass unbalance of the tip tank. Table I gives the inertial properties of the tank for each of these weight conditions with no additional weights added.

The geometrical properties of both tip tanks and fins are also given in table I. The fairing at the juncture of the wing and tank A can be seen in figure 1(b). This fairing was completely covered by the center section of tank B.

Figure 10 indicates the manner in which additional weights were mounted in the tanks to simulate a given fuel load. As previously noted, no effort was made to take into account the effective changes in the tip-tank inertial characteristics due to fuel sloshing. The tip-tank weight is hereinafter referred to in terms of the weight ratio μ which is defined as the ratio of the tip-tank weight to wing-panel weight by the relation

$$\mu = \frac{W_t}{W_w} = \frac{W_t}{10}$$

since $W_w = 10$ pounds.

Figure 11 is included for the purpose of relating μ to full-scale fuel loads for both size tip tanks. In view of the results of reference 14 concerning the effective weight of sloshing fluid in a tank, the fuel loads simulated in the present investigation by means of solid weights correspond to increased actual fuel loads. Although tank B had three times the internal volume of tank A, the full-scale fuel capacity of both tanks was considered to be the same. The empty weight of tank B was based on a further assumption that the larger full-scale tank housed fixed equipment whose weight was approximately 50 percent of the weight of its full fuel load. The weight of this fixed equipment accounts for the large differences in μ corresponding to the tank-empty condition in figure 11. The minimum weight condition indicated by the dotted boundary in the figure, and applying to a solid fuel load of 25 percent full, corresponds to the lightest weight of the flutter-arresting device for tank A with fin. (See table I.)

Fuselage. - The main structural member of the fuselage was a hollow steel section to which the wings were mounted through steel brackets welded to the root of each wing spar. This center section was made hollow so as to permit passage of the instrument wires leading from the model to the control room. The fairings forming the external contours of the fuselage were attached to either end of the main member, as may be seen in figure 1(b) which shows model with middle fairings removed. The elastic properties of the fuselage were not intended to be representative of current fighter designs; the fuselage was, in fact, essentially rigid with respect to the wings. Bearings were housed at either end of the center section to permit a rolling degree of freedom of $\pm 180^\circ$. Low stiffness springs were housed within the fuselage to position the model horizontally in the tunnel when the model was given freedom to roll. Small aerodynamic control tabs (fig. 1(a)) were located at the rear end of the fuselage to provide manual control of the model in roll. The rolling degree of freedom could be completely locked out so as to obtain essentially the cantilever or symmetric boundary condition. The actual measured rolling inertia

of the model fuselage was 2.36 in-lb-sec^2 which is somewhat larger than the scaled value of a typical fighter fuselage (the scaled rolling inertia of the Lockheed F-94B is approximately 1.39 in-lb-sec^2).

Instrumentation.- All the frequencies in both the natural vibration survey and the flutter investigation were measured by means of resistance wire strain gages located at three different stations along each wing spar as indicated in figure 3(a). The bending gages were mounted to the inside surfaces of the overhanging flanges, and the torsion gages were mounted to the vertical web members. The signals from these strain gages were fed into a recording oscilloscope. The position of the model in roll could be determined by means of a slide wire-position indicator located at the forward end of the main center-section member of the fuselage.

In order to determine the vertical acceleration of the fuselage during flutter, an accelerometer was located on the main center-section member at the juncture of the fuselage center line and the wing elastic axis.

High-speed motion pictures were taken of the model during flutter from a position outside the tunnel and in line with the span of the wing. The only other item of model instrumentation was associated with the operation of the flutter-arresting device, discussed in the following section.

Flutter-arresting gear.- A desirable and important feature of wind-tunnel flutter testing is a reliable means of preventing a destructive buildup of amplitude once a flutter condition is attained. The more common methods used at low speeds such as restraining wires or mechanical means within the flow are not too satisfactory at transonic speeds. Several alternative methods have been suggested. The Wright Air Development Center (WADC), for instance, has successfully restrained rudder flutter in flight by quickly changing the mass balance of the control surface. One of the objectives in this series of tests was to evaluate a flutter-arresting device involving a rapid shift of the tip-tank center of gravity and its possible application to flight flutter-testing techniques. The shift of the tip-tank center of gravity was accomplished by moving a piston, within a cylinder running the length of each tank, from its extreme rearward position to its extreme forward position or conversely. The piston could not be stopped at an intermediate position. The position of the piston was controlled by an observer or by an electronic device that monitored the electrical outputs of one of the strain gages on the wings. When the oscillating stress at that station exceeded a predetermined level, the piston was automatically fired to its other position.

Included in figure 3(a) is a simplified sketch of the flutter-arresting gear. Forward travel of the piston was obtained by supplying

air under pressure through the rearward end of the cylinder, whereas rearward movement was accomplished by applying a vacuum. Electrical contacts were placed at each end of the cylinder in order that the extreme forward and rearward locations of the pistons could be recorded by an oscillograph.

The mass of the cylinder, being only 0.53 pound or 6 percent of the tank A full weight, imposed no weight penalties except in cases where low fuel loads were to be simulated. The pistons used weighed 0.40, 0.78, and 1.07 pounds, corresponding respectively to 4.8, 9.2, and 12.7 percent of the tank A full weight.

MODEL TESTS

Vibration Survey

Before the flutter tests were started, natural frequencies of vibration of the model were measured with the model mounted in a horizontal position on a dummy sting. The flexibility of this sting was made approximately equivalent to that of the sting in the Langley 16-foot transonic tunnel so that the model frequencies obtained in this survey would be comparable with those obtained on the sting in the tunnel. The model was excited both manually and with an electrodynamic shaker attached at various points along the wing.

Wind-Tunnel Test Procedure

Figure 1(a) shows the model mounted on the sting in the Langley 16-foot transonic tunnel. The flutter tests were conducted at Mach numbers up to 0.94 and at Reynolds numbers per foot up to 4.2×10^6 .

In conducting the flutter tests, the tunnel speed was increased gradually and maintained at various speeds while the model response to random tunnel disturbances was observed and recorded with the flutter-arresting piston in the forward and rearward positions of the tip tank. Since only two positions of the piston were possible (extreme forward or extreme rearward) during the approach to flutter, the piston was left in the position that appeared to have the least damping as observed by the aforementioned response of the model to the random tunnel disturbances.

The wind-tunnel tests were terminated either when flutter was encountered or when the test could not proceed further, because of tunnel power limitations or lack of effectiveness of the flutter-arresting device.

When flutter was encountered, the tunnel conditions were recorded simultaneously with the operation of the recording oscillograph and movie camera. At the same time, the piston was fired to the position which appeared to have more damping, and it was hoped that this would result in a condition that was not in a flutter region (a condition which was usually obtained). The oscillograph records and movies were generally taken continuously before, during, and immediately after the firing of the piston.

The model was excited manually by plucking the wing tips in bending and torsion prior to and often after each flutter run, and records were made of the bending and torsional vibration frequencies. These frequencies were measured after the flutter runs to provide checks on the structural integrity of the model.

RESULTS AND DISCUSSION

For convenience most of the experimental and calculated results of this investigation are indexed in table II. Figures 12 to 18 listed in this table show flutter Mach number plotted against e_t for both experimental and calculated results. Figures 19 to 23 listed in the table show frequency plotted against e_t .

Experimental Results

Table III compares some of the results of the vibration survey with the results (available in ref. 10) of vibration tests on a current unswept-wing fighter-type airplane with tip tanks. The comparisons are made between model frequencies obtained during the vibration survey and frequencies scaled from reference 10 for the closest wing and tip-tank inertial conditions available for both model and airplane. The frequencies and tip-tank inertial conditions taken from reference 10 were scaled according to the scale factors listed earlier in the section entitled "Description of Model." The agreement shown by the limited comparisons in table III for first bending and first torsion indicate how well the flutter model may have represented a current fighter-type airplane, namely, the Lockheed F-94B. The fact that the two scaled second bending frequencies listed for the airplane were considerably higher than the model second bending frequencies could be partly due to reduced fuel rolling inertia effects (see ref. 15) which may have been present in the airplane but were not realized in the model.

Table IV presents the results of the flutter tests in which the tip-tank inertial properties were systematically varied so as to obtain flutter

for ratios of uncoupled wing bending frequency to torsion frequency f_{h1}/f_{α_1} near unity. In this table the tip-tank weight ratio μ and moment of inertia for each flutter run are represented by a simple designation. In this designation the letter "A" or "B" identifies the tip tank used, the set of numbers following the first dash refers to μ , and the set of numbers following the second dash gives the uncoupled frequency ratio f_{h1}/f_{α_1} . As previously noted, the value of μ was determined from the ratio of tip-tank weight to wing-panel weight; the frequency ratio was determined from figures 24 and 25. The phase angle indicated in table IV is the angle by which the bending strain led the torsion strain.

Effect of tip-tank center of gravity. - The effect of e_t on flutter speed may be seen in figures 12 to 18 for various values of μ and frequency ratio f_{h1}/f_{α_1} . The various frequency ratios correspond to different moments of inertia for a given value of μ . Speeds where flutter was encountered are represented by the solid points and the open points indicate speeds reached in the tests without encountering flutter.

With the exception of figure 16, the results presented in figures 12 to 18 were obtained with the fuselage locked to prevent roll; thus, these results are for symmetric flutter, that is, flutter with both wing panels oscillating in phase. These figures, except for figure 12, apply to the smaller tip tank (tank A). In general, as may be observed, flutter speeds are increased for center-of-gravity positions forward of the elastic axis and tend to decrease as the ratio of uncoupled wing bending frequency to torsion frequency approaches unity. (See, for example, fig. 14.)

The flutter frequencies corresponding to the flutter speeds (shown in figs. 12 to 16) are presented in figures 19 to 23. In addition, figures 19 to 23 show the first and second measured wing natural frequencies with the model on the sting, the first and second calculated coupled frequencies, and the first bending and first torsional uncoupled frequencies. Each figure applies to a given tip-tank weight ratio μ and a given calculated frequency ratio f_{h1}/f_{α_1} . The fact that the experimental flutter frequency consistently fell between the measured first bending and first torsional wing frequencies of the model mounted on the sting indicates that the wing with tip tanks fluttered mainly in a combination of the first bending and first torsional structural modes. This type of motion was observed on the model during flutter. To show this, a typical flutter cycle, figure 26, is reproduced from the motion pictures taken during flutter.

Effect of tip-tank weight. - A comparison of the data of figure 13 ($f_{h_1}/f_{\alpha_1} = 0.93$; $\mu = 0.59$) with the data of figure 15 ($f_{h_1}/f_{\alpha_1} = 0.92$; $\mu = 1.005$) indicates that an increase of μ from 0.59 to 1.005 is accompanied by only a moderate decrease in flutter speeds for any given value of e_t . However, the flutter data given in table IV are insufficient to show the effect at low values of μ .

An appraisal of the flutter-arresting gear. - In figures 12 to 15 the effect of the tip-tank center of gravity on the symmetric flutter boundary indicates that, in general, the forward position of the piston should have resulted in a flutter-free condition. The fact that this proved to be the case is attested to by the motion pictures and the oscillograph records which were taken continuously when flutter occurred to provide complete time histories of the flutter response and subsequent damping action caused by the change in position of the piston. Figure 27 is a typical flutter oscillogram which shows clearly how the forward position of the piston damped the oscillations. For all conditions where the tip-tank center of gravity was shifted forward of the elastic axis, the flutter-arresting gear was effective in damping flutter.

Despite the effectiveness of this device, the shapes of the flutter boundaries were such as to impose certain restrictions on the practical application of the variable unbalance feature of the device. These restrictions are evident in a comparison of figures 15 and 16 which show increasing flutter speeds for tip-tank centers of gravity rearward of certain locations. Figure 15 shows that it was possible to traverse a small portion of the flutter region into a safe region without dangerous amplitudes building up. However, figure 16 shows a flutter condition where this was not possible. With the center of gravity approximately 3.6 inches rearward of the elastic axis, firing the piston forward established a condition also very close to the flutter boundary as indicated by the open point at approximately 1.4 inches rearward of the elastic axis. Since this shift did not change the center of gravity to a position in the safe region, this test could not be safely conducted beyond a Mach number of 0.37.

A further restriction in the application of the arresting device to flight-flutter use may be seen by examining the weight and size of a full-scale flutter-arresting device. If a full-scale device of this type were reproduced according to the scale factors applicable to the flutter model, the flutter arresting tube would be 6 times as long, or approximately 12 feet. The full-scale piston would be 216 times as heavy, or would weigh approximately 230 pounds for the heaviest piston.

The cumbersome features of a mass this large moving such a distance in a full-scale tank may be offset by the time of travel of the piston from one end of the tube to the other. In order for the piston travel

to be accomplished in the same number of flutter cycles for both model and airplane, the full-scale piston would have to traverse the arresting tube length in about $2\frac{1}{2}$ seconds.

It is recognized that flutter conditions can occur which may be insensitive to a change in mass unbalance and that under such conditions more suitable flutter-arresting devices may be those which suddenly cause a large increase in the damping of the structure. However, for the symmetric flutter encountered in the present study, the shifting mass-unbalance principle proved very effective within the limitations discussed in the preceding paragraphs.

Effect of tip-tank size. - The effect of the size of the tip tank on flutter can be seen in figure 12 by a comparison of the curve through the large symbols (pertaining to the large tank) with the curve through the small symbols (pertaining to the small tank), both tanks having nearly the same value of μ and moment of inertia (resulting in nearly the same frequency ratio $f_{h1}/f_{\alpha 1}$). The reduction in flutter speed for the large tip tank, which was as much as 15 percent in the region covered by the tests, is probably due mainly to the increased aerodynamic forces resulting from the larger tank, although it should be noted that approximately $1\frac{1}{2}$ percent of the area of the half-wing was covered by the large tip tank. (See fig. 3(a)).

Effect of tip-tank fins. - Most of the flutter runs were conducted with a horizontal fin attached near the trailing edge of the tip tank on the outboard side. Some tests were conducted with the fin removed, and the effect of this alteration on the flutter speed may be seen by comparing certain tests in table IV for both large and small tip tanks. In some of these cases the fin appeared to be beneficial and in other cases it was not. For tip tank A, for example, comparisons between tests 4 and 5 for a low tip-tank weight and between tests 25 and 26 for a high tip-tank weight show that the use of the fin significantly increased the flutter speed. In contrast, however, comparisons between tests 6 and 7 for tip tank A and between tests 40 and 41 for tank B indicate that the addition of fins had little effect on the flutter speed and actually reduced the flutter speed slightly for the large tank.

Observations on fuselage freedoms. - The effect of freeing the fuselage to roll about its longitudinal axis is shown in figure 16. These data pertain to the large tip tank for $\mu = 1.02$ and an uncoupled symmetric frequency ratio of 1.04. The solid curve through the circles corresponds to the fuselage-locked condition, whereas the squares apply to tests in which the rolling freedom was permitted. This additional freedom produced little or no effect on the flutter speed in the region where

symmetric flutter was encountered. Here, as in previous figures, the open points represent speeds reached without encountering flutter. Previous experiences with antisymmetric flutter (see, for example, ref. 13) have indicated that this type of flutter can be critical for forward tip-tank centers of gravity. In that case, firing the piston rearward would be necessary to move away from the flutter boundary and arrest flutter. For these tests, however, antisymmetric flutter was not encountered over the range of tank weights and frequency ratios covered. The failure to locate this boundary may be attributed, first, to the fact that the uncoupled first antisymmetric bending to first torsional frequency ratio was 3.36, whereas the first symmetric frequency ratio was 1.04; and, second, to the inability of the control surfaces on the tail and the soft torsional spring inside the fuselage to keep the model positioned in a near-horizontal attitude sufficiently well to permit satisfactory tests at Mach numbers higher than 0.80 for the fuselage free-to-roll condition.

The term symmetric flutter as used in this paper applies to flutter where the wings were moving in phase and was obtained when the fuselage was locked to prevent roll. However, from observation and motion pictures made during the tests, together with oscillograms of a strain gage on the sting and an accelerometer on the model center line at the wing elastic axis, it is clear that vertical motion of the fuselage was present. This motion was particularly noticeable for more violent flutter responses in which the entire model and the sting appeared to be pitching about some axis in the sting support system. Subsequent static and dynamic studies of the sting support system revealed that the sting has considerable flexibility and that an axis of rotation exists in part of the supporting structure just beneath the tunnel floor. Some information on the elastic and inertial properties of the sting support system is given in the appendix. Furthermore, the fundamental natural frequency of the entire sting model system appears to be well within the range of the model frequencies. These dynamic characteristics of the sting mount should be kept in mind when interpreting the symmetric flutter results obtained in this investigation.

Remarks on model flutter results and related full-scale flight flutter experience.. Under certain special tip-tank inertial loading conditions involving the use of lead weights in the tip tanks, flutter was experienced on the Lockheed F-80A airplane in flight tests conducted by WADC. Some uncertainties existed in the actual inertial loading conditions, particularly with regard to the distribution of fuel within the wing. Exploring such conditions on the model would have necessitated removal of the flutter-arresting device and was, therefore, postponed until the end of the experimental program. However, an attempt to reproduce the flight flutter point with the model would have had uncertain value since the inertial properties of the model wing did not duplicate the scaled values of the airplane wing (figs. 4 to 6). (It is of interest to note in passing, that, at least for vibration and flutter studies, the

wing of the Lockheed F-80A may be considered identical to that of the Lockheed F-94B.) Furthermore, the effect of the sting flexibility as an additional degree of freedom would make comparisons between model and full-scale results difficult. For these reasons, the conducting of the postponed test without the flutter-arresting device was not considered advisable. Despite the important differences that existed between the model and flight flutter conditions, some results have been chosen for conditions which, although far removed from those of the airplane, are as near as could be approached in the experimental program to those that are believed to have existed at the time the full-scale airplane fluttered. These results are presented in figure 28 in terms of Mach number at flutter as a function of the ratio of uncoupled wing bending frequency to torsion frequency and show that the model fluttered in the same Mach number range for comparable frequency ratios. Better agreement might be expected if, as indicated previously, more accurate inertial properties of the airplane had been reproduced in the model and if the dynamic properties of the sting support system could have been adjusted to represent the body degrees of freedom existing in the airplane.

Calculations and Correlation of Experiment and Theory

Methods of calculations.— The calculated flutter speeds and flutter frequencies presented in this paper were determined by application of a Rayleigh-Ritz type of analysis in which a combination of uncoupled vibration modes was employed to represent the flutter mode. By use of the measured wing inertial and stiffness properties given in figures 4 to 8, these modes were computed by means of the iterative method presented in reference 18. The uncoupled cantilever first bending and first torsional frequencies computed by this method are shown as functions of μ and I_{at} in figures 24 and 25, respectively. The corresponding mode shapes are shown in cross-plot form in figures 29 and 30. The uncoupled cantilever second bending and second torsional mode shapes and frequencies are given in figure 31. Figure 32 shows the uncoupled antisymmetric first bending mode shapes and frequencies.

In addition to approximating the flutter mode by means of a limited number of uncoupled modes, the flutter calculations also involved the following simplifying assumptions:

- (1) The oscillating aerodynamic forces and moments acting on the wing were those derived by Theodorsen in reference 16 on the basis of two-dimensional incompressible potential-flow theory (except for one case involving compressibility noted later). The effect of wing taper was accounted for in two different ways, one of which amounted to weighting or grading the aerodynamic forces and moments according to the taper ratio as recommended in reference 19. The station at three-fourths of the span was arbitrarily chosen as a reference station and the

$F + iG$ parts of the aerodynamic coefficients for k at this reference station were held constant along the span, whereas the remaining parts of the aerodynamic coefficients were allowed to vary with span according to the semichord ratio b/b_r . This method is for convenience identified herein by the term "graded coefficients." In the other method, labeled "constant coefficients," the reference station was also at three-fourths of the span but all parts of the aerodynamic coefficients were held independent of span for k at this station.

(2) Aerodynamic forces and moments on the tip tank were not included.

(3) The effect of structural damping in bending or torsion was taken into consideration in the manner recommended in reference 20; that is, it was assumed that $g_{h_1} = g_{a_1} = \text{Constant}$. For most of the calculations this constant was taken as zero; but for a number of cases, a value of 0.035 was used. This value was chosen on the basis of the experimental vibration data and has already been mentioned in the section on scale factors.

With these assumptions included in the analysis, flutter calculations were performed for three different wing-root boundary conditions, two of which were symmetric and the third antisymmetric to correspond, respectively, to the locked and unlocked fuselage in the flutter experiments. The first of these boundary conditions was the ideal cantilever-wing condition, whereas the second condition was that the pitching motion of the sting was approximated by means of a simple spring-inertia system whose properties are given in the appendix and was introduced into the flutter calculations as an additional elastic degree of freedom. For the antisymmetric condition, corresponding to the unlocked fuselage, the calculations included the first antisymmetric wing bending modes given in figure 32 for two different fuselage and tip-tank rolling moments of inertia. The entire program of flutter calculations has been classified, according to the degrees of freedom used, by the code designation given in the following table in order to facilitate identification of important features in specific applications of the analysis:

Identification of analysis	Boundary condition	Aerodynamic assumptions for wing taper	Degrees of freedom	
			Fuselage	Wing
A-1	Symmetric (cantilever)	Graded coefficients	None	First bending, first torsion
A-2		Constant coefficients		First bending, first torsion
A-3		Constant coefficients		First bending, first torsion Second bending, second torsion
A-4		Constant coefficients (compressible)		First bending, first torsion
B-1	Symmetric (sting flexible)	Constant coefficients	Fuselage pitch	First bending, first torsion
C-1	Antisymmetric	Constant coefficients	Fuselage free to roll	First asymmetric bending, First torsion
C-2		Constant coefficients		First asymmetric bending including tip-tank rolling inertia, First torsion

For convenience in comparing the calculated and experimental results, the analytical identifications given in this table are repeated in table II. In studying the effects of structural damping as stipulated by assumption (3) given previously, only analysis A-1 was used.

The calculated flutter speeds and flutter frequencies are given in table V, which is divided into six parts, each part being identified according to the code given in the preceding paragraph. Tables V(a), V(b), and V(c) apply to the ideal cantilever-wing boundary condition. Calculations using approximations to the flexibility in the model mounting system are given in table V(d), and antisymmetric flutter solutions are given in tables V(e) and V(f).

Results of analyses A-1 and A-2. Comparison of the results given in table V(a) for analysis A-1 (for zero damping) with those given in table V(b) for analysis A-2 for the same tip-tank inertial conditions indicates that the use of constant aerodynamic coefficients yielded flutter speeds that were as much as 30 percent higher than those obtained using graded coefficients. This trend toward higher flutter speeds due to the former and simpler application of two-dimensional aerodynamic coefficients was also found by Jahn and Buxton in reference 21, in which flutter speeds calculated by using various constant-coefficient approximations were appreciably higher than those calculated by using a graded-coefficient representation that essentially involved integration of both $F + iG$ and k along the span. The calculations in this reference were performed for a conventional bare wing of considerably lower frequency ratio and somewhat higher taper ratio than the frequency and taper ratios of the present configuration.

The results of analyses A-1 and A-2 without damping are compared, on the basis of Mach number, with experimental flutter results in figures 13 to 18, except for figure 17 in which the effect of damping is also shown. Although for some cases the comparison suffers for lack of a more complete fix on the experimental flutter boundaries, notably in figures 17 and 18, it is nonetheless evident that the disagreement between experiment and calculation was enlarged as the ratio of uncoupled bending frequency to torsion frequency approached unity. Furthermore, there were consistent tendencies for the calculations to be excessively conservative when the tip-tank centers of gravity were within 1 inch to the rear of the elastic axis, and for experimental and calculated flutter speeds to converge on one another for tip-tank centers of gravity further to the rear of the elastic axis. As was pointed out in reference 11, this behavior may be due to the failure to include some estimated tip-tank aerodynamic forces and moments in the calculations. (See assumption (2) in the preceding section.) Figures 12 and 16 show that flutter speeds calculated by using constant coefficients were in better agreement with experiment than were those calculated by using graded coefficients.

Effects of structural damping. - Table V(a) and figure 17 show some effect of introducing a damping coefficient of 0.035 into the simple two-mode flutter calculations involving graded aerodynamic coefficients (analysis A-1). The increases in flutter speeds, due to damping, were generally greater for tip-tank centers of gravity within 1 inch to the rear of the elastic axis than for tip-tank centers of gravity further to the rear. Case 40 for $e_t = 0$ shows that the flutter-speed increase was very abrupt. Moreover, it can be noted in this table that the increase in flutter speed also tended to be greater as the uncoupled frequency ratio ω_{h1}/ω_{x1} approached and exceeded unity. (Compare, for example, case 34 with case 47 and case 35 with case 49 for approximately the same values of μ and e_t .) This trend is in general agreement with that found in the extensive theoretical flutter studies of reference 22. The effects of this small damping coefficient materially improved the agreement between the calculated and experimental results, particularly for cases where the calculations without damping yielded excessively conservative answers.

Effects of higher uncoupled modes and compressible aerodynamic coefficients. - Table V(c) corresponding to analysis A-3 shows that the introduction of various combinations of higher uncoupled modes into analysis A-2 produced a negligible effect on flutter speed and flutter frequency for the case considered, namely case 64. On the basis of the results of reference 5, it is reasonable to expect a greater influence of higher modes for conditions of greater mass unbalance (corresponding to high e_t values in the present investigation) than the mass unbalance of case 64.

Although, as previously noted, most of the flutter calculations presented in this paper were based on incompressible-flow theory for the aerodynamic approximations, the effects of compressibility were explored by means of analysis A-4, which was based on constant coefficients corresponding to a Mach number of 0.7 as given in reference 23. The calculations made by using this analysis were also applied to case 64, and the results, listed for case 65 of table V(b), indicate that the flutter speed was not appreciably affected here by compressibility. As an approximate check on this effect, examination of figure 1 in reference 23 showed that the κ and frequency ratio of the model for this calculation fell approximately in a region where the same flutter speeds could be obtained with either compressible ($M = 0.7$) or incompressible ($M = 0$) coefficients.

The case chosen for these studies was one for which there existed a wide disagreement between theory and experiment and it is apparent that no improvement was obtained by introducing either higher uncoupled modes or compressible aerodynamic coefficients.

Note on coupled modes of vibration. - Along with the other frequencies in figures 19, 20, and 23 are shown also the first two coupled cantilever frequencies which were calculated from the flutter stability determinants with the aerodynamic terms omitted. These computations were performed for the purpose of estimating how much of the discrepancy between measured frequencies and calculated uncoupled frequencies was due to coupling in the system. As may be observed, coupling constitutes a relatively small part of this discrepancy, especially for the first mode. The remaining gap, of as much as 30 percent, between measured and calculated coupled frequencies is probably due in large measure to the fact that the measured frequencies include a strong influence of the sting support system.

Effect of sting flexibility. - The effect of flexible pitching in the sting mount, as simulated by means of analysis B-1, is shown in table V(d) and figure 33. Case 64 was used in this study which included a range of sting frequencies f_s and equivalent sting-fuselage pitching moments of inertia I_{f_s} . The calculated flutter speed is seen to be sensitive to frequency f_s , but relatively insensitive to inertia I_{f_s} .

In order to compare the results of analysis B-1 with experiment, estimates of the parameters ($I_{f_s} = 26.4 \text{ ft-lb-sec}^2$ and $f_s = 16.8 \text{ cps}$) are made in the appendix and are shown as dashed lines on figure 33. By using the estimated values of the parameters, it can be observed that there is very little effect of sting flexibility on flutter speed for the case considered. However, the large effect of frequency f_s indicates that sting flexibility may be important when the flutter frequency is close to the sting frequency.

Antisymmetric boundary condition.- The results of the antisymmetric flutter calculations are given in tables V(e) and V(f) for analyses C-1 and C-2, respectively. These calculations involved the first uncoupled antisymmetric bending-mode shapes and frequencies presented in figure 32. The fact that the flutter speeds and flutter frequencies are considerably higher than those obtained from cantilever analysis A-2 for the same tip-tank weight and moment of inertia is due to the greatly increased frequency ratios based on the antisymmetric bending frequency. An overall picture of the effect of frequency ratio in relation to tip-tank center-of-gravity location is shown for three frequency ratios in figure 34 and corresponds to analysis C-1. As may be seen, the frequency-ratio effect was considerably more pronounced for forward tip-tank centers of gravity than for rearward tip-tank centers of gravity. Notice also the reversed effect of this parameter on flutter speed as the tip-tank center of gravity is moved from a position forward of the elastic axis to a position rearward of the elastic axis. The value of I_{fr} used in analysis C-1 was estimated during the design of the model. The higher value of I_{fr} used in analysis C-2 was based on measured data obtained after completion of the model. However, the differences in flutter speeds between tables V(e) and V(f) are attributed more to the effect of I_{tr} than of I_{fr} . This contention is based on the existence of a small difference between the antisymmetric bending frequencies due to the two different values of I_{fr} , as compared with the larger difference caused by modifying the tip bending-moment boundary condition from zero to a finite value determined from the estimated tip-tank rolling inertia about the wing tip. (See fig. 32.) However, as comparison between tables V(e) and V(f) shows, the effect of this parameter on flutter speed was small.

The theoretical antisymmetric flutter trend plotted in figure 16 (for analysis C-2) serves to show the location of the experimental symmetric flutter region. As is implied in figure 34, this region might well have fallen within the speed range covered by the experiments, particularly for forward tip-tank centers of gravity, had the ratio of uncoupled antisymmetric bending frequency to torsion frequency been closer to unity. Preliminary analytical work during the construction of the model indicated that this condition might be realized for tip-tank weights approaching an empty condition, a condition which was not attainable in this investigation.

CONCLUSIONS

An extensive investigation has been made of flutter of a true-speed dynamically scaled model representative of current unswept-wing fighter-type airplanes with tip tanks. The model was one-sixth the size of a

hypothetical fighter prototype having an aspect ratio of 6 and was of spar-balsa segment-type construction with a flutter-arresting device in each tip tank. The following conclusions can be drawn from the results of this investigation:

1. A true-speed dynamically scaled model can be built to satisfy a given set of elastic and inertial specifications for flutter tests at high subsonic speeds.
2. In general, symmetric flutter speeds were increased for tip-tank center-of-gravity positions forward of the elastic axis and tended to decrease as the ratio of uncoupled wing bending frequency to torsion frequency $f_{h1}/f_{\alpha 1}$ approached unity.
3. Increasing the volume of the tip tanks by a factor of 3 tended to decrease the flutter speed. The installation of a horizontal fin at the rearward end of the tank may have had a beneficial effect on the flutter speed for the small tank, but may have had a slightly detrimental effect for the larger tanks.
4. Symmetric flexure-torsion flutter was effectively arrested when the tip-tank center of gravity was quickly shifted forward of the elastic axis. For cases where the center of gravity could not be shifted this far forward, the effectiveness was not as positive and was in some cases negative. In applications to flight flutter use, the weight, size, and time factors involved in the effectiveness of this device must be considered.
5. Calculated flutter speeds based on assumptions involving structural damping, higher structural modes, compressible aerodynamic coefficients, and sting-support flexibility (and not including aerodynamic forces and moments on the tip tanks) were, in general, excessively conservative for tip-tank centers of gravity near the elastic axis. However, the introduction of structural damping improved the agreement between calculation and experiment and resulted in greater increases in calculated flutter speeds, especially for ratios of uncoupled wing bending frequency to torsion frequency near unity. The effects of sting-support flexibility showed that this modification to the calculation may be important where the natural frequency of the sting system was near the flutter

frequency, and further work on these effects is in order. In addition, this sting flexibility should be kept in mind in interpreting the experimental flutter results.

Langley Aeronautical Laboratory,
National Advisory Committee for Aeronautics,
Langley Field, Va., September 29, 1954.

APPENDIX

CHARACTERISTICS OF MODEL MOUNTING SYSTEM

Description

The model was mounted in the Langley 16-foot transonic tunnel in the manner shown in figure 1(a). This mounting system essentially consisted of two main parts, the sting and the sting-support structure. The juncture between these two parts was 95 inches rearward of the elastic axis along the tunnel center line, and the actual connection was made by means of bolts approximately 1 inch in diameter located around the periphery. The sting had a joint whose center line was located 60 inches rearward of the elastic axis along the tunnel center line. At the free or upstream end of the sting a sting extension was mounted which was part of the main structural member of the model fuselage.

The sting support structure was made up of a massive streamlined strut mounted to a circular-shaped track that was part of the mechanism used to provide a change in angle of attack on models in the tunnel. The top of the strut to which the base of the sting was connected was cylindrical in shape with the longitudinal axis of the cylinder lying along the tunnel center line.

Stiffness Distribution

Figure 35 gives the stiffness distribution along the length of the sting. The variation shown is based on both calculation and experiment, the experimental values being obtained from measurements of the bending slope with the sting subjected to vertical loads applied to the main structural member of the fuselage at the elastic axis. Along the solid portion of the curve the calculated and experimental values were in close agreement. The dotted portions of the curve apply to the various joints and connections in the system and represent the most reasonable stiffness values corresponding to the actual measured slopes over these discontinuities. The experiments further revealed that the sting support structure was, for all practical purposes, rigid in the vertical or pitch direction, but that there was a finite stiffness contribution from the strut mount on the circular track. An estimation of this stiffness in terms of a spring constant for the pitching degree of freedom is 596×10^6 in-lb/radian, based on the approximate location of the actual axis of rotation in the base of the sting support structure.

Weight Distribution

Figure 36 shows the variation of weight per unit length with the distance along the tunnel center line. This distribution was calculated from the specifications of the sting.

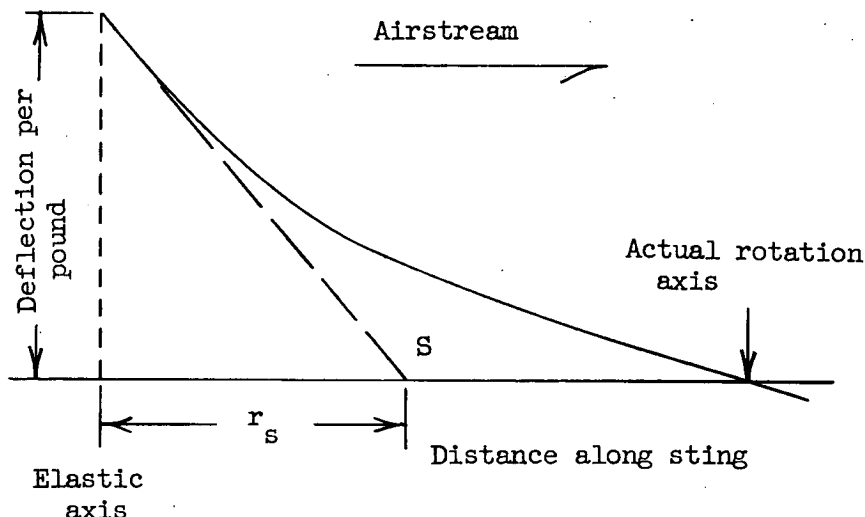
Fuselage Inertial Properties

The weight and pitching moment of inertia of the fuselage, including the main structural center section, wing spar root brackets (see fig. 3(a)), nose, center, and rearward fairings with control-surface assembly, are given as follows:

Fuselage weight, lb	157
Mass pitching moment of inertia of fuselage about elastic axis, in-lb-sec ²	75.3
Fuselage center of gravity, rearward of elastic axis, in.	5.92

Simplified Representation of Sting Flexibility

A scheme is advanced herewith for approximating the actual elastic behavior of the sting mount by means of an equivalent one-degree-of-freedom system oscillating in pitch about a point S in the manner shown in the following sketch:



The equivalent elastic properties consisted of a spring constant k_s and an effective rotation arm r_s . These parameters were determined from static loadings at the elastic axis together with deflection-curve measurements along the sting. As indicated in the foregoing sketch, the slope of the deflection curve at the elastic axis established the point S as being the effective axis of rotation and r_s as the effective rotation arm. From these measurements the following values were found for these two parameters:

$$k_s = 4015 \text{ lb/in.}$$

and

$$r_s = 42 \text{ in.}$$

In addition,

$$I_{f_s} = 26.4 \text{ ft-lb-sec}^2$$

which is based on the measured fuselage inertial properties given previously and includes the effective sting mass corresponding to $r_s = 42$ inches.

On the basis of the foregoing structural and inertial properties, the estimated frequency of the fuselage-equivalent sting combination is

$$f_s = \frac{1}{2\pi} \sqrt{\frac{k_s r_s^2}{2^4 I_{f_s}}} = 16.8 \text{ cps}$$

REFERENCES

1. Lambourne, N. C., and Weston, D.: An Experimental Investigation of the Effect of Localized Masses on the Flutter of a Model Wing. R. & M. No. 2533, British A.R.C., 1944.
2. Runyan, Harry L., and Sewall, John L.: Experimental Investigation of the Effects of Concentrated Weights on Flutter Characteristics of a Straight Cantilever Wing. NACA TN 1594, 1948.
3. Biot, M. A.: Flutter Analysis of a Wing Carrying Large Concentrated Weights. GALCIT Rep. No. 1A (Contract No. 41-2579, Part of Item 1, Material Div., Air Corps), Jan. 1942.
4. Minhinnick, I. T., and Yarwood, Jennifer: Interim Note on the Theoretical Effects of an Engine Mass on Wing Flutter. R.A.E. Tech. Note No. S.M.E. 143, May 1943.
5. Woolston, Donald S., and Runyan, Harry L.: Appraisal of Method of Flutter Analysis Based on Chosen Modes by Comparison With Experiment for Cases of Large Mass Coupling. NACA TN 1902, 1949.
6. Woolston, Donald S., and Runyan, Harry L.: On the Use of Coupled Modal Functions in Flutter Analysis. NACA TN 2375, 1951.
7. Runyan, Harry L., and Watkins, Charles E.: Flutter of a Uniform Wing With an Arbitrarily Placed Mass According to a Differential-Equation Analysis and a Comparison With Experiment. NACA Rep. 966, 1950. (Supersedes NACA TN 1848.)
8. Pepping, R. A.: Model F2H-2 - Summary Report. Theoretical Investigation of Aero-Elastic Stability of Wings Carrying Full and Partially Full Tip Tanks. Rep. No. 1704 (Contract NOa(s)-9768), McDonnell Aircraft Corp., May 26, 1950.
9. Bellan, T. M.: Models XF2H-1 and F2H-2 - Flutter Analysis of Wing With Tip Tanks. Rep. No. 1324 (Contracts NOa(s)-6130 and NOa(s)-9768), McDonnell Aircraft Corp., Aug. 5, 1949.
10. Oldaker, M. R., and Leppert, E. L.: Flutter Investigation of the F-94B Airplane With Fletcher 230 Gallon Tip Tanks. Rep. No. 8262, Lockheed Aircraft Corp., Nov. 15, 1951.
11. Gayman, William H.: An Investigation of the Effect of a Varying Tip Weight Distribution on the Flutter Characteristics of a Straight Wing. Jour. Aero. Sci., vol. 19, no. 5, May 1952, pp. 289-301.

12. Kinnaman, E. Berkeley: Flutter Analysis of Complex Airplanes by Experimental Methods. Preprint No. 363, S.M.F. Pub. Fund Preprint, Inst. Aero. Sci., Jan.-Feb. 1952.
13. Andropoulos, T. C., Chee, C. F., and Targoff, W. P.: The Effect of Engine Locations on the Antisymmetric Flutter Mode. AF Tech. Rep. No. 6353, Air Research and Development Command, U. S. Air Force, Aug. 1951.
14. Merten, Kenneth F., and Stephenson, Bertrand H.: Some Dynamic Effects of Fuel Motion in Simplified Model Tip Tanks on Suddenly Excited Bending Oscillations. NACA TN 2789, 1952.
15. Widmayer, Edward, Jr., and Reese, James R.: Moment of Inertia and Damping of Fluid in Tanks Undergoing Pitching Oscillations. NACA RM L53E01a, 1953.
16. Theodorsen, Theodore: General Theory of Aerodynamic Instability and the Mechanism of Flutter. NACA Rep. 496, 1935.
17. Taylor, A. S.: The Laws of Aeroelastic Similarity and Their Application, With Particular Reference to the Design and Testing of Elastic Wind Tunnel Models. Rep. No. Aero. 2393, British R.A.E., Aug. 1950.
18. Houbolt, John C., and Anderson, Roger A.: Calculation of Uncoupled Modes and Frequencies in Bending or Torsion of Nonuniform Beams. NACA TN 1522, 1948.
19. Scanlan, Robert H., and Rosenbaum, Robert: Introduction to the Study of Aircraft Vibration and Flutter. The Macmillan Co., 1951, pp. 211-212.
20. Smilg, Benjamin, and Wasserman, Lee S.: Application of Three-Dimensional Flutter Theory to Aircraft Structures. ACTR No. 4798, Materiel Div., Army Air Corps, July 9, 1942.
21. Jahn, H. A., and Buxton, G. H. L.: Comparative Calculations of the Critical Speed for Flexural-Torsional Flutter of a Typical Cantilever Wing. Tech. Note No. S.M.E. 3225, British R.A.E., Nov. 1942.
22. Theodorsen, Theodore, and Garrick, I. E.: Mechanism of Flutter - A Theoretical and Experimental Investigation of the Flutter Problem. NACA Rep. 685, 1940.
23. Garrick, I. E.: Bending-Torsion Flutter Calculations Modified by Subsonic Compressibility Corrections. NACA Rep. 836, 1946. (Supersedes NACA TN 1034.)

TABLE I.- GEOMETRICAL AND INERTIAL PROPERTIES OF MODEL TIP TANKS

(a) Small tip tank: tank A (scaled 230-gallon tip tank)

[Length, 30.3 in.; maximum diameter, 4.24 in.;
 span of fin (from tank center line), 4.38 in.;
 exposed area of fin, 11.2 in.²]

Piston weight, lb	Without fin			With fin		
	W _t , lb	e _t , in.	I _{at} , in-lb-sec ²	W _t , lb	e _t , in.	I _{at} , in-lb-sec ²
0.40	2.70	1.46	0.280	2.78	1.96	0.332
.78	3.08	2.49	.378	3.16	2.92	.430
1.07	3.37	3.22	.466	3.45	3.59	.520

(b) Large tip tank: tank B

[Length, 43.7 in.; maximum diameter, 6.12 in.;
 span of fin (from tank center line), 6.31 in.;
 exposed area of fin, 23.9 in.²]

Piston weight, lb	Without fin			With fin		
	W _t , lb	e _t , in.	I _{at} , in-lb-sec ²	W _t , lb	e _t , in.	I _{at} , in-lb-sec ²
0.40	4.77	1.22	0.698	5.00	1.92	0.803
.78	5.15	1.73	.680	5.38	2.48	.901
1.07	5.44	2.22	.769	5.67	2.92	.990

TABLE II.-- INDEX TO RESULTS

Table	Description
III	Experimental - comparable natural frequencies of model and a typical full-scale fighter configuration
IV	Experimental - results of model flutter program
V	Analytical - results of flutter calculations

Figure	Tank size	μ	$f_{h1}/f_{\alpha 1}$	e_t , in.	Wing-root boundary condition	Analysis
Ordinate, M; abscissa, e_t						
12	A and B	0.60	0.92	-4.9 to 1.7		None
13		.59	.84, .93	-4.9 to 3.5		A-1, A-2
14	A	.82	.90, .96, 1.02	-3.1 to 4.0	Fuselage clamped	A-1
15		1.005	.92	-2.4 to 4.0		A-1
			1.04	-2.4 to 4.0		A-1, A-2
16		1.02	3.36	-2.6 to 1.6	Fuselage free to roll	None
			3.36	0 to 2.4		C-2
17	B	.895	.98	-3.8 to 4.0	Fuselage clamped	A-1
18		1.29	1.01, 1.09	-2.1 to 4.0		A-1
Ordinate, f; abscissa, e_t						
19		.595	.84	-1.0 to 2.8		A-2
			.84	-2.0 to 3.5		First two coupled frequencies
20	A	.59	.93	-4.8 to 1.7		A-2
			.93	-1.25 to 1.6	Fuselage clamped	First two coupled frequencies
21		.82	1.02	-.9 to 2.5		A-1
22		1.005	.92	-2.3 to 4.0		A-1
23	B	1.02	1.04	-2.4 to 4.0		A-2
			1.04	0 to 3.2		First two coupled frequencies

TABLE III.- COMPARISON OF MODEL VIBRATION DATA WITH SCALED

VIBRATION DATA OF THE LOCKHEED F-94B AIRPLANE

	Tip-tank fuel load, gal	Scaled tip-tank inertial properties			Symmetric			Asymmetric bending	Test condition
		Wt., lb	et, in	I _{tot} , in-lb-sec ²	f _{b1} , cps	f _{t1} , cps	f _{b2} , cps		
Model Airplane	---	3.04	1.96	0.358	20.5	32.3	84.6	---	I
	75	3.15	---	.327	20.4	34.8	106	56.8	A
Model Airplane	---	3.70	0	506	19.6	29.5	83.8	---	I
	100	3.89	---	.401	18.9	31.2	103	---	A
Model Airplane	---	3.86	4.08	642	18.2	36.3	---	---	II
	100	3.89	3.80	.443	17.4	37.5	---	67.2	B

I Model mounted on dummy sting for vibration survey. (See fig. 1(b).)

II Model mounted on sting in tunnel. (See fig. 1(a).) Data from test 5 in table IV.

A Airplane in level attitude resting on its main landing gear with tires at normal pressure and fuel in integral wing tanks. (See ref. 10.)

B Airplane, with empennage and afterburner removed, inclined at 19° angle of attack with landing gear on chocks and blocks, tires at normal pressure, and fuel in integral wing tanks. (See ref. 10.)

TABLE IV - RESULTS OF EXPERIMENTAL FLUTTER PROGRAM

Test	Configuration	e_t , in.	Aerodynamic data				Frequency data				Phase angle, deg	Remarks	
			Piston forward	Piston rearward	M	V_f , fpm	$\frac{D_{sec}^2}{ft^4}$	R, per foot	f_{b1} , cps	Before flutter	After flutter		
1	A-.32-.82	.3.81	1.21	0.94	1.013	0.0015154	4.2 \times	10 ⁶	20.1	21.3	14.4	40.2	No flutter within test range; bursts of torsional oscillations from approximately $M = 0.60$ to $M = 0.80$
2	A-.335-.86	4.35	1.92	.78	.852	.001674	4.0		17.65	16.2	30.5	37.2	No flutter within range of available tunnel power
3	A-.36-.88	4.77	2.52	.78	.853	.001671	4.0		16.1	17.4	38.4	37.0	No definite flutter point at available tunnel power; flutter in bursts over wide range of Mach number below top point
4	A-.38-.81, no fin	3.77	.73	.73	.803	.001706	3.8		18.5	17.4	36.4	28.9	Incipient flutter
5	A-.385-.86	4.08	-.03	.84	.921	.001546	4.0		18.2	17.65	36.3	27.8	No flutter within range of available tunnel power
6	A-.405-.90, no fin	5.06	.62	.686	.001892	3.5			15.0	34.5	32.3		Incipient flutter; piston relatively ineffective
7	A-.49-.92	5.29	.65	.719	.001810	3.6			14.7	15.4	30.8	34.5	Very close to flutter; forward center-of-gravity shift due to firing piston appeared to be ineffective in arresting flutter
8	A-.565-.91	3.98	2.04	.68	.740	.001859	3.8		14.6	25.5	28.7	63	Symmetric flutter involving fuselage translation
9	A-.505-.93	-1.03	-.88	.99	.00188	3.8			15.2	25.2	22.8		No flutter
10	A-.505-.93	.37	-.542	.69	.774	.001718	3.6		15.8	21.3	21.3		Flutter
11	A-.505-.93	1.72	-2.07	.61	.683	.001859	3.5		15.1	22.3	19.3		Flutter
12	A-.595-.84	2.77	-.95	.77	.866	.002377	3.6		15.3	26.6	26.6		No flutter; near to flutter at $M = 0.73$
13	A-.595-.84	2.77	-.95	.73	.816	.001659	3.8		15.1	22.3	18.6		Repeat of test 12; burst of flutter at $M = 0.73$; test continued to $M = 0.81$ without obtaining flutter
14	A-.645-.107, no fin	.73	-.72	.45	.491	.002158	2.9		14.6	18.2	18.2	16.5	Flutter
15	A-.635-.90	3.79	1.08	.64	.719	.001777	3.4		14.4	14.2	19.4	19.7	Flutter
16	A-.825-.96	-.09	-2.77	.64	.910	.001650	4.2		15.5	12.7	22.5	15.8	No flutter
17	A-.825-.96	.04	-2.64	.60	.867	.001672	4.1		15.5	19.5	18.5		No flutter; random oscillations appeared to be slightly worse with piston forward
18	A-.825-.96	1.11	-1.57	.64	.695	.001910	3.7		13.6	14.6	19.05	15.0	Flutter
19	A-.825-.96	2.06	-.62	.50	.544	.002096	3.2		13.5	14.4	19.45		Test discontinued; right tip tank loose
20	A-.825-.96	2.06	-.62	.57	.629	.002399	3.5		13.4	18.2	19.35	16.0	Flutter

CONFIDENTIAL

NACA RM L54I19

TABLE IV - RESULTS OF EXPERIMENTAL FLUTTER PROGRAM - Continued

Test	Configuration	e_t , in.	Aerodynamic data				Frequency data				Remarks			
			Piston forward	Piston rearward	M	V_f , fps	ρ , lb-sec ² /ft ⁴	B, per foot	f_{t1} , cps Before flutter	f_{t1} , cps After flutter				
21	A-.85-.97	2.22	-.47	.65	669	.001931	3.7 \times 10 ⁶	12.4	12.1	25.3	19.0	15.4	27	Violent flutter; symmetric mode involving fuselage translation
22	A-.82-.1.02	-.38	-3.07	.65	939	.001516	3.9						No flutter	
23	A-.82-.1.02	1.05	-1.64	.65	709	.001973	3.7		13.9	17.4	15.6	33	Flutter	
24	A-.82-.1.02	1.83	-.36	.47	517	.002132	3.1	15.1	14.9	18.05	15.3	35	Flutter	
25	A-.85-.95, no fin	.15	-.73	.73	790	.001797	4.0	12.9	13.0	18.0	16.3	16.7	25	Visual evidence of flutter; piston in forward position appeared very effective in arresting flutter
26	A-.86-.95	.32	-2.28	.81	872	.001683	4.2	12.9	12.6	18.9	17.9	17.7	No flutter; torsional oscillations appeared stronger and less damped with piston forward than with piston rearward	
27	A-.90-.1.01, no fin	-.72	-1.73	.57	574	.002012	3.4	12.4	12.4	19.7	19.0		Very close to flutter; piston appeared ineffective in arresting flutter	
28	A-1.005-.92	-.10	-2.31	.81	890	.001587	3.9	12.8	11.6				No flutter within range of test; fitting for left wing tank loosened during test	
29	A-1.005-.92	-.78	-1.43	.63	692	.001871	3.6	13.3	12.3	16.9	16.5	15.1	Flutter	
30	A-1.005-.92	2.02	-.19	.57	632	.001949	3.4	11.8	12.65	17.2	16.95	14.5	35	Flutter
31	A-1.005-.92	2.53	-.32	.61	668	.001986	3.5	12.9	13.3				Flutter	
32	B-.595-.94	-.13	-1.49	.65	708	.001882	3.7	14.95	14.8	20.4	20.7	21.5	27	Flutter
33	B-.605-.93	1.09	-.152	.56	622	.001985	3.4	14.7	14.7	21.7	22.3	19.4	20	Flutter
34	B-.625-.90	.02	-1.29	.58	615	.001931	3.4	14.7	14.8	20.9	21.2	21.5	22	Flutter
35	B-.625-.90	.91	-.40	.56	626	.001955	3.3	14.7	14.7	23.1		21.0		Flutter
36	B-.85-.98, no fin	1.18	-.41	.460	.002028	2.6		13.05	13.1	17.65	17.9	16.6	21	Flutter in bursts
37	B-.855-.98	-.1	-.32	.78	890	.001701	4.1	13.4		17.6			No flutter within range of available tunnel power; action of piston very effective in preventing flutter	
38	B-.855-.98	.36	-.214	.69	759	.001613	3.7	11.1		19.9			Flutter; action of piston very effective in preventing flutter	
39	B-.85-.1.02, no fin	.70	-.38	.40	128	.002124	2.4	13.0	15.75	16.9	17.4	15.0	26	Flutter; piston effective in stopping flutter
40	B-.875-.1.04, no fin	.99	-.153	.40	137	.002211	2.7	12.9	12.75	17.45	17.2	14.5	31	Flutter

CONFIDENTIAL

TABLE IV - RESULTS OF EXPERIMENTAL FLUTTER PROGRAM - Concluded

Test	Configuration	e_t , in.	Piston forward	Aerodynamic data			Frequency data			Remarks			
				M	V _P , fps	$\frac{P}{lb \cdot sec^2}$	R, per foot	f_{bl} , cps	f_{tl} , cps	Phase angle, deg	f_t , cps	f_t , cps	
41	B-1.025-1.04	1.19	.36	396	0.002255	2.4×10^6	12.4	12.7	12.9	14.8	16	Flutter	
42	B-1.02-1.04	-.27	.84	929	.001544	3.9	11.7	12.6	16.85	16.7		No flutter; wing showed strong bending tendencies	
43	B-1.02-1.04	.65	-.154	687	.001872	3.5	11.6	11.0	15.1			Flutter; strong torsion response	
44	B-1.01-1.04	1.04	.62	427	.002213	2.6	12.1	12.0	14.1	15.8	14.2	Flutter	
45	B-1.01-1.05	1.03	-.116	.39	.002232	2.5	12.3	12.2	15.15	15.55	14.0	Flutter; amplitude of oscillations increased slowly prior to flutter	
46	B-1.025-1.04	1.62	.42	472	.002135	2.7	11.0	11.0	15.3	14.0	14.4		
47	B-1.025-1.04	3.58	.37	1.40	.002135	2.7	12.15	11.5	15.1	15.0	13.5	Flutter	
48	B-1.30-1.01	-.57	.71	10.65			11.3	11.3	15.5	15.4	13.5		
49	B-1.31-1.07	-.22	-.06	10.5			11.3	11.5	15.1	15.0	14.7	Test discontinued; no flutter observed	
50	B-1.28-1.09	.76	-.97	10.1			10.1	10.1	15.1	15.0	12.8	No flutter; predominant bending response	
51	B-1.025-1.04	-.41	-.92	764	.001766	3.7	11.4	11.3	15.3	15.3	12.4	Sustained flutter; predominantly torsion; piston very effective	
52	B-1.02-1.04	.76	-.97	3.9	.002223	2.6	10.8	11.1	13.4	13.5	12.4	No flutter; model free to roll	
53	B-1.02-1.04	-.41	-.92	426	.002223	2.6	11.4	10.6	13.3	13.3	12.4	No flutter; model free to roll; very unstable in roll; records indicate model less damped with piston in forward position near top Mach numbers	
54	B-1.02-1.04	.55	-.259	781	.001710	3.8	13.3 (symmetric) 13.7 (antisymmetric) 16.4 (symmetric) 16.6 (antisymmetric)	10.6	14.8	15.4	14.6	14.6	No flutter; model free to roll; very unstable in roll; records indicate model less damped with piston in forward position near top Mach numbers
55	B-1.02-1.04	-.27	.60	701	.001900	3.5	13.2 (symmetric) 14.2 (antisymmetric) 14.6 (symmetric)	11.1	15.1	15.1	14.8	14.8	Flutter; model free to roll; piston forward effective in stopping flutter
56	B-1.02-1.04	.55	-.246	.60	.001912	3.5	14.2 (symmetric) 14.3 (antisymmetric) 14.3 (antisymmetric)	10.6	16.0	15.1	14.6	14.6	Flutter; model free to roll; piston forward effective in stopping flutter
57	B-1.025-1.04	1.63	-.164	.40	.002179	2.6	12.5 (symmetric) 12.9 (symmetric) 14.2 (antisymmetric)	11.1	14.4	14.6	14.6	14.6	Flutter in bursts; model free to roll; strong torsion response

TABLE V.- RESULTS OF FLUTTER CALCULATIONS

(a) Cantilever-wing boundary condition, graded coefficients,
first bending and first torsion (analysis A-1)

Case	e_t , in.	$g_{h1} = g_{\alpha_1} = 0$			$g_{h1} = g_{\alpha_1} = 0.035$		
		v_f , fps	f_f , cps	$1/k_r$	v_f , fps	f_f , cps	$1/k_r$
A-.565-.91 configuration							
1	3.925	699	20.8	13.09			
A-.59-.93 configuration							
2	-1.16						
3	0	501	22.7	8.60			
4	.24	443	22.6	7.66	562.5	22.25	9.85
5	.50	461	22.5	8.00	523	22.2	9.18
6	1.00	519	22.2	9.12	547	22.1	9.63
7	1.59	558	21.8	9.96	583.5	21.95	10.35
A-.59-.84 configuration							
8	0	993	24.1	16.05			
9	.50	774	23.7	12.74	849	23.2	14.28
10	1.00	748	23.3	12.51	774	23.0	13.1
11	1.75	761	22.6	13.13	783	22.7	13.43
12	2.64	785	21.8	14.04	831	22.3	14.54
13	3.50	803.5	21.1	14.84	886	21.9	15.75
A-.815-.90 configuration							
14	0	655	19.9	12.82			
15	1.00	561	19.4	11.26	582	19.3	11.74
16	2.00	615	18.6	12.9	658.5	19.0	13.51
17	3.00	652	17.9	14.2	729	18.5	15.31
18	3.695	667	17.4	14.95	777	18.3	16.56
19	4.00	672	17.2	15.23	781	18.0	16.9
A-.825-.96 configuration							
20	0	329	18.9	6.78			
21	.50	367	18.8	7.60	422	18.65	8.80
22	1.02	442	18.5	9.32	475.5	18.6	9.98
23	1.97	516	17.9	11.23	574	18.3	12.23
24	3.00	563	17.2	12.75	656	17.9	14.27
25	4.00	592	16.6	13.9			

TABLE V.-- RESULTS OF FLUTTER CALCULATIONS - Continued

(a) Cantilever-wing boundary condition, graded coefficients, first bending and first torsion (analysis A-1) - Concluded

Case	e_t , in.	$g_{h1} = g_{\alpha_1} = 0$			$g_{h1} = g_{\alpha_1} = 0.035$		
		v_f , fps	f_f , cps	$1/k_r$	v_f , fps	f_f , cps	$1/k_r$
A-.82-1.02 configuration							
26	0	255	18.1	5.49			
27	.50	317	18.0	6.85			
28	.96	384	17.8	8.40			
29	1.74	439	17.4	9.82			
30	2.50	484.5	17.0	11.11			
31	3.00	507	16.75	11.8			
32	4.00	540	15.2	12.98			
A-1.005-.92 configuration							
33	.25	477	17.5	10.6			
34	.71	465	17.3	10.48			
35	1.95	538	16.6	12.62			
36	2.47	570	16.3	13.63			
37	3.00	595	16.0	14.43			
38	4.00	620	15.4	15.68			
B-.895-.98 configuration							
39	-1.015						
40	0	217.5	18.0	4.705			
41	.69	376	17.8	8.22			
42	1.50	472	17.3	10.64			
43	2.50	536	16.7	12.5			
44	4.00	585	15.8	14.43			
B-1.02-1.04 configuration							
45	-.27						
46	.0135	537	16.3	12.85			
47	.65	328	15.9	8.03			
48	.94	362	16.0	8.81			
49	1.96	426	15.6	10.65			
50	3.58	483.5	14.5	12.96			
51	3.99	497	14.6	13.28			
B-1.29-1.01 configuration							
52	-.35						
53	.50	288	14.75	7.62			
54	1.50	407	14.5	11.1			
55	2.50	465	13.8	13.14			
56	4.00	508	13.1	15.15			
B-1.29-1.09 configuration							
57	.99	338	13.8	9.54			
58	1.50	360	13.6	10.33			
59	2.50	404	13.2	11.92			
60	4.00	446	12.6	13.77			

TABLE V.- RESULTS OF FLUTTER CALCULATIONS - Continued

(b) Cantilever-wing boundary condition, constant coefficients,
first bending and first torsion (analysis A-2)

Case	e_t , in.	v_f , fps	f_f , cps	l/k_r
A-.565-.91 configuration				
61	3.925	762	20.9	14.25
A-.59-.93 configuration				
62	-1.16			
63	0	664	22.7	11.39
64	.24	486	22.6	8.39
65a	.24	488	22.2	8.67
66	.50	491	22.6	8.50
67	1.00	524	22.8	8.97
68	1.59	604	21.9	10.8
A-.59-.84 configuration				
69	-2.00			
70	0	999	24.1	16.16
71	.50	831	23.7	13.66
72	1.00	813	23.3	13.61
73	1.75	819	22.6	14.14
74	2.64	855	21.8	15.3
75	3.50	890	21.1	16.45
B-1.02-1.04 configuration				
76	-.27			
77	.0135	720	16.2	17.35
78	.50	374	16.1	9.05
79	.94	407	15.9	9.95
80	1.50	442	15.9	10.86
81	1.96	475	15.6	11.86
82	2.75	511	15.2	13.08
83	3.22	532	15.0	13.82
84	3.99	556	14.7	14.71

^aComputed using Mach number 0.7 coefficients
(analysis A-4)

TABLE V.- RESULTS OF FLUTTER CALCULATIONS - Continued

(c) Cantilever wing boundary condition, constant coefficients, first bending, first torsion, second bending, and second torsion

[(Analysis A-3); configuration A-.59-.93; $e_t = 0.24$ in.]

Case	Identification of modes used	v_f , fps	f_f , cps	l/k_r
85	First bending, first torsion, second bending, second torsion	479	22.7	8.23
86	First bending, first torsion, second bending	476	22.6	8.20
87	First bending, first torsion, second torsion	476	22.6	8.20
64	First bending, first torsion	486	22.6	8.39

(d) Symmetric (sting-fuselage pitching) boundary condition, constant coefficients, flexible sting pitching, first cantilever wing bending, and first cantilever wing torsion

[(Analysis B-1); configuration A-.59-.93; $e_t = 0.24$ in.]

Case	I_{f_s} , ft-lb-sec ²	v_f , fps	f_f , cps	l/k_r
$f_s = 14.5$ cps				
88	25	465	23.0	7.87
89	39.8	431	23.0	7.29
90	50	427	23.3	7.13
91	70	435	22.75	7.45
92	100	447	22.8	7.63
$f_s = 16.7$ cps				
93	10	518	22.7	8.90
94	25	509	23.05	8.61
95	40	463	23.0	7.82
96	50	428	22.9	7.28
97	70	447	22.8	7.64
98	100	426	22.9	7.26
$f_s = 20$ cps				
99	10	461	22.9	7.84
100	25	658	23.1	11.075
101	39.8	526	23.1	9.05
102	50	528	23.1	8.91
103	70	469	22.9	7.97
$f_s = 23$ cps				
104	10	995	23.0	16.85
105	25	1,112	23.3	18.58
106	40	970	24.35	15.52
107	50	990	23.1	16.72
108	70	999	23.0	16.90

TABLE V.- RESULTS OF FLUTTER CALCULATIONS - Continued

(e) Antisymmetric (fuselage free to roll) boundary condition, constant coefficients, first asymmetric bending, and first cantilever wing torsion

[Analysis C-1; configuration B-1.02-1.04;
 $I_{fr} = 0.0605 \text{ ft-lb-sec}^2$; $I_{tr} = 0$]

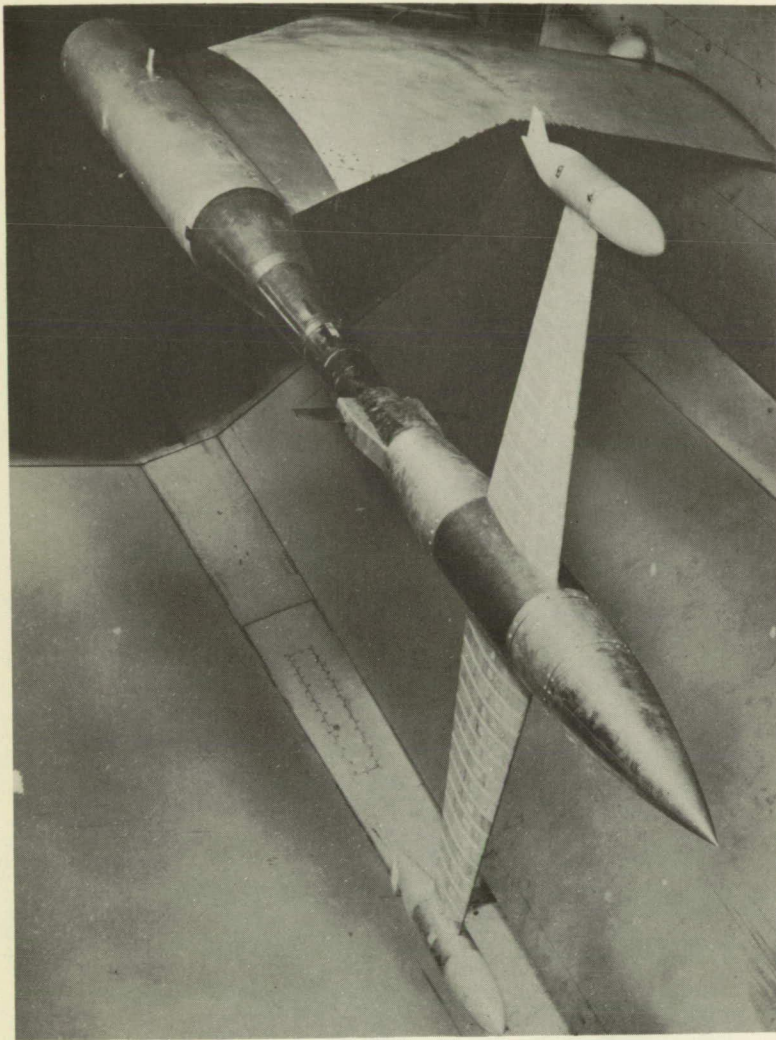
Case	e_t , in.	v_f , fps	f_f , cps	l/k_r
109	-2.50	3,441	31.6	42.5
110	-2.00	4,213	31.9	51.55
111	-1.00	7,125	31.3	88.8
112	-.75	9,995	31.0	125.7
113	-.50	2,829	15.4	71.7
114	0	1,427	15.1	36.7
115	1.19	1,088	14.6	29.2
116	2.375	1,027	14.0	28.6

TABLE V.- RESULTS OF FLUTTER CALCULATIONS - Concluded

(f) Antisymmetric (fuselage free to roll) boundary condition, constant coefficients, first asymmetric bending, and first cantilever wing torsion

[Analysis C-2; configuration B-1.02-1.04; $I_{fr} = 0.0984 \text{ ft-lb-sec}^2$;
 $I_{tr} = 0.0192 \text{ ft-lb-sec}^2$]

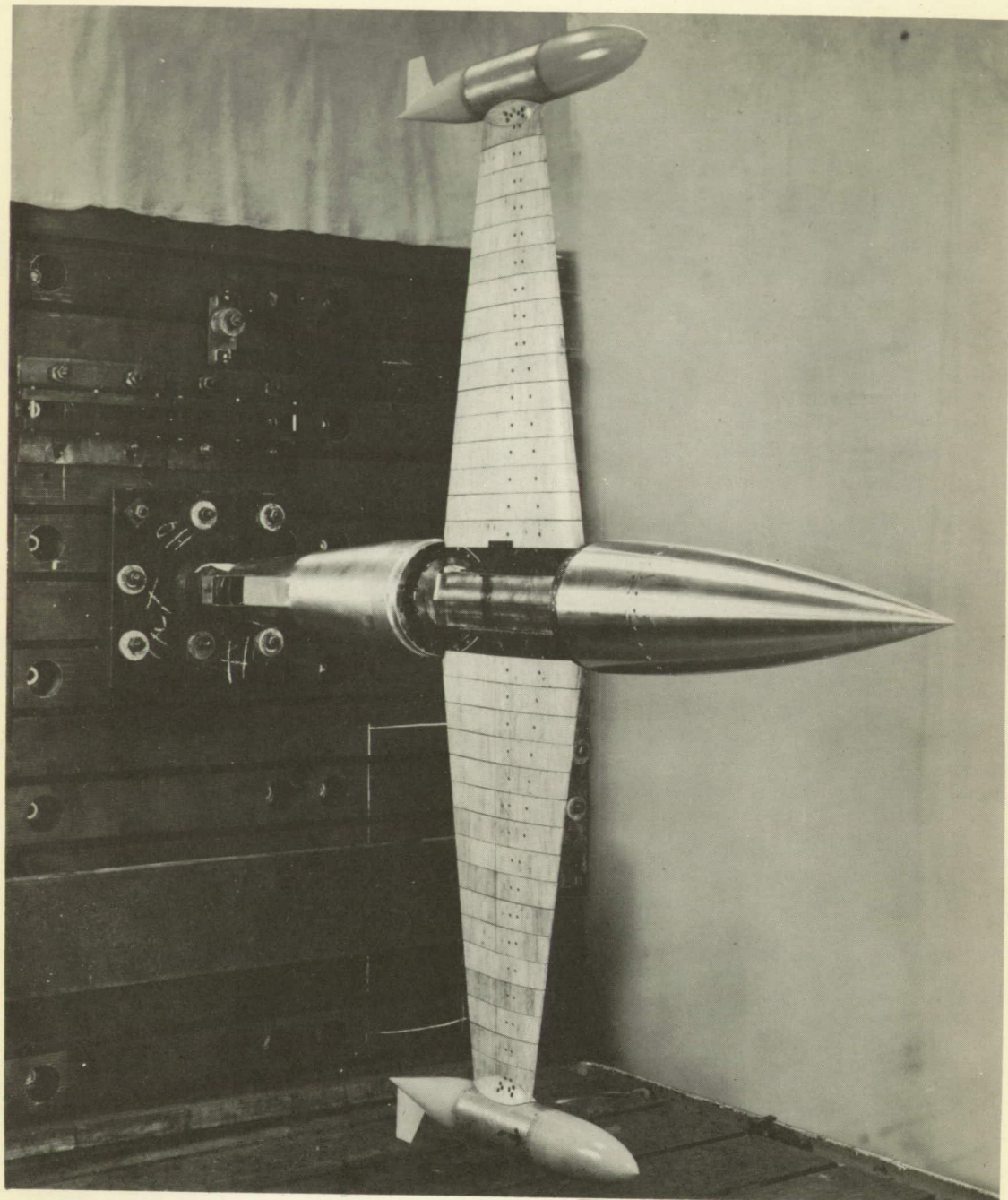
Case	e_t , in.	v_f , fps	f_f , cps	l/k_r
117	0	1,489	15.05	38.6
118	1.19	1,131	14.4	30.6
119	2.375	1,059	13.8	29.9



(a) Model in the Langley 16-foot transonic tunnel.

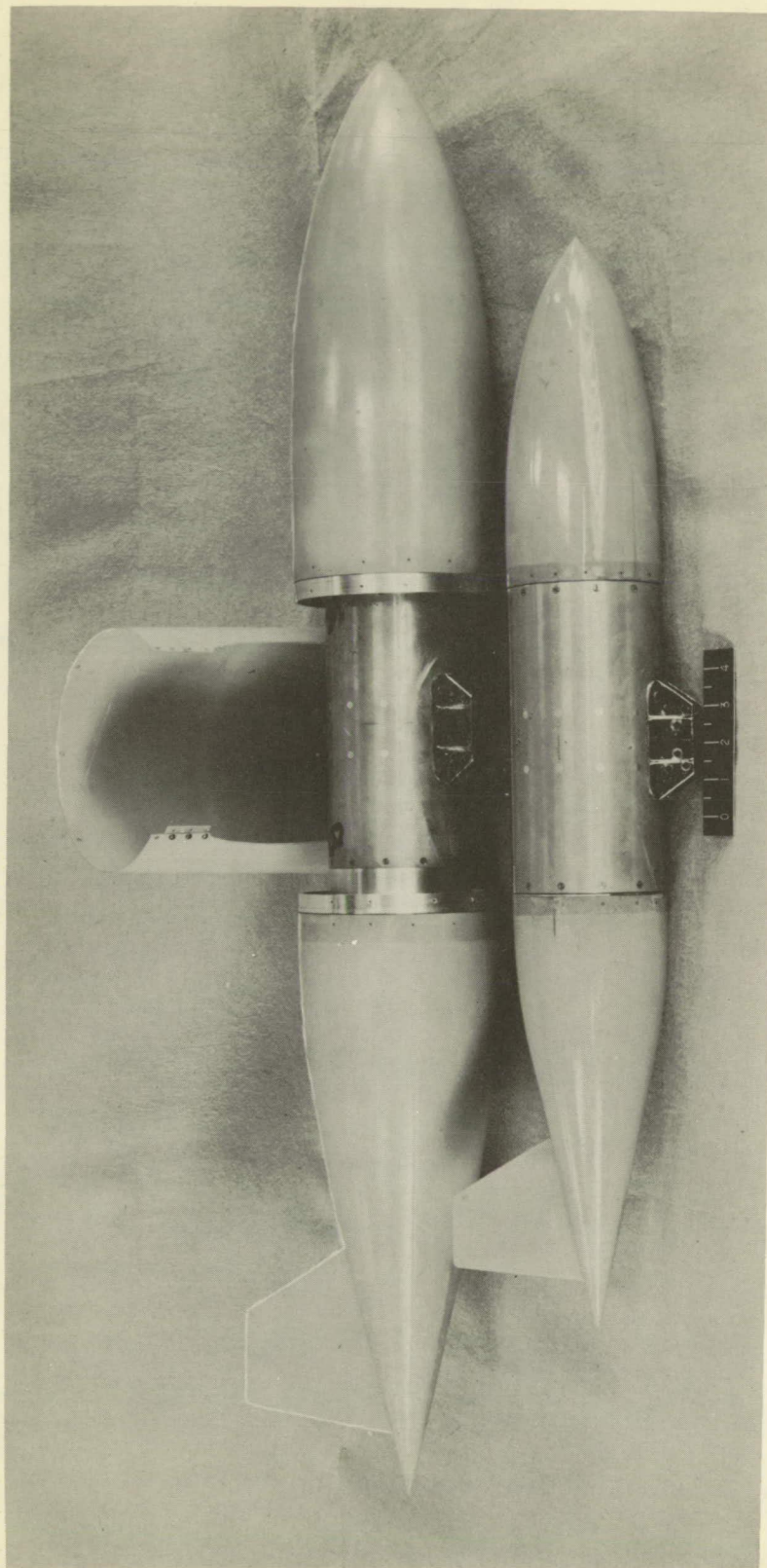
L-77976.1

Figure 1.- Photographs of dynamic model.

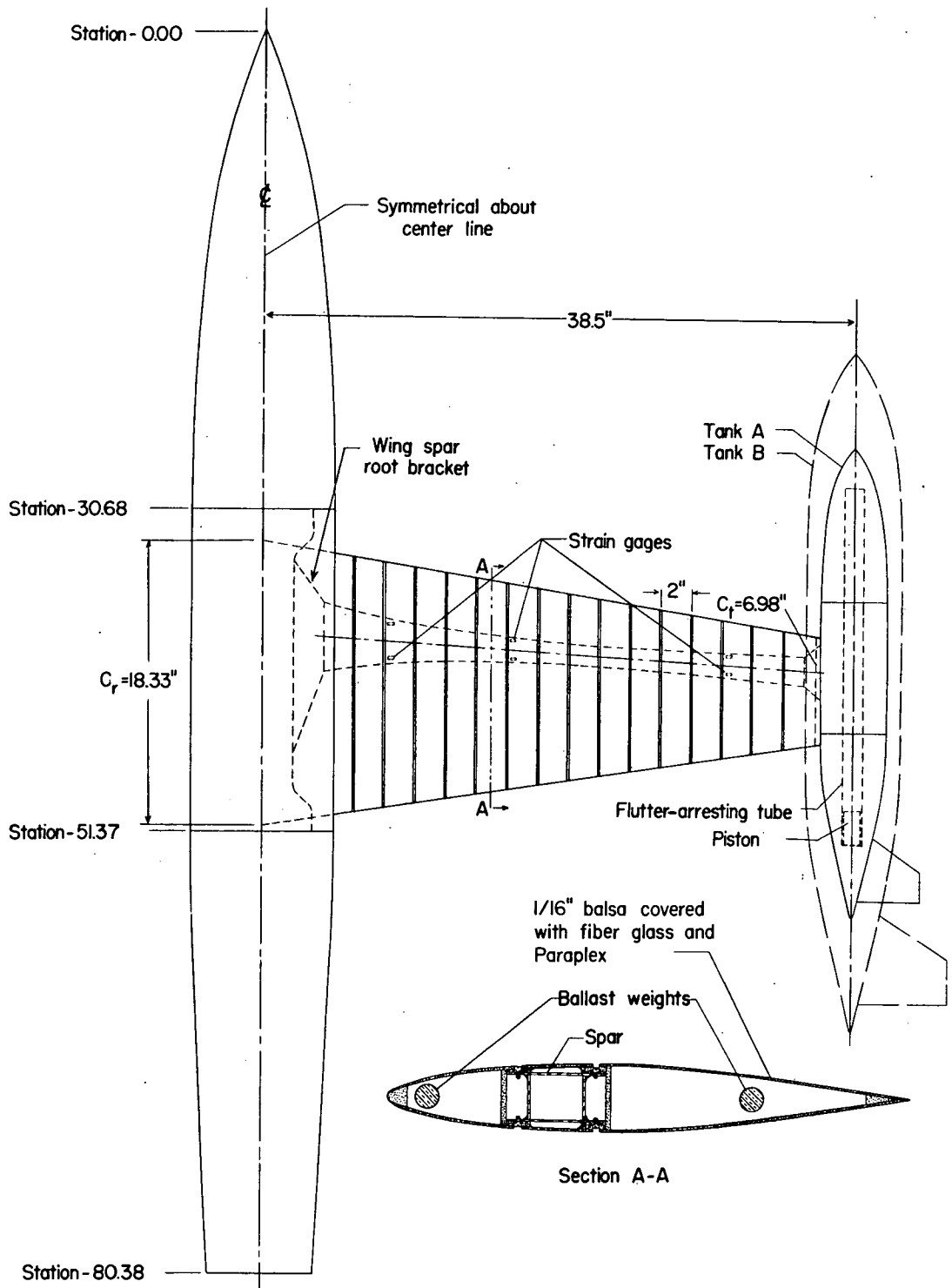


(b) Model mounted on dummy sting for vibration survey. L-77439

Figure 1.- Concluded.

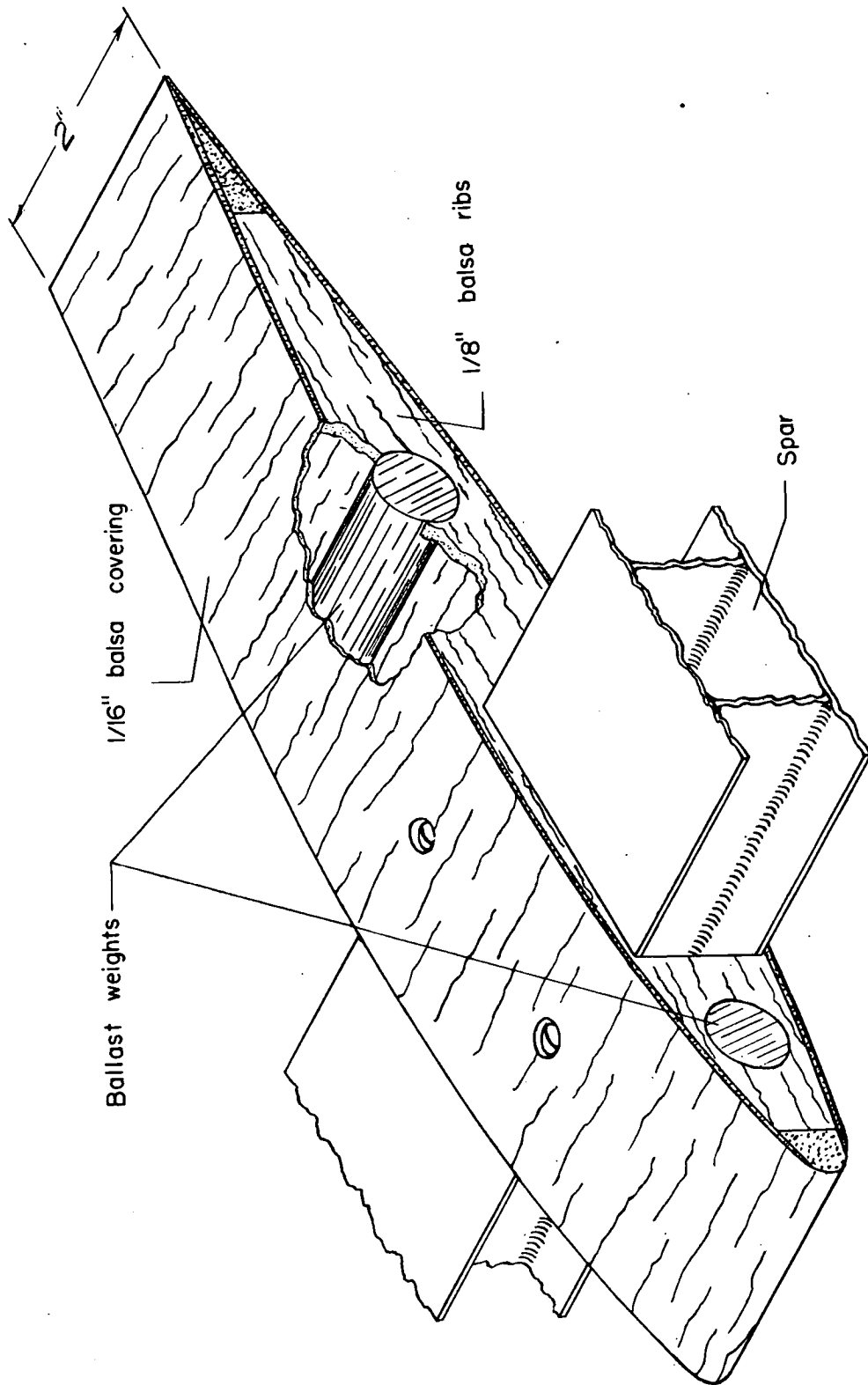


L-77443
Figure 2.- Tip tanks used in investigation.



(a) Plan view of model.

Figure 3.- Sketches of dynamic model.



(b) Sketch showing balsa segment construction for a single segment.

Figure 3.- Concluded.

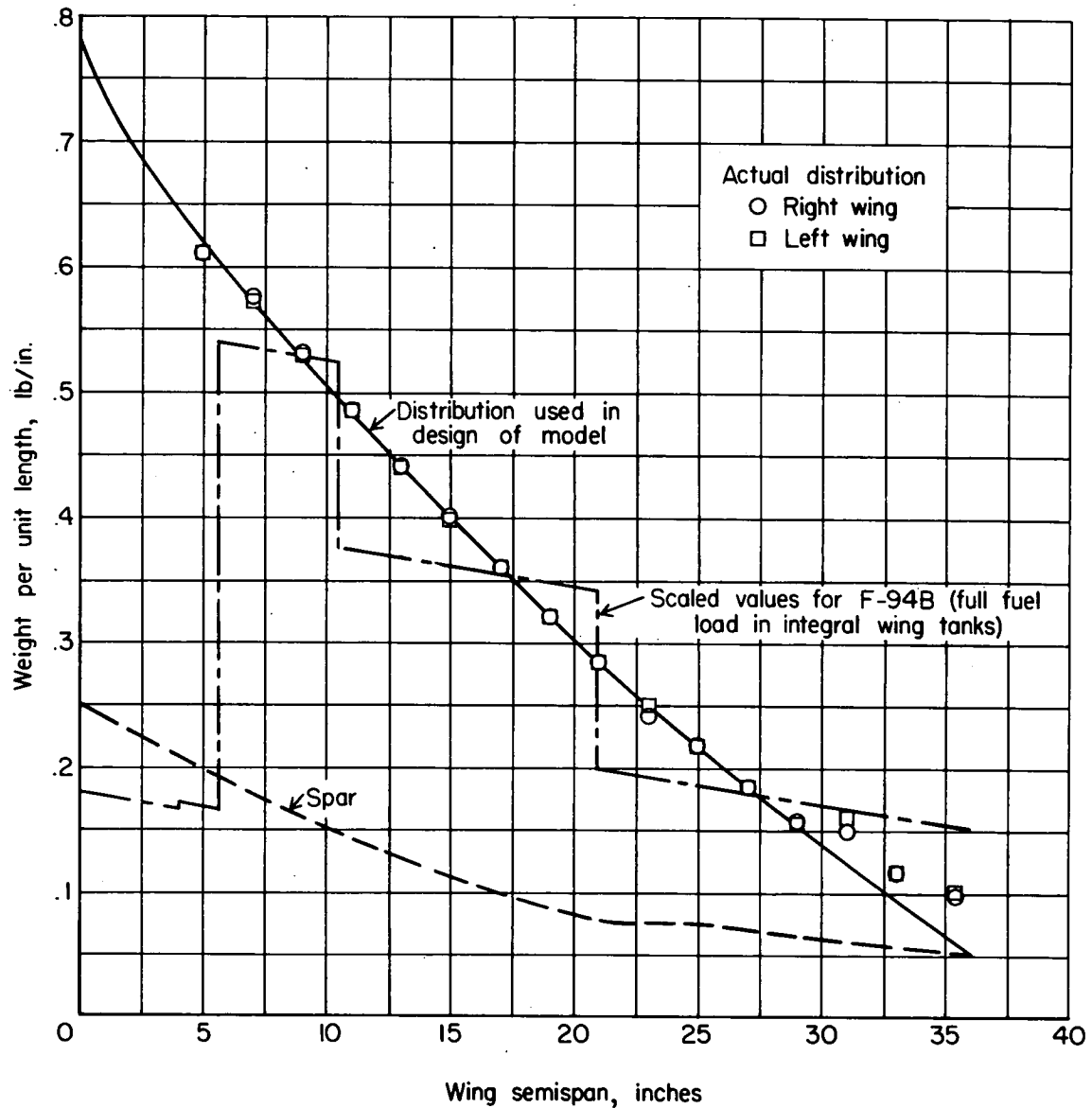


Figure 4.- Spanwise weight distribution.

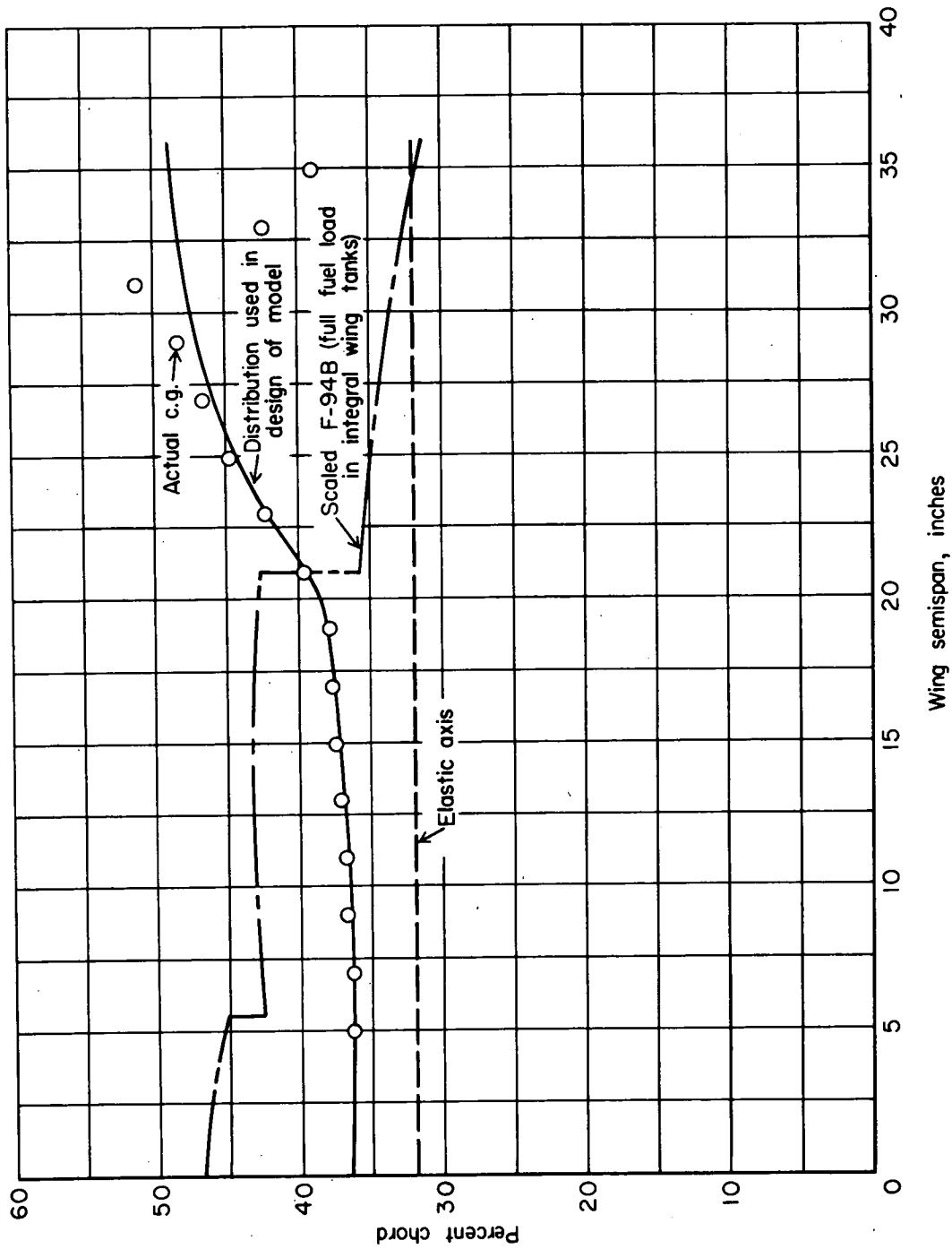


Figure 5.- Variation of center of gravity and elastic axis with span.

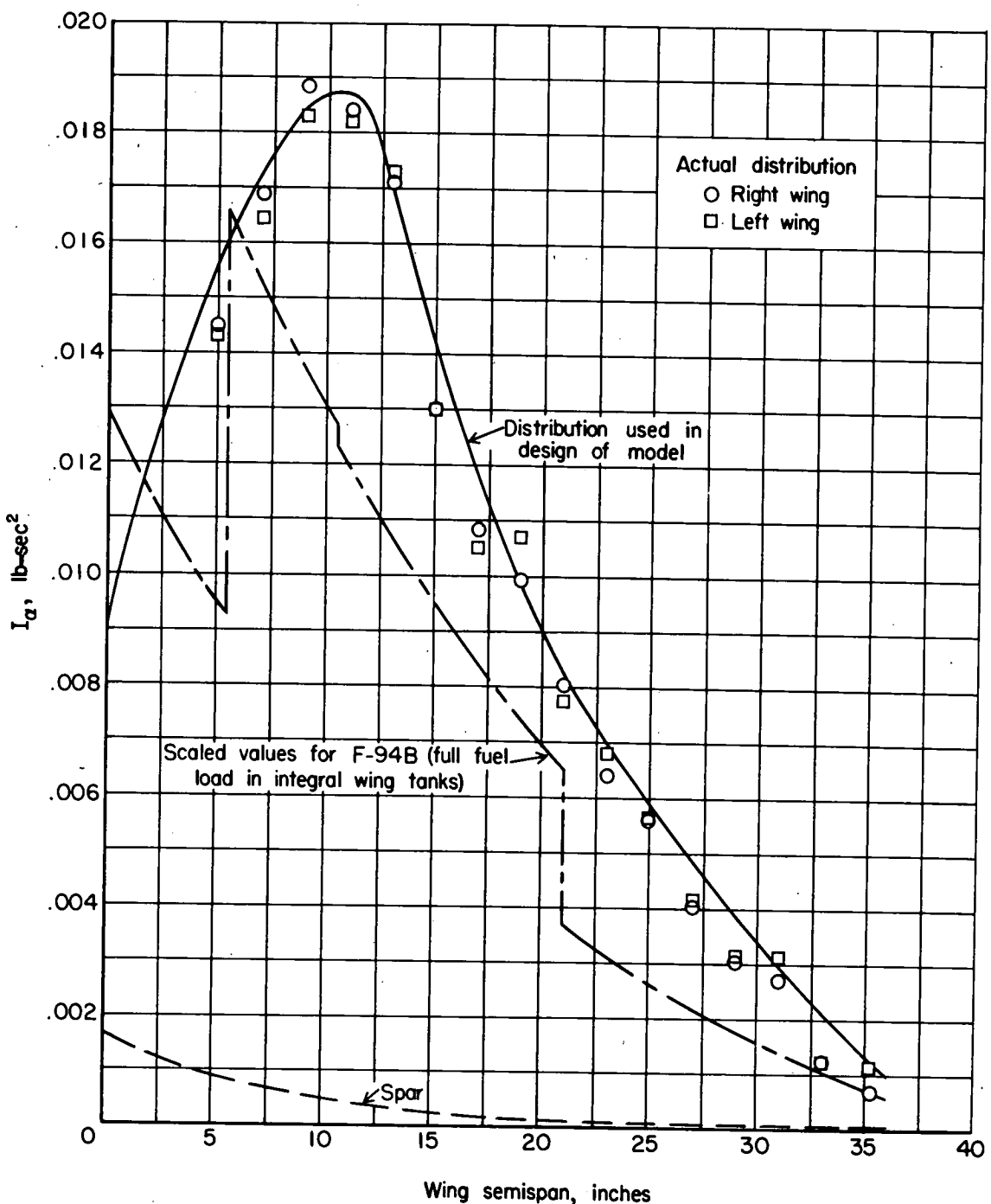


Figure 6.- Variation of moment of inertia with span.

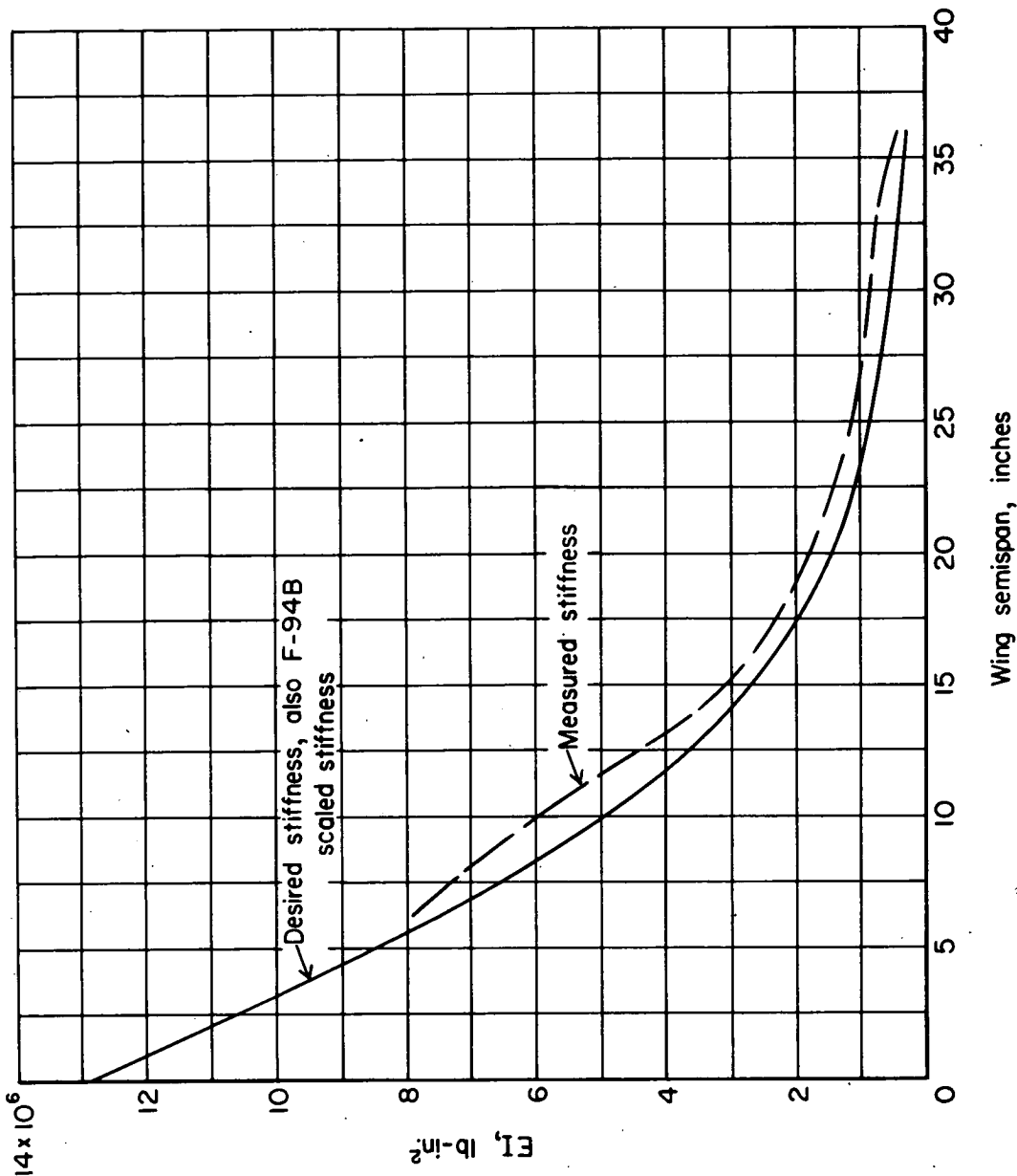


Figure 7.- Variation of bending stiffness with span.

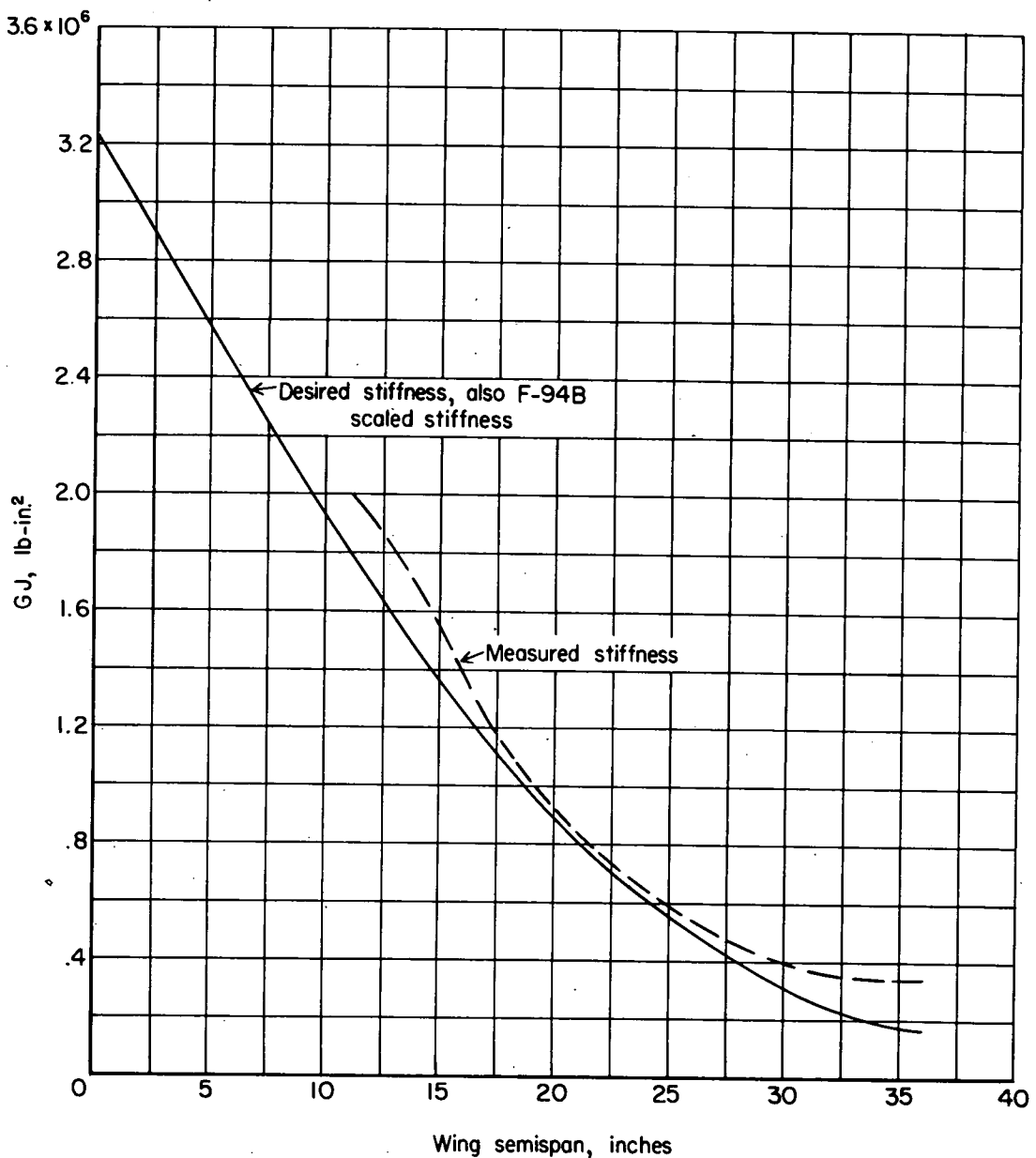


Figure 8.- Variation of torsional stiffness with span.

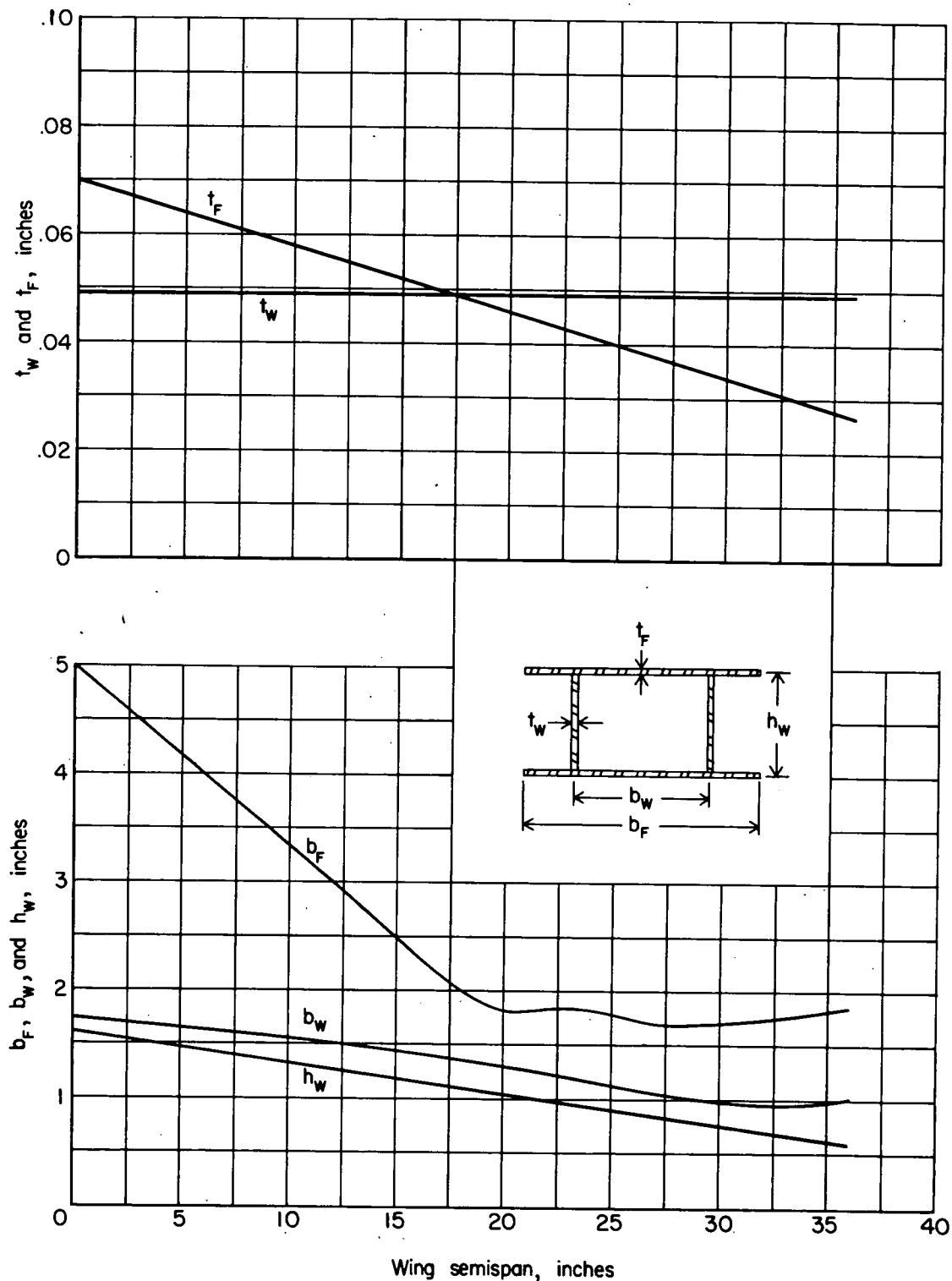


Figure 9.- Design specifications for wing spar.

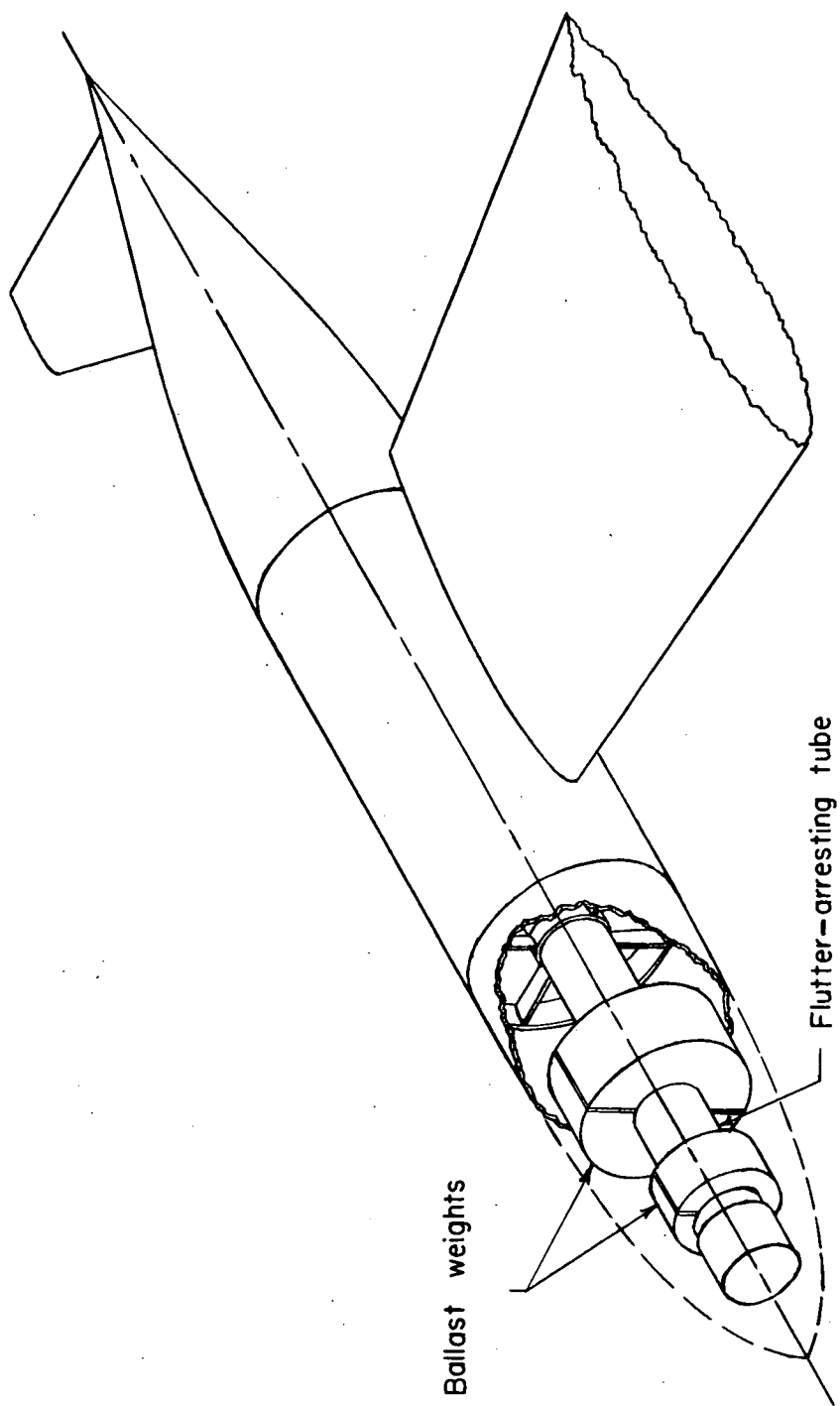


Figure 10.- Sketch of tip tank A showing ballast weights.

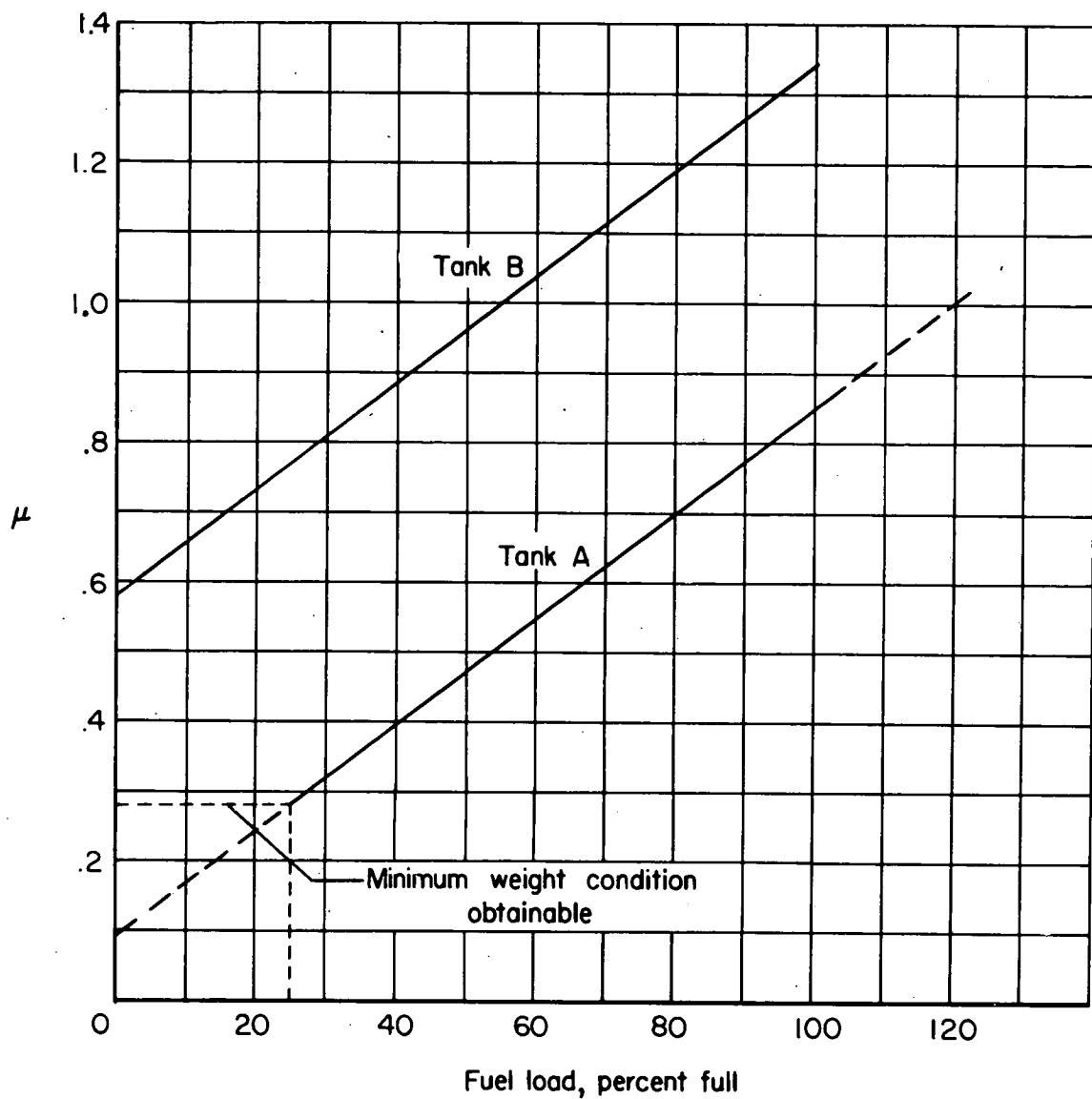


Figure 11.- Correlation of model tip-tank weight ratio with prototype fuel load.

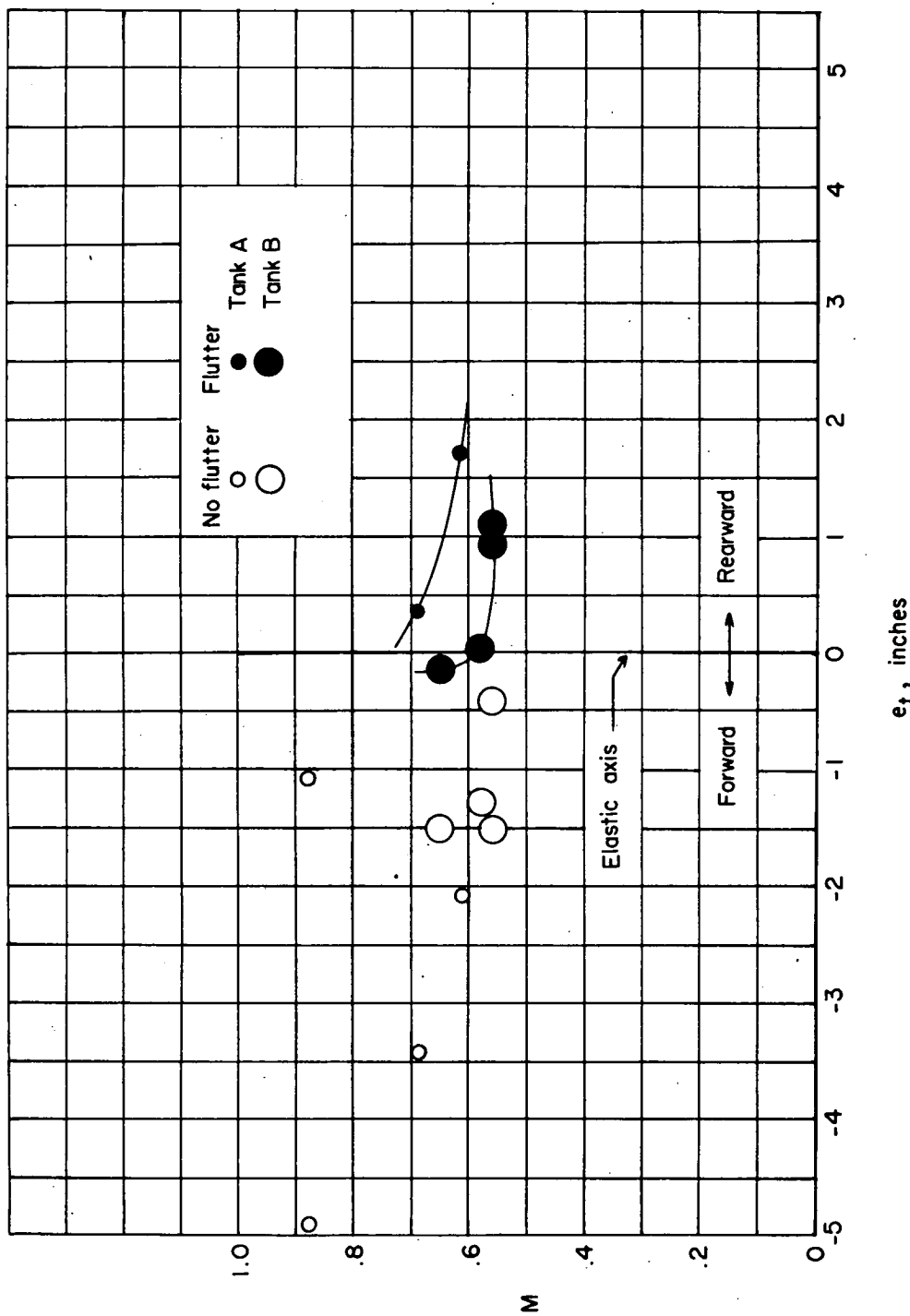


Figure 12.- Variation of flutter Mach number with tip-tank center of gravity for both small and large tanks ballasted to the same weight and moment of inertia. $f_{h1}/f_{c1} = 0.92$; $\mu = 0.60$; fuselage clamped.

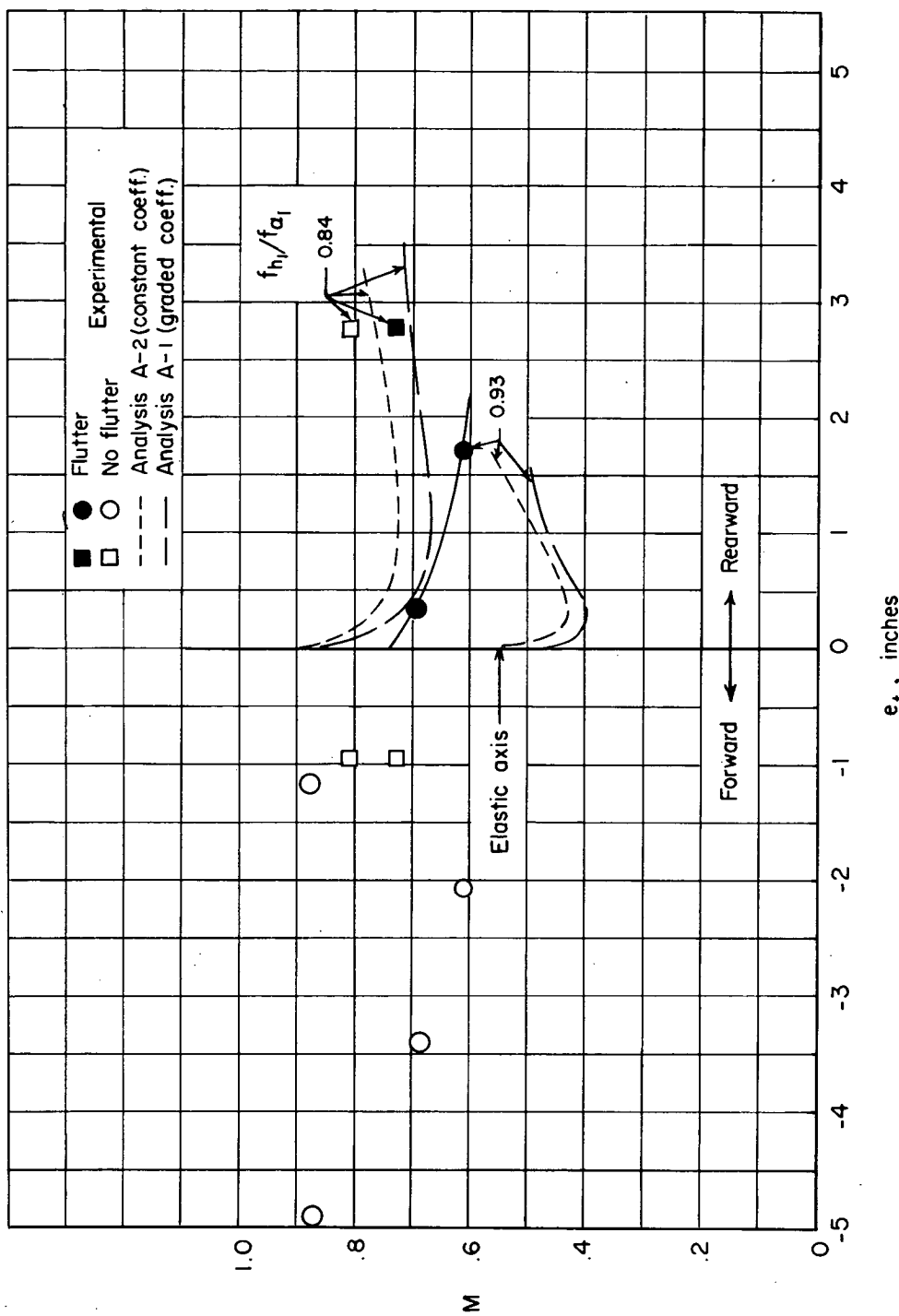


Figure 13.- Variation of experimental and theoretical flutter Mach numbers with tip-tank center of gravity for two values of f_{h1}/f_{α_1} . Tank A;
 $\mu = 0.59$; fuselage clamped.

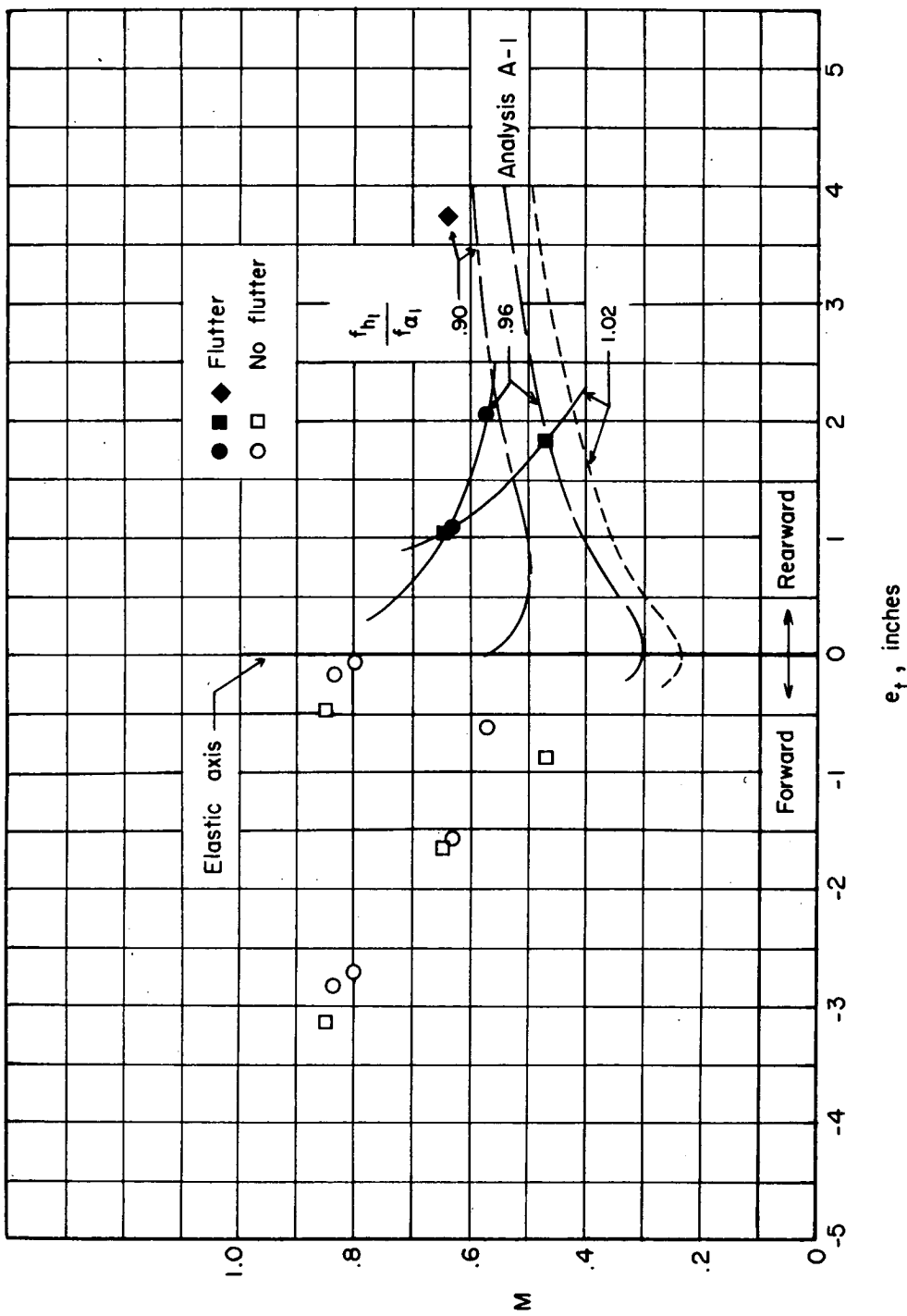


Figure 14.- Variation of experimental and theoretical flutter Mach numbers with tip-tank center of gravity for three values of f_{h1}/f_{a1} . Tank A;
 $\mu = 0.82$; fuselage clamped.

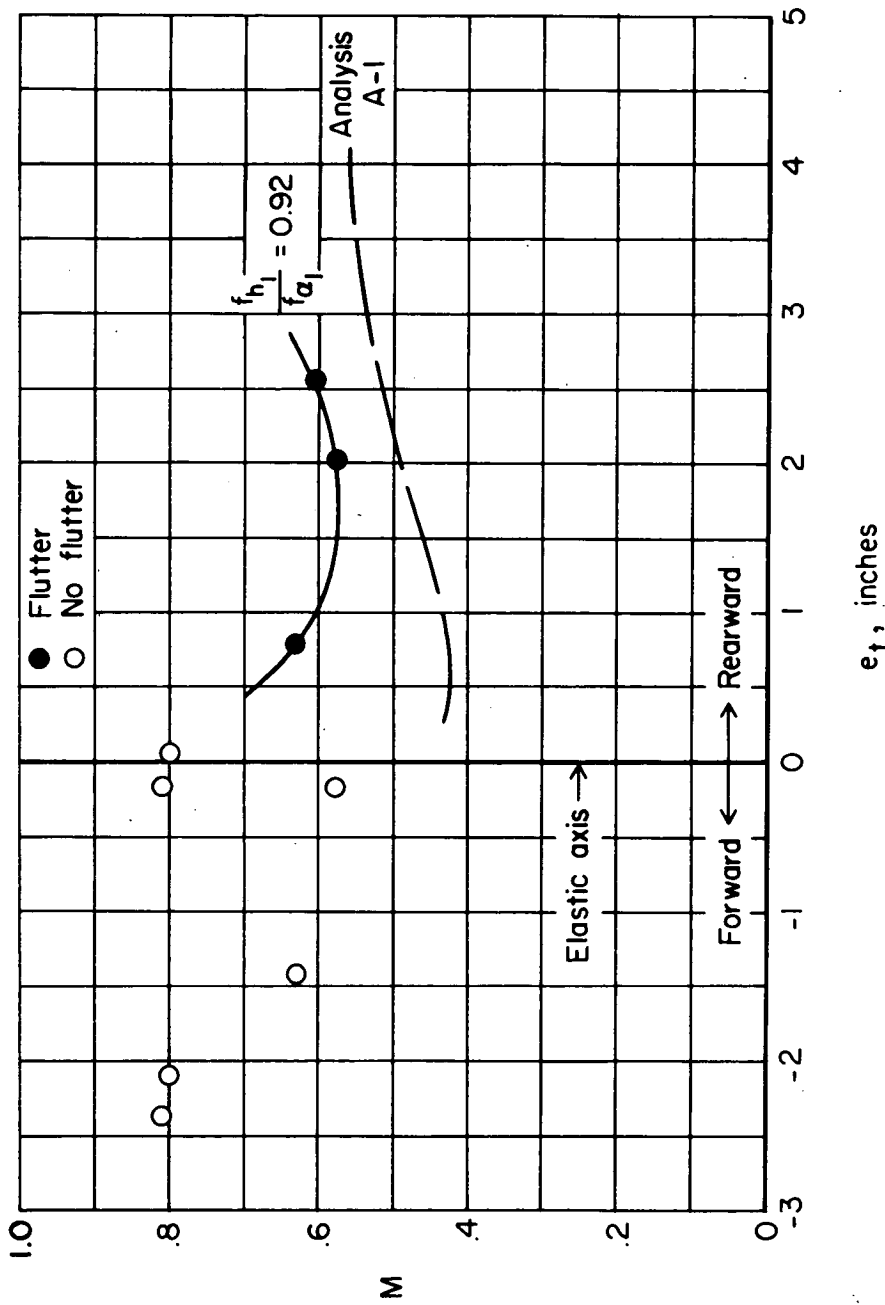


Figure 15.- Variation of experimental and theoretical flutter Mach numbers with tip-tank center of gravity. Tank A; $\mu = 1.005$; fuselage clamped.

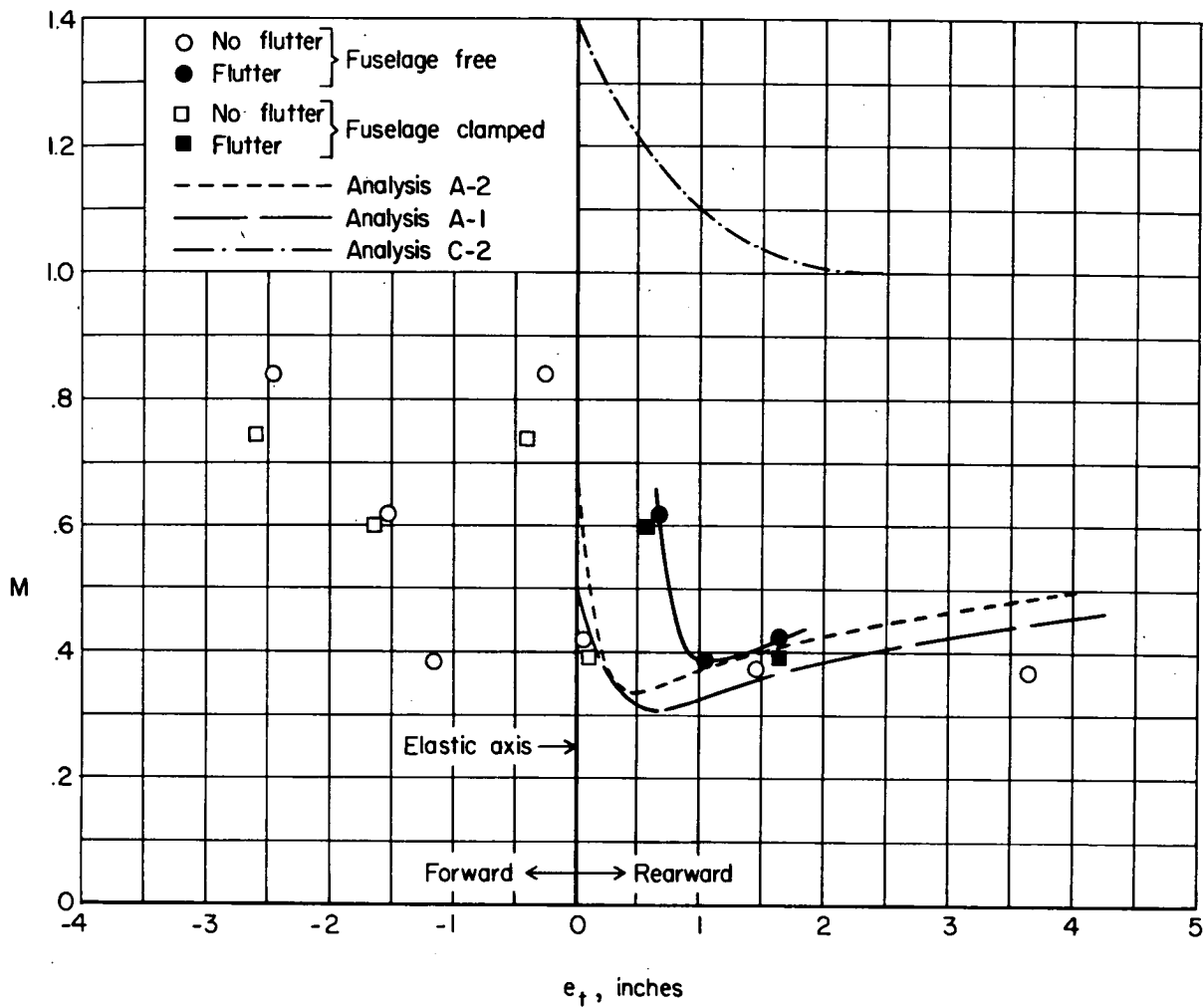


Figure 16.- Variation of experimental and theoretical flutter Mach numbers with tip-tank center of gravity with fuselage clamped and fuselage free to roll. Tank B; $\mu = 1.02$; $f_{h1}/f_{\alpha 1} = 1.04$.

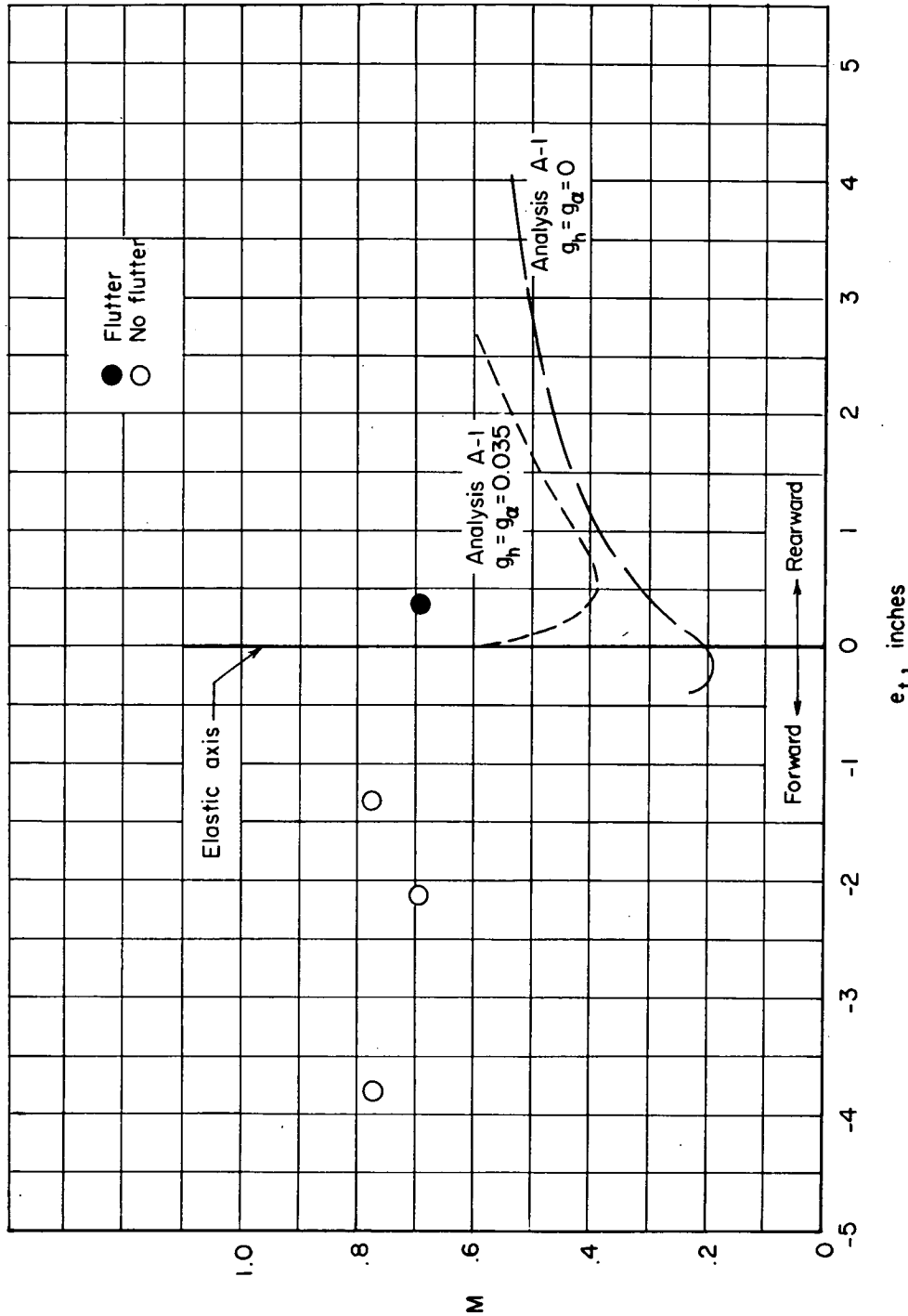


Figure 17.- Variation of experimental and theoretical Mach numbers with tip-tank center of gravity for $f_{h1}/f_{\alpha_1} = 0.98$. Tank B; $\mu = 0.895$; fuselage clamped.

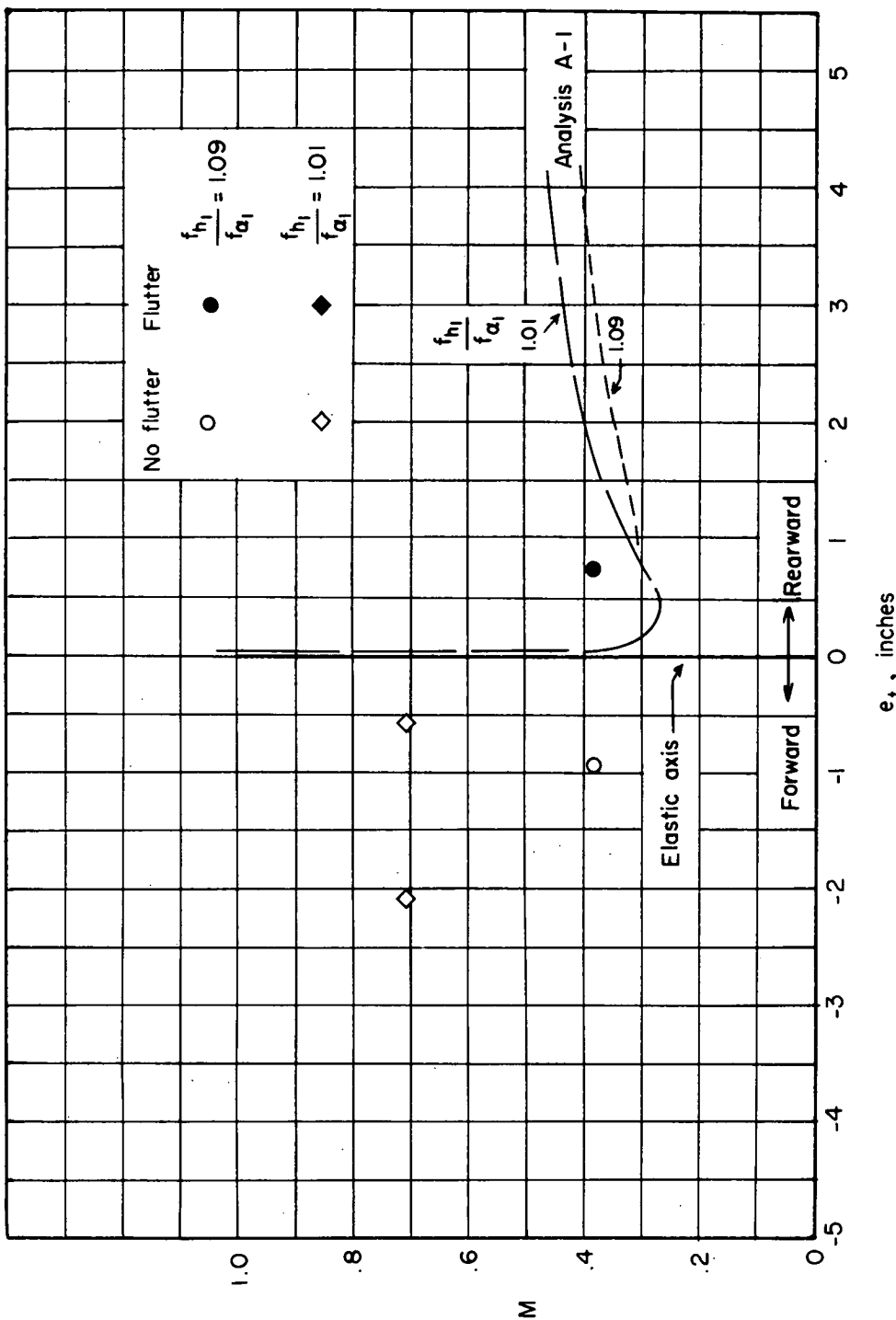


Figure 18.- Variation of experimental and theoretical flutter Mach numbers with tip-tank center of gravity. Tank B; $\mu = 1.29$; fuselage clamped.

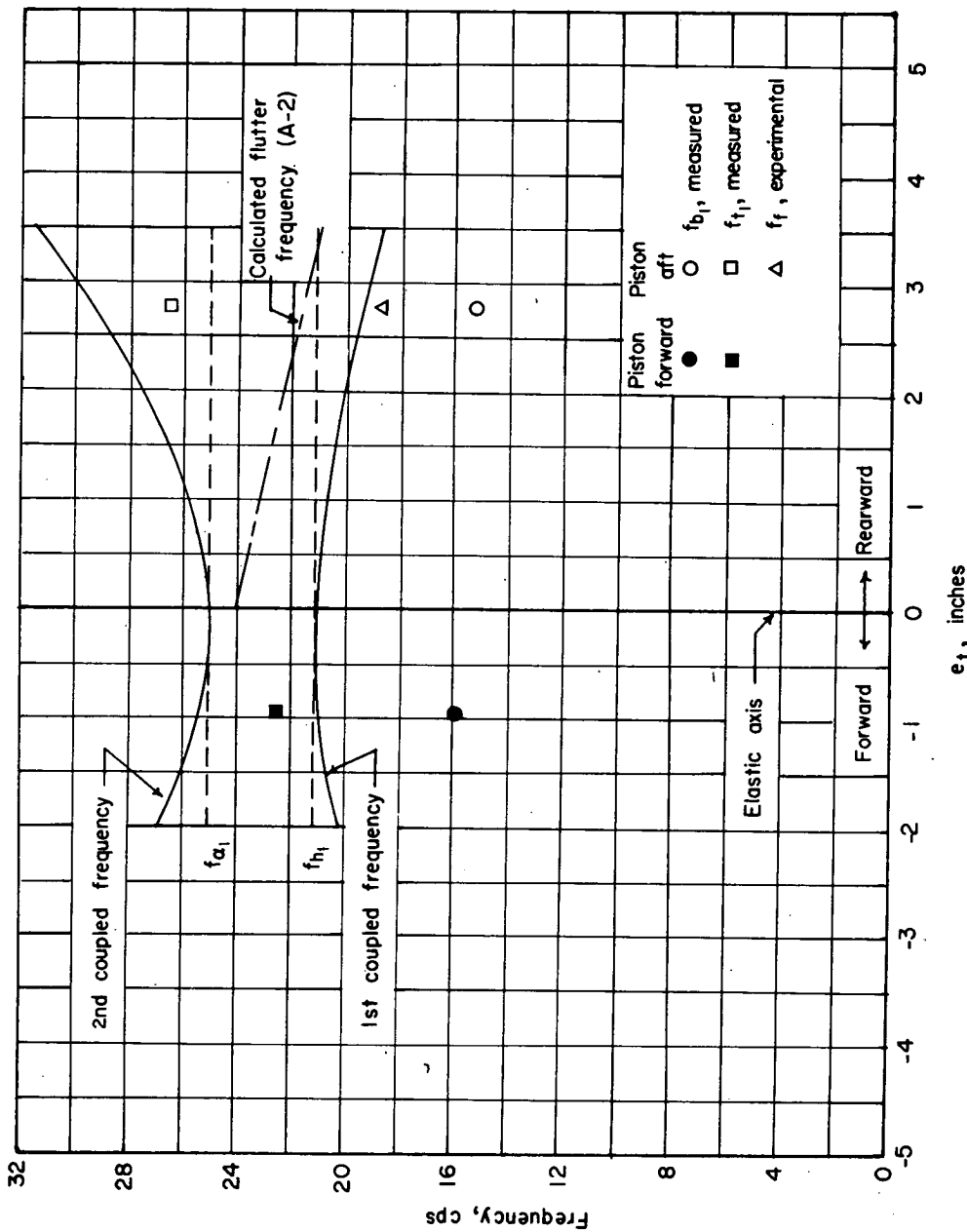


Figure 19.- Comparison of analytical and measured frequencies as a function of tip-tank center of gravity. Tank A; $\mu = 0.595$; $f_{b1}/f_{\alpha_1} = 0.84$; fuselage clamped.

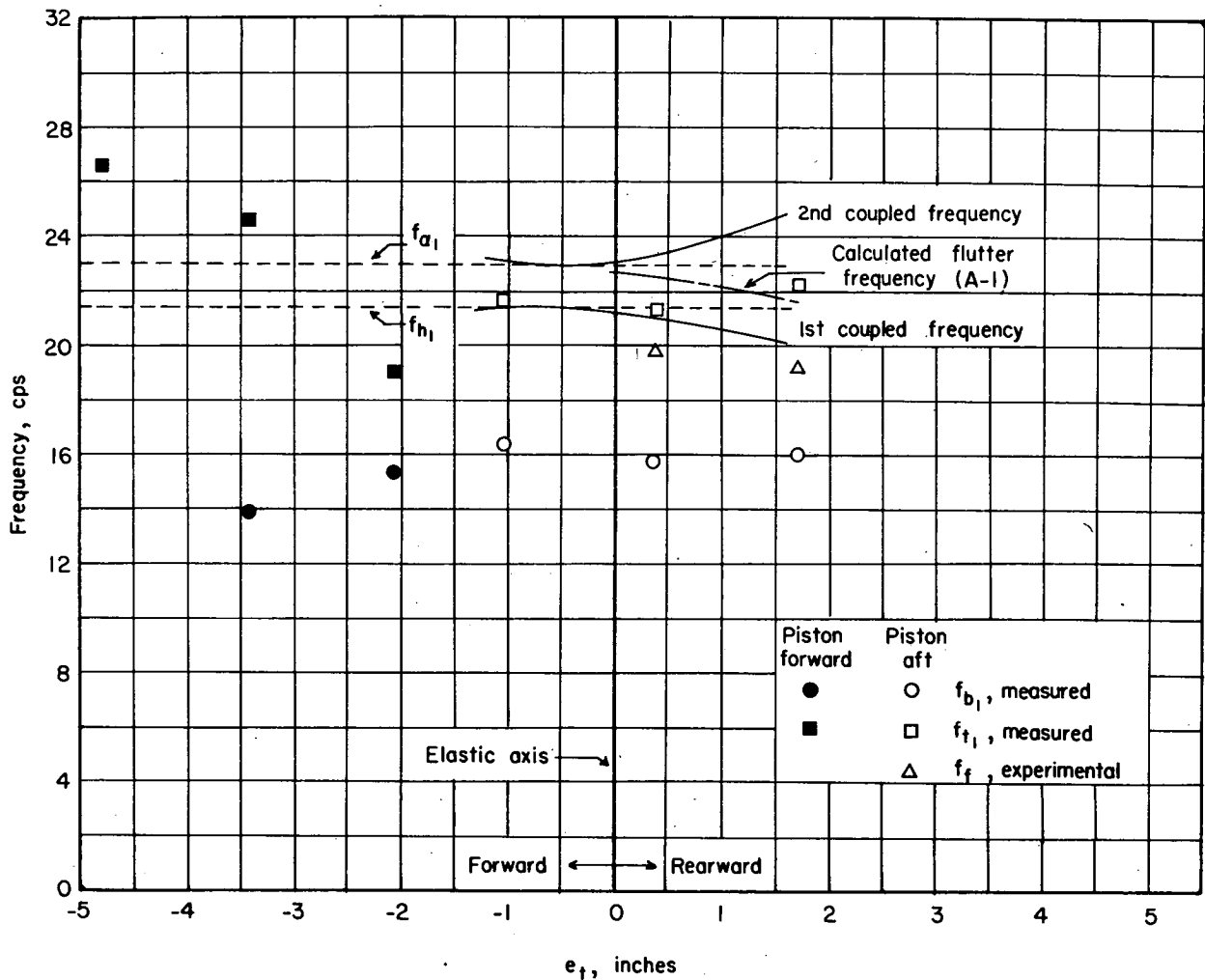


Figure 20.- Comparison of analytical and measured frequencies as a function of tip-tank center of gravity. Tank A; $\mu = 0.59$; $f_{h1}/f_{\alpha 1} = 0.93$; fuselage clamped.

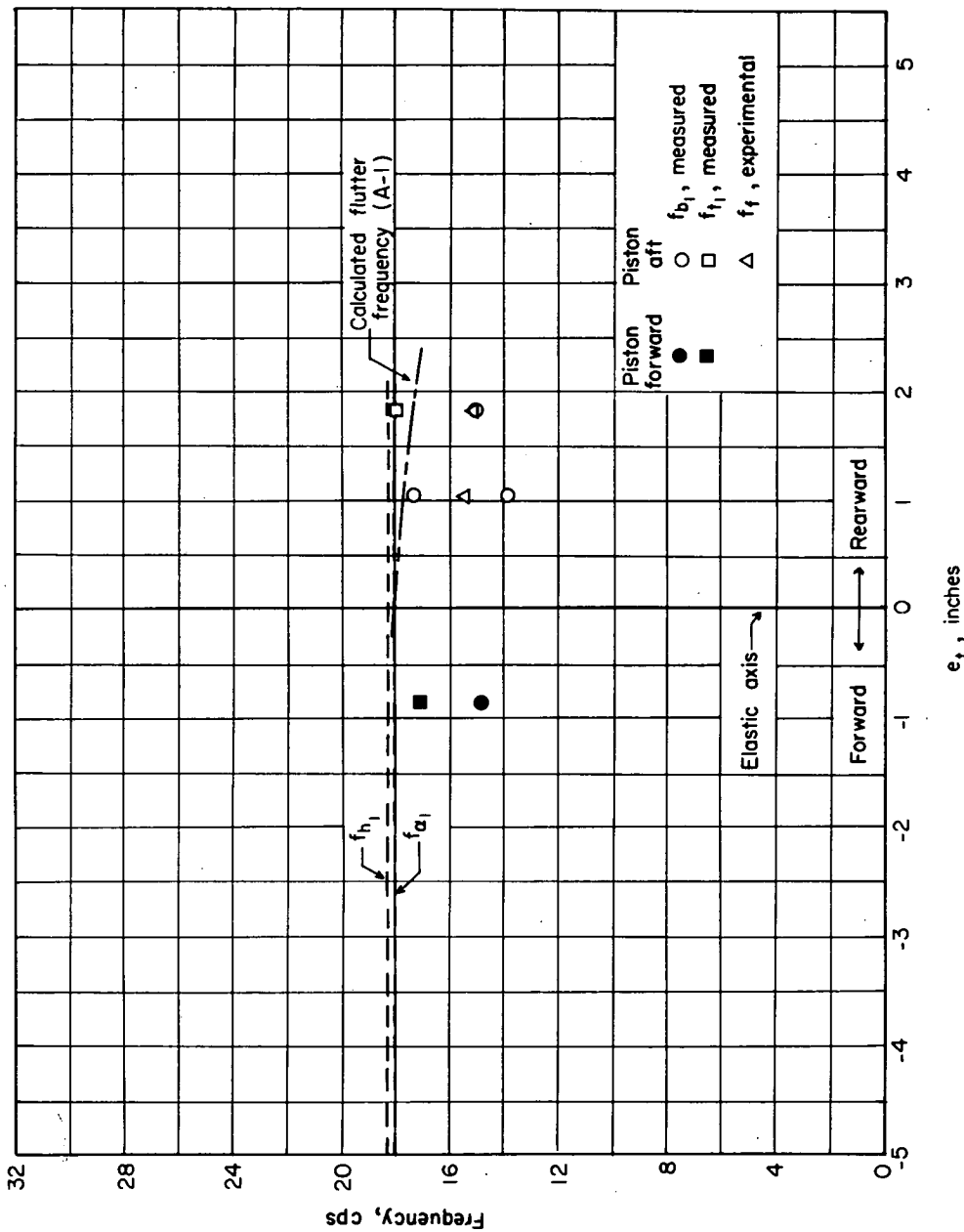


Figure 21.- Comparison of analytical and measured frequencies as a function of tip-tank center of gravity. Tank A; $\mu = 0.82$; $f_{h_1}/f_{\alpha_1} = 1.02$; fuselage clamped.

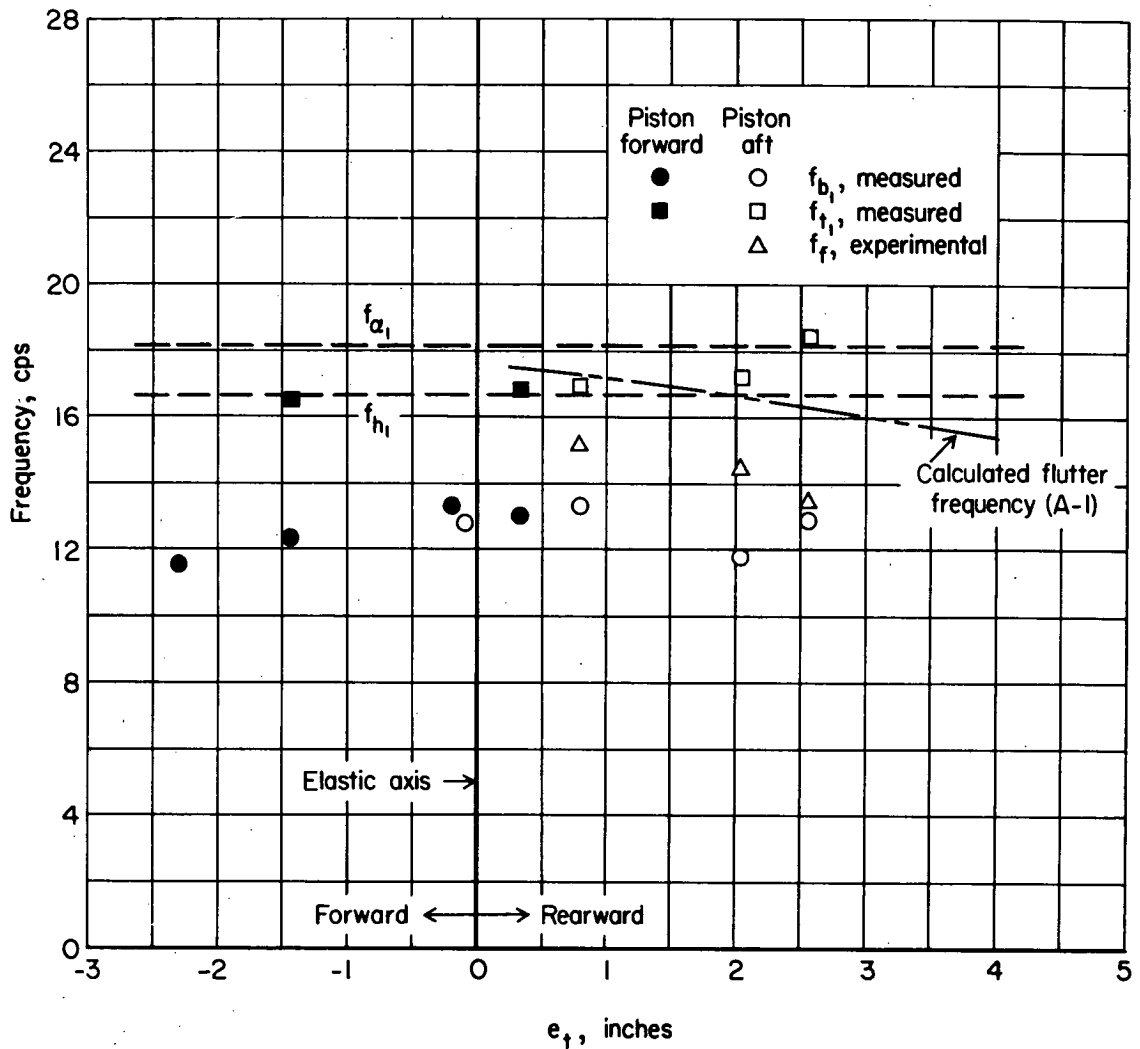


Figure 22.- Comparison of analytical and measured frequencies as a function of tip-tank center of gravity. Tank A; $\mu = 1.005$; $f_{h_1}/f_{\alpha_1} = 0.92$; fuselage clamped.

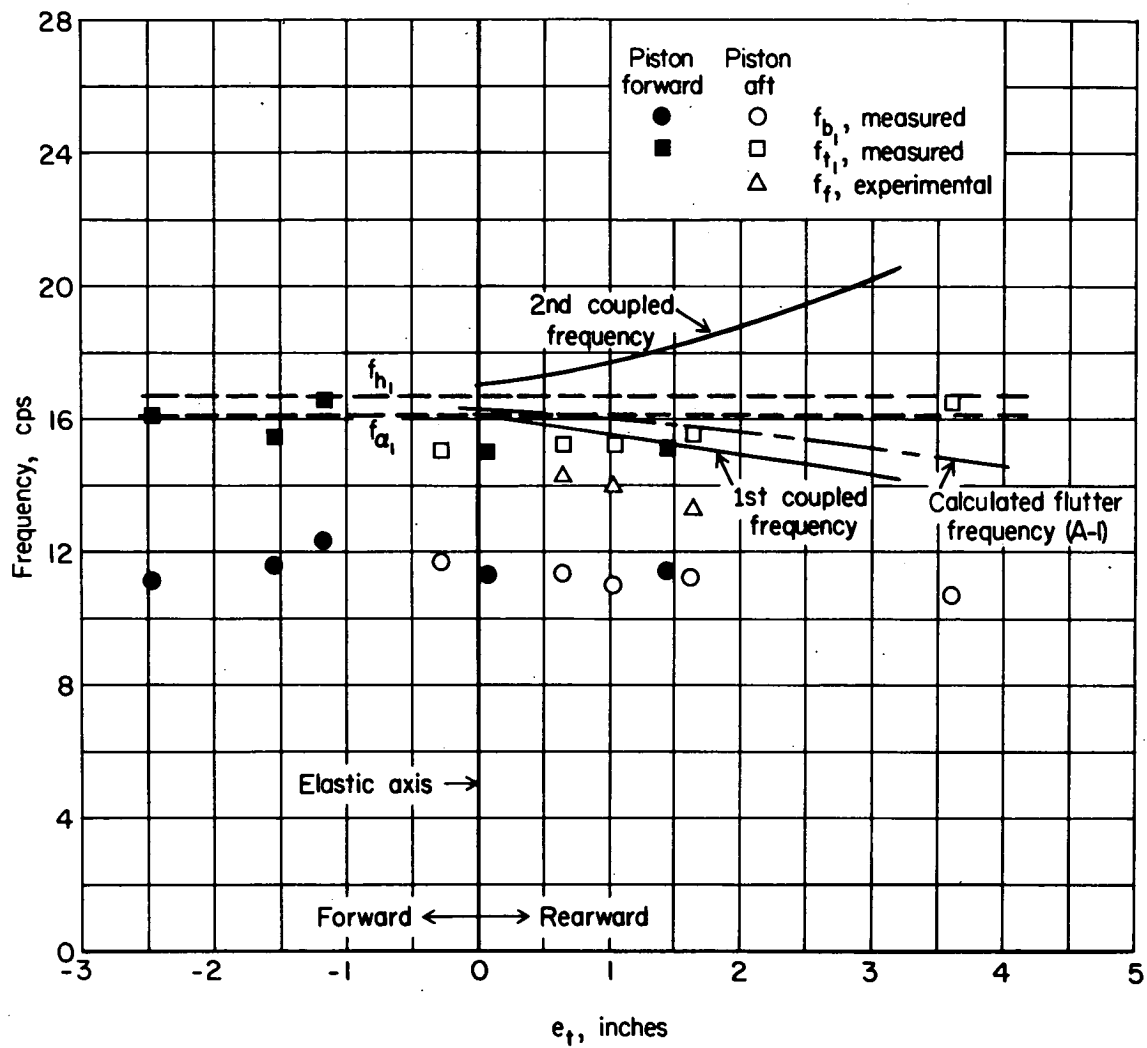


Figure 23.- Comparison of analytical and measured frequencies as a function of tip-tank center of gravity. Tank B; $\mu = 1.02$; $f_{h_1}/f_{\alpha_1} = 1.04$; fuselage clamped.

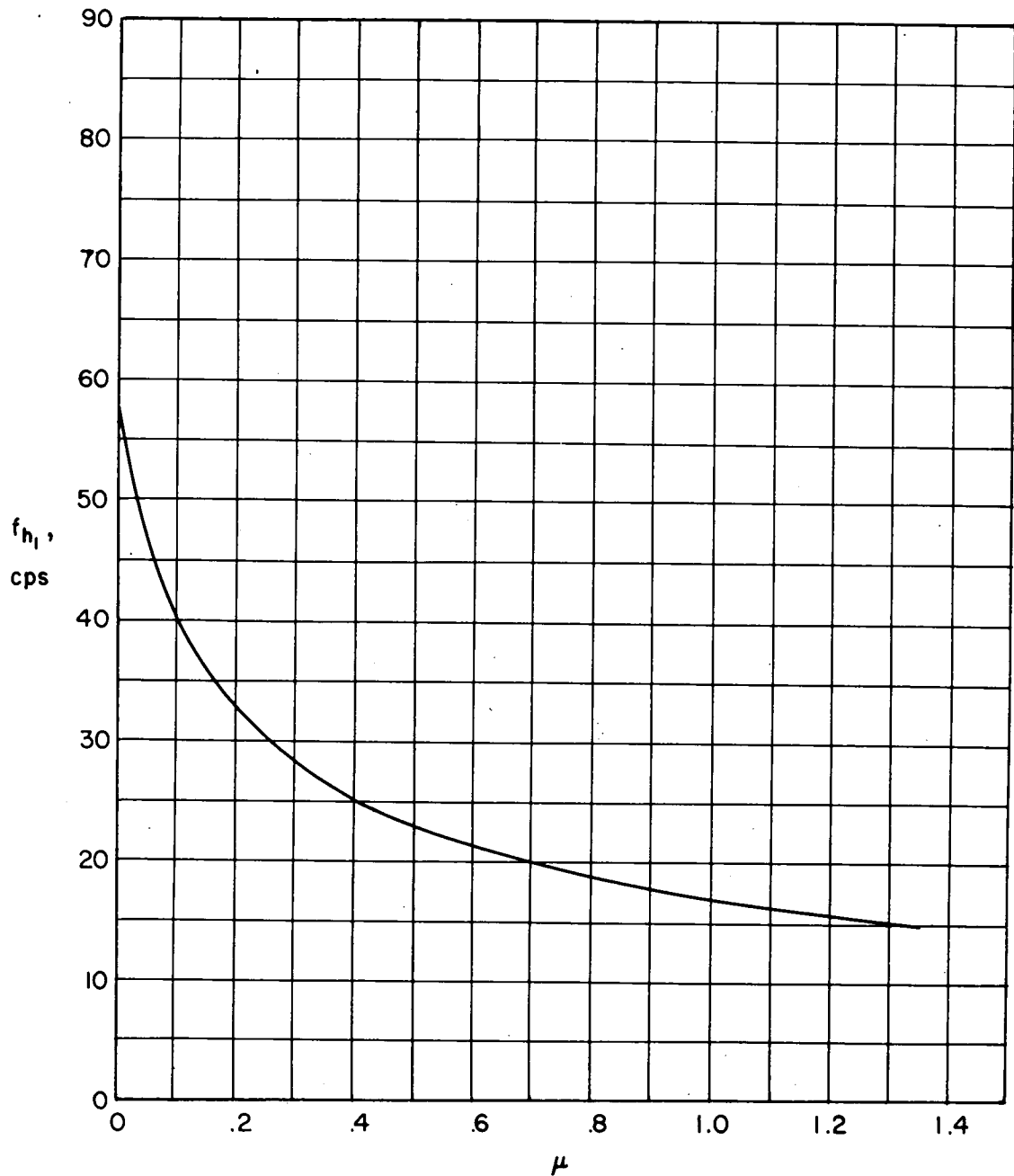


Figure 24.- Variation of first uncoupled bending frequency with tip-tank weight ratio.

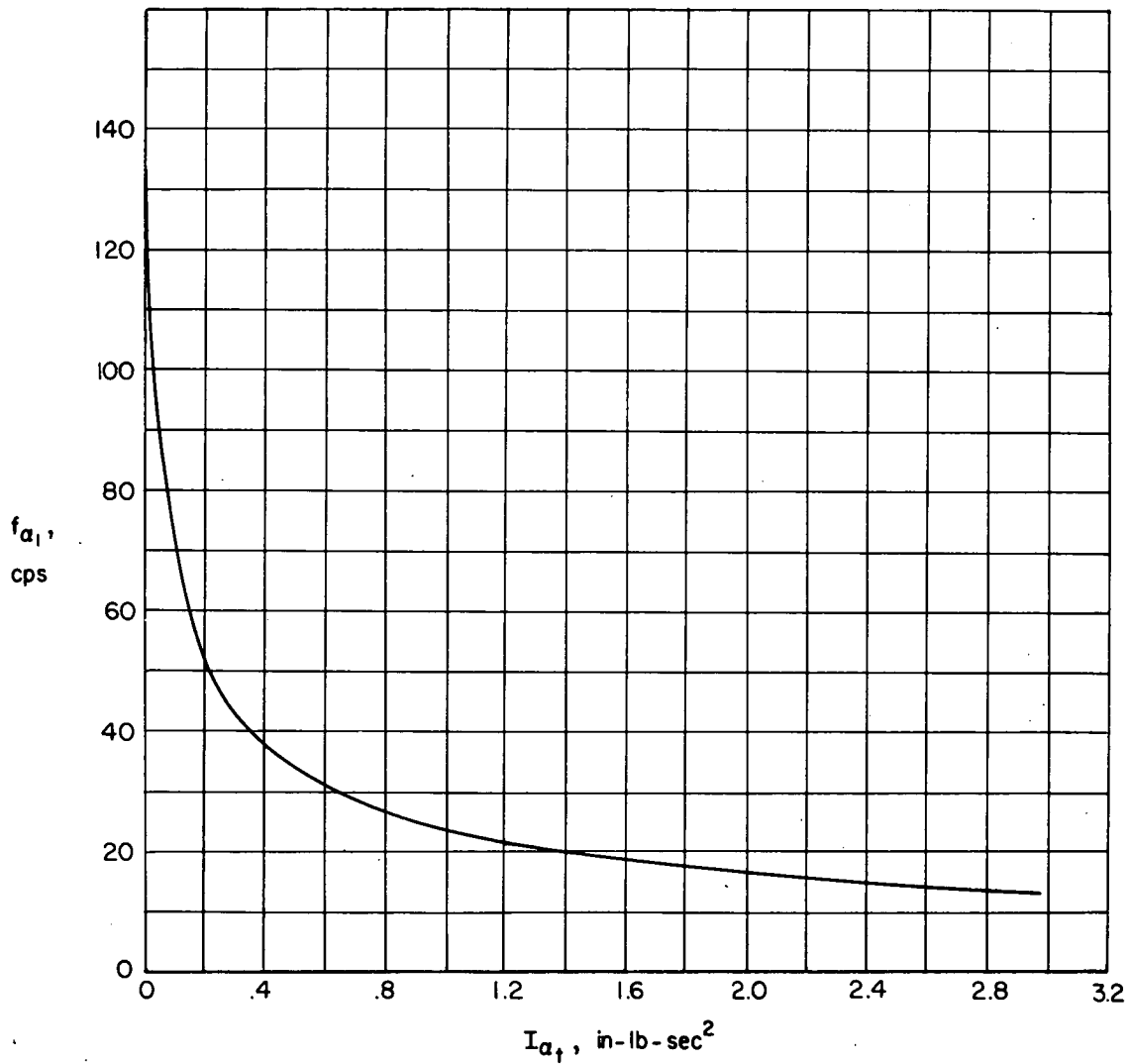
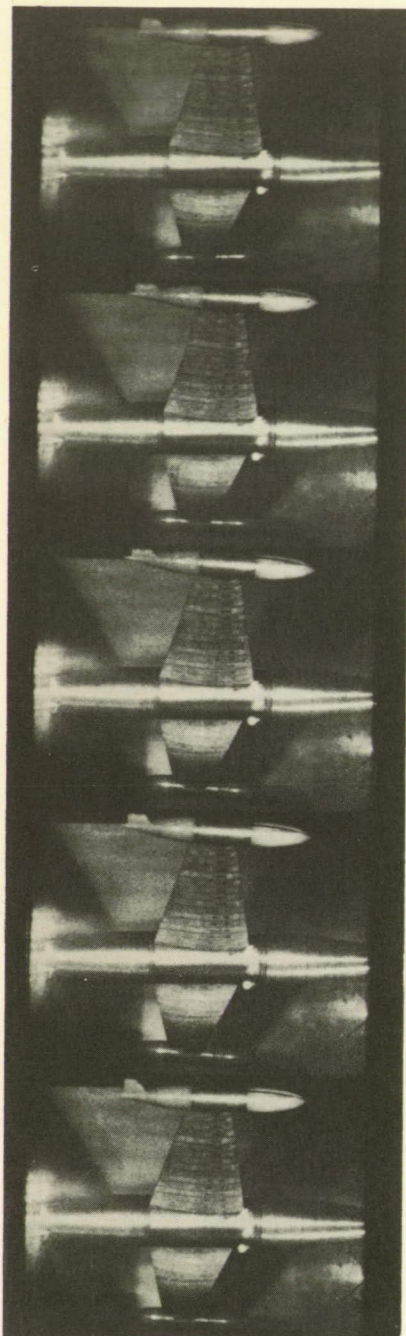


Figure 25.- Variation of first uncoupled torsional frequency with tip-tank moment of inertia.

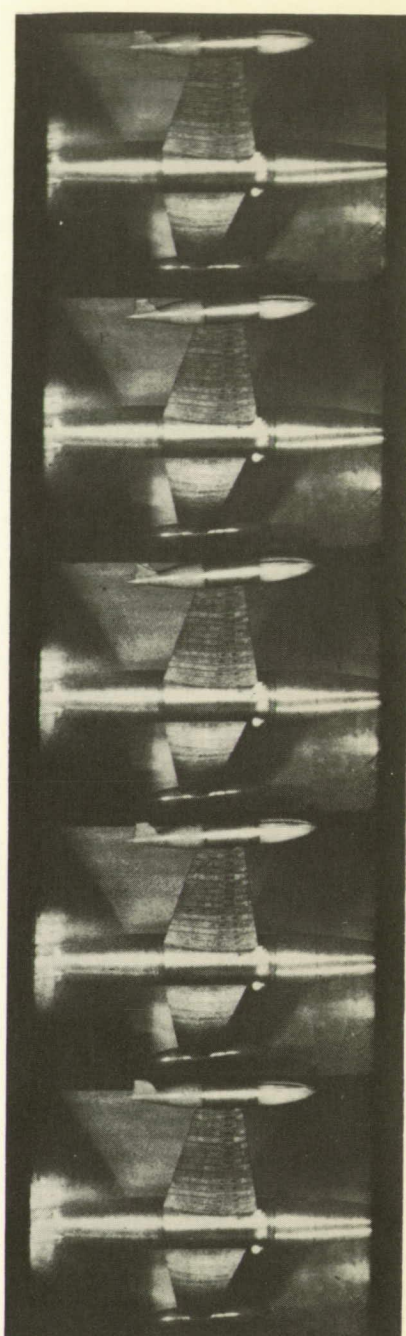
Frame

1



2

6



3

7

4

8

5

9

L-86439

Figure 26.- High-speed motion pictures showing a typical cycle of symmetric flutter. The direction of increasing time is from top to bottom beginning with frame 1.

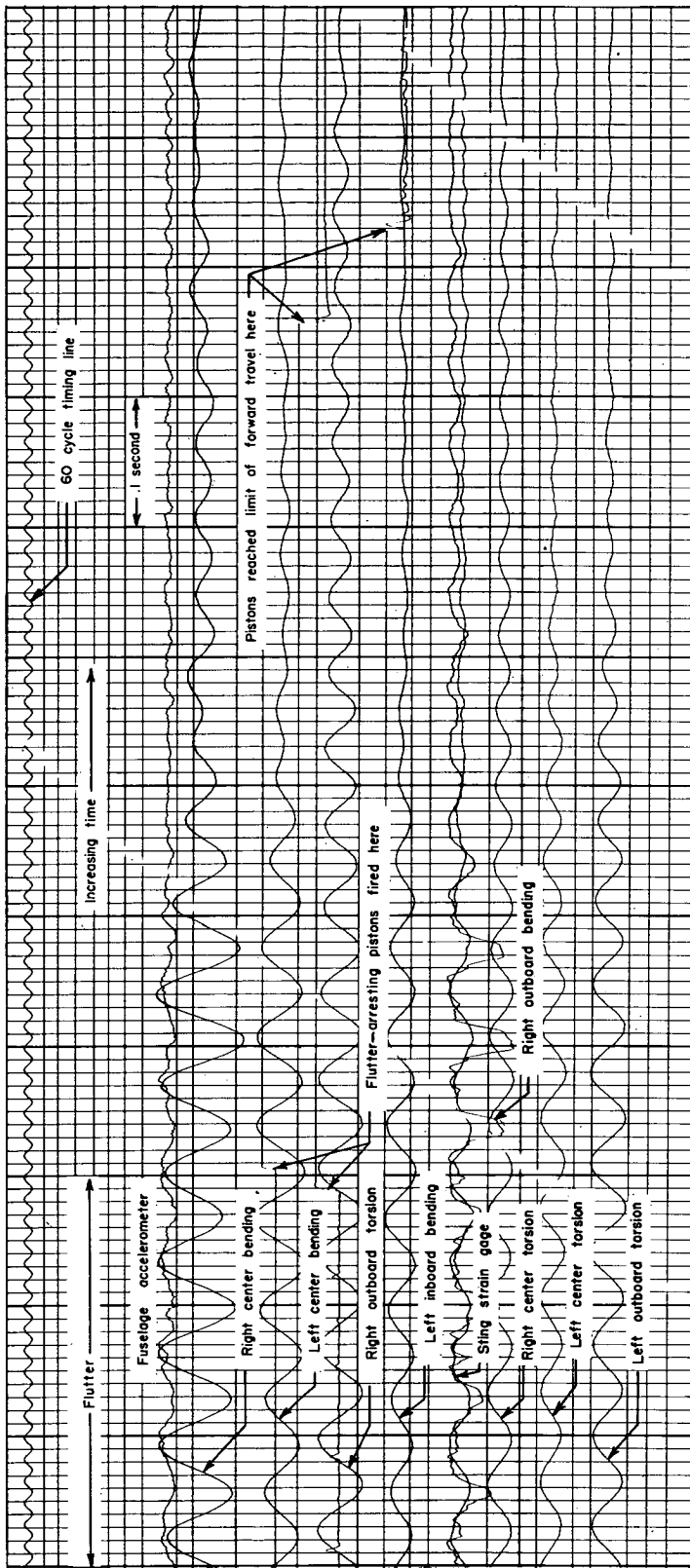
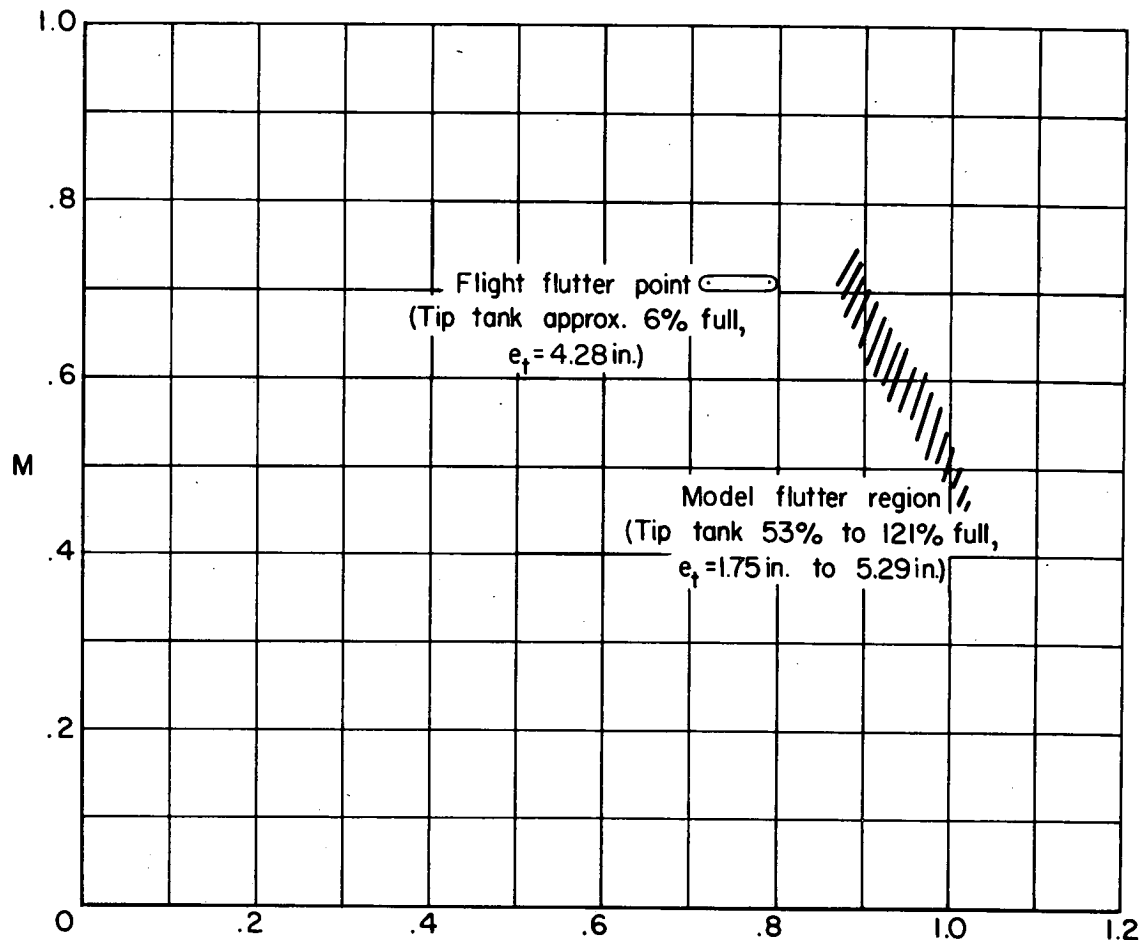


Figure 27.- Portion of oscillogram taken at flutter showing effect of flutter-arresting device.



$$\frac{\omega_{h_1}}{\omega_{\alpha_1}}$$

Figure 28.- Mach number against frequency ratio for model flutter region and flight flutter experience.

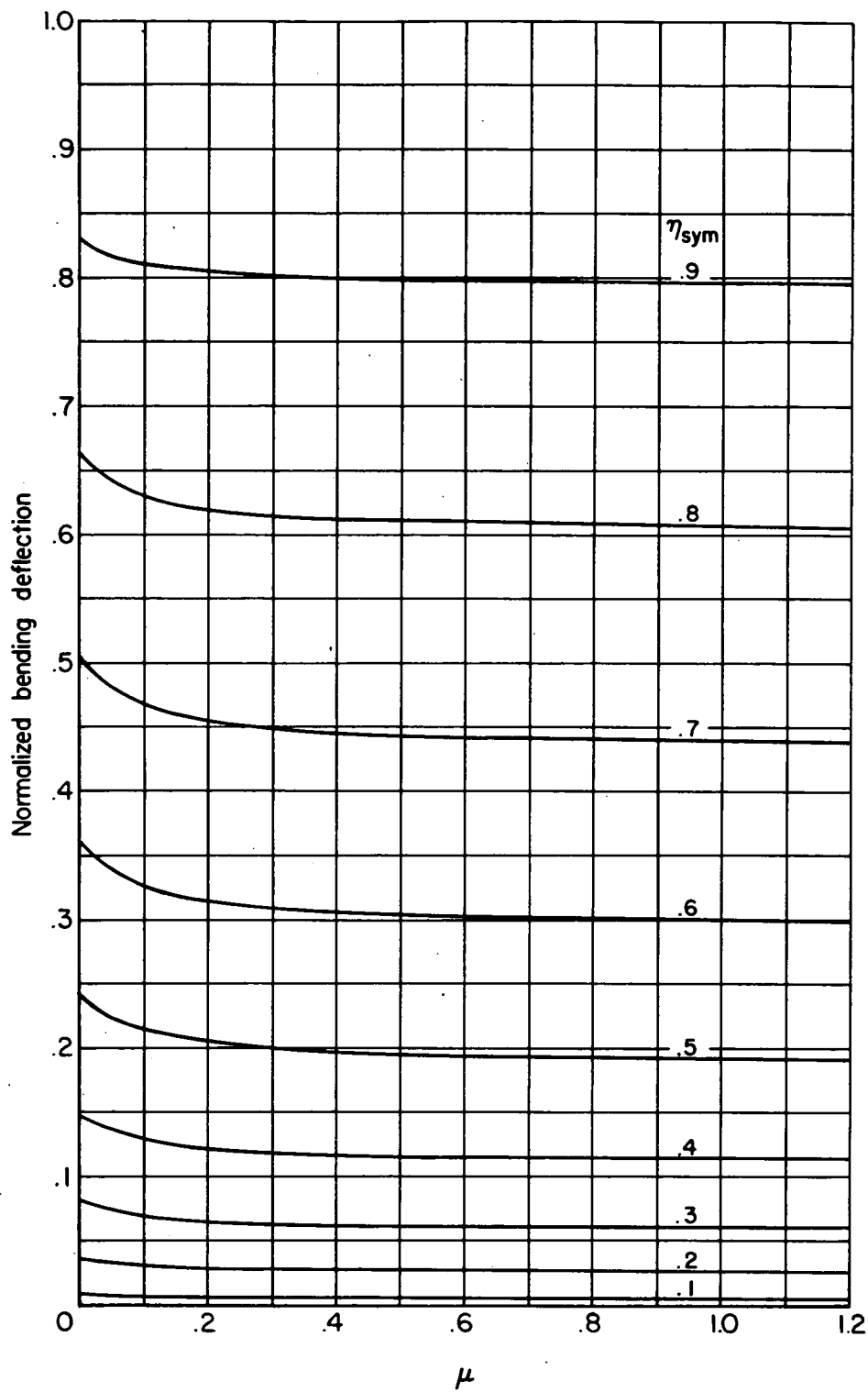


Figure 29.- Cross plot of uncoupled cantilever bending-mode shape as a function of tip-tank weight ratio.

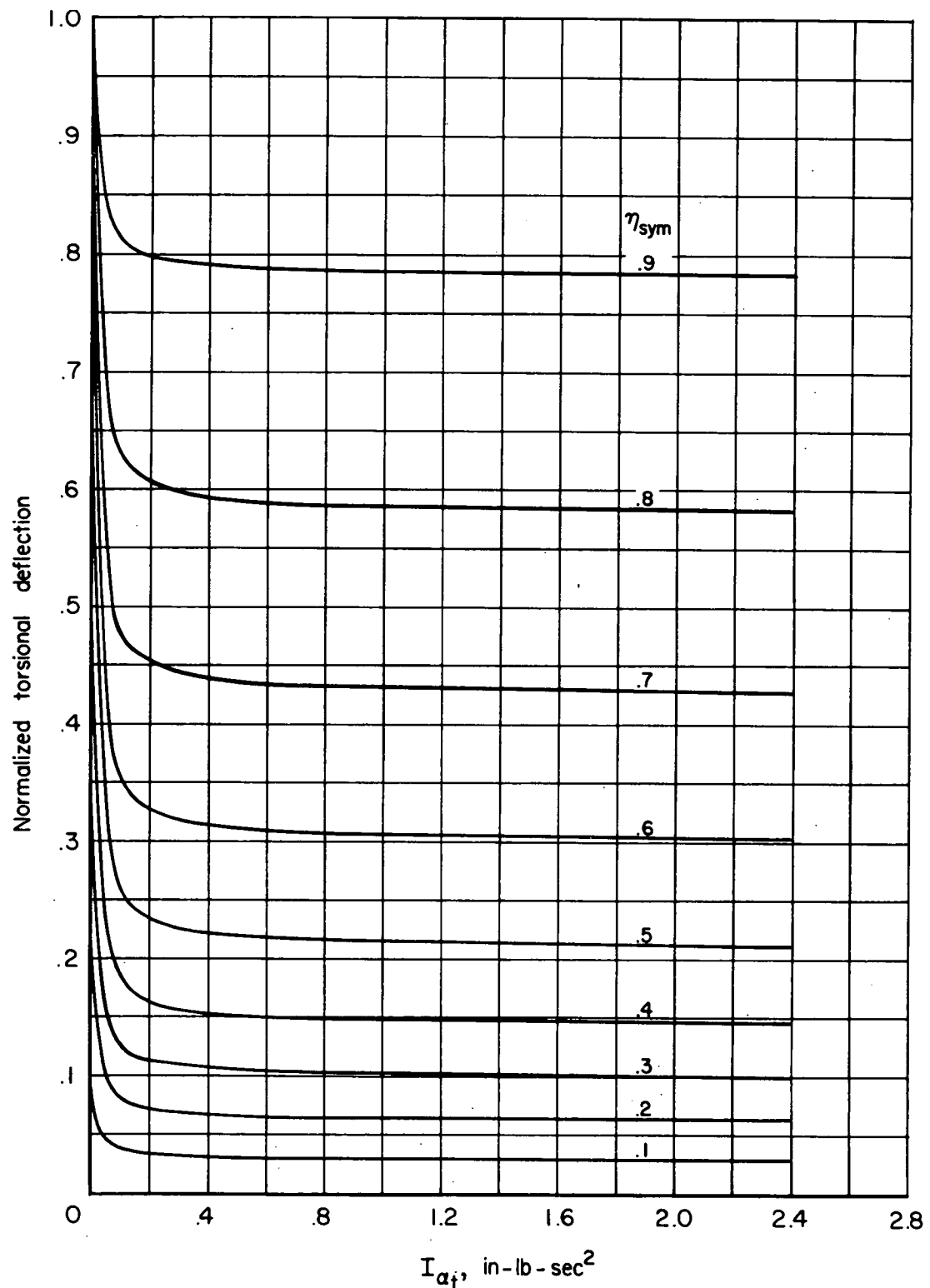


Figure 30.- Cross plot of uncoupled cantilever torsion-mode shape as a function of tip-tank moment of inertia.

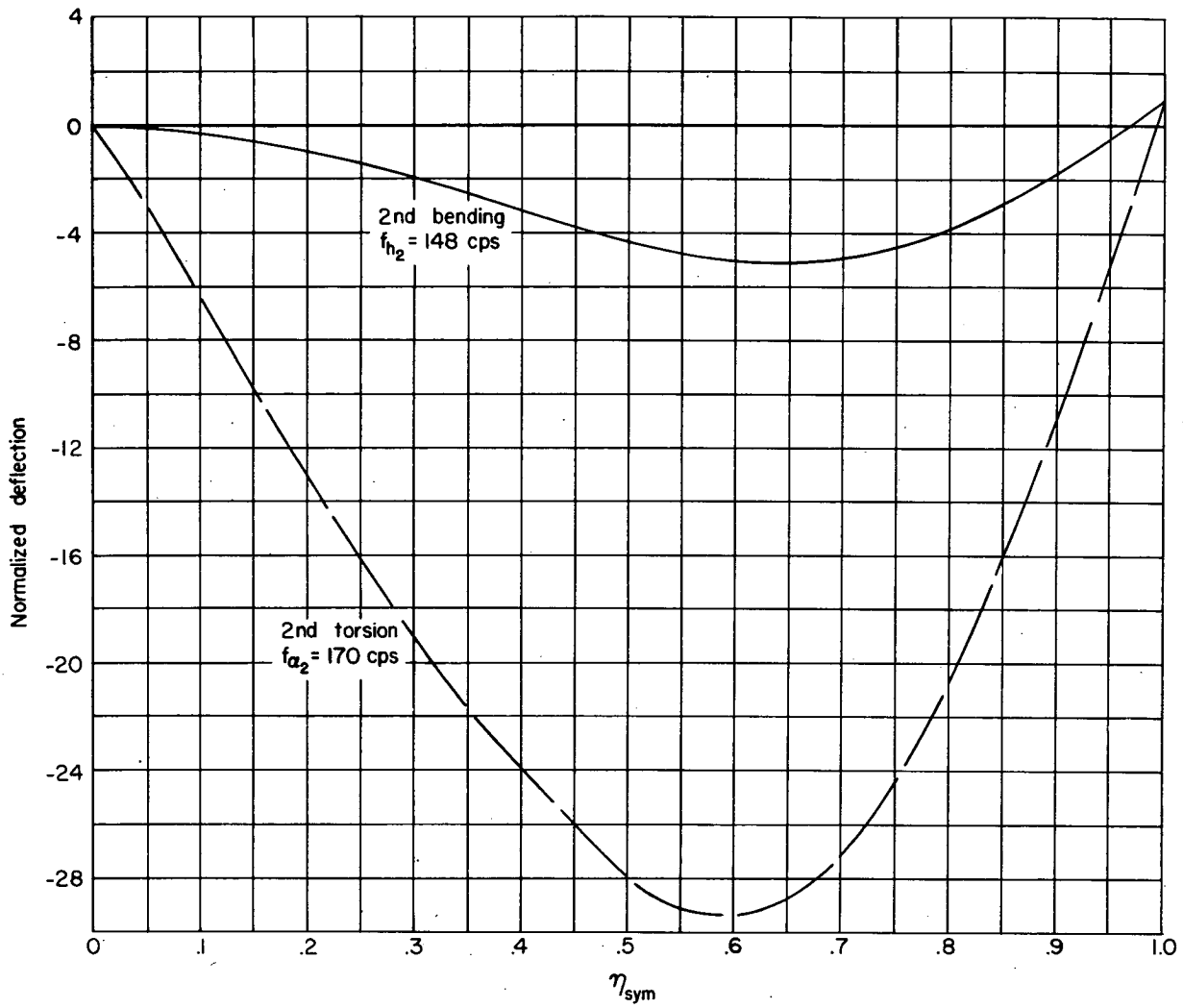


Figure 31.- Second uncoupled bending and torsion-mode shapes. Tank A;
 $\mu = 0.59$; $f_{h_1}/f_{\alpha_1} = 0.93$.

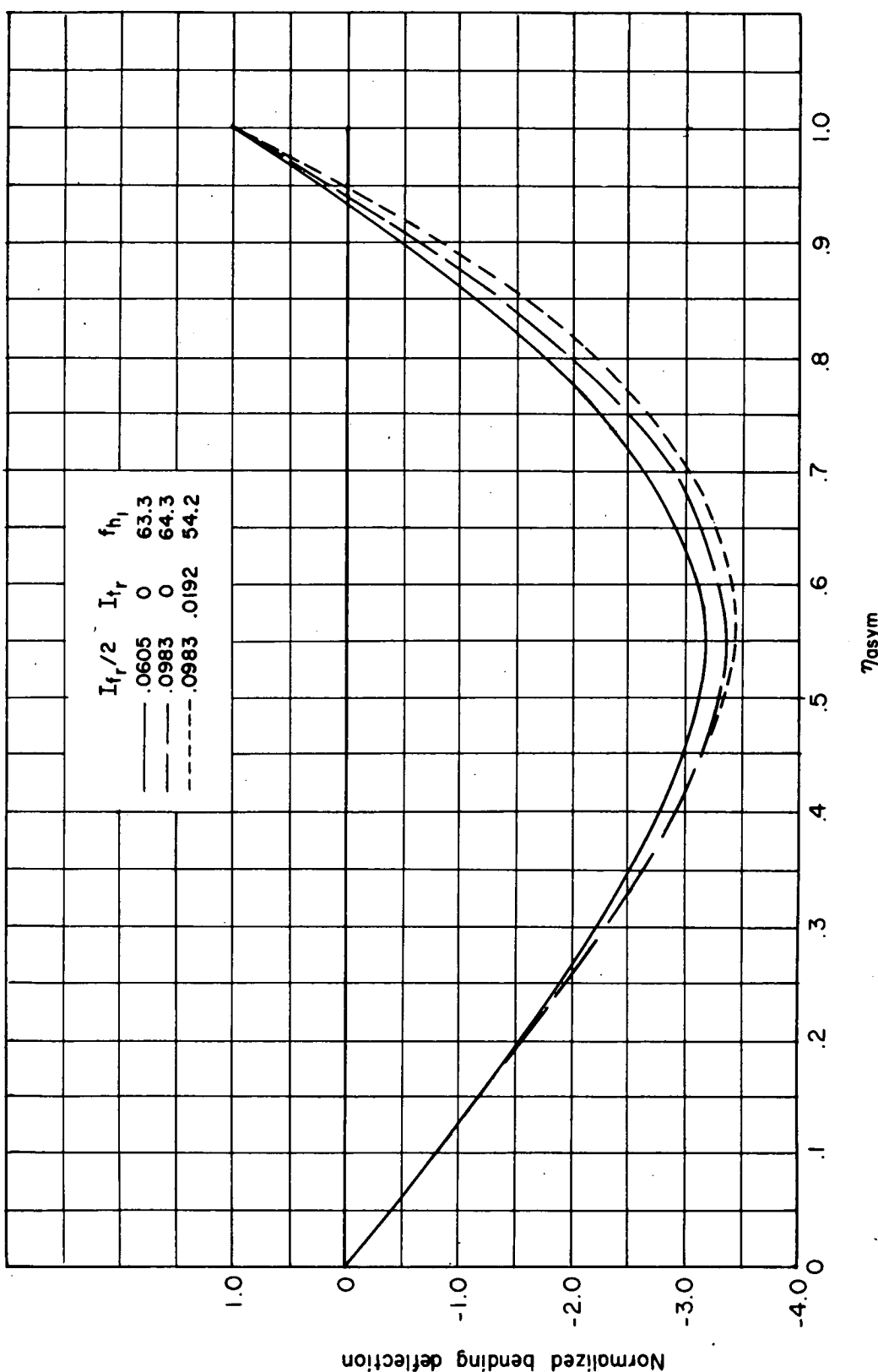
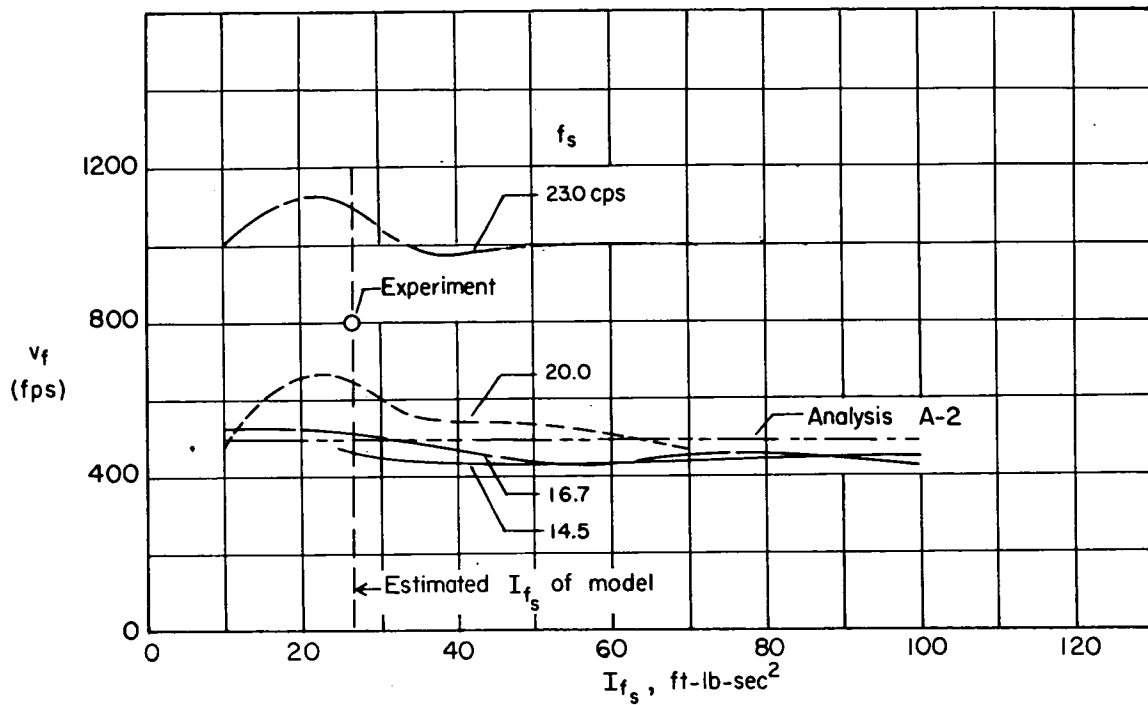
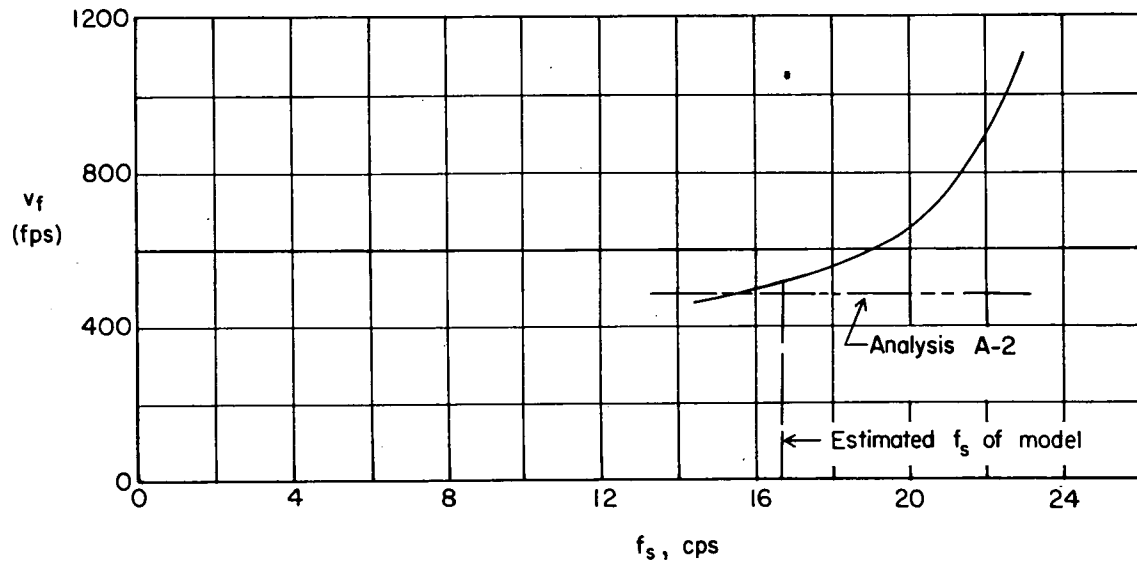


Figure 32.- First uncoupled antisymmetric bending-mode shape. Tank B;
 $\mu = 1.02$.



(a) Effect of sting-fuselage pitching moment of inertia I_{f_s} on flutter speed for four values of sting-fuselage frequency f_s .



(b) Effect of sting-fuselage frequency on flutter speed for $I_{f_s} = 26.4$.

Figure 33.- Correlation of experimental with theoretical flutter speeds including effects of sting flexibility (analysis B-1).

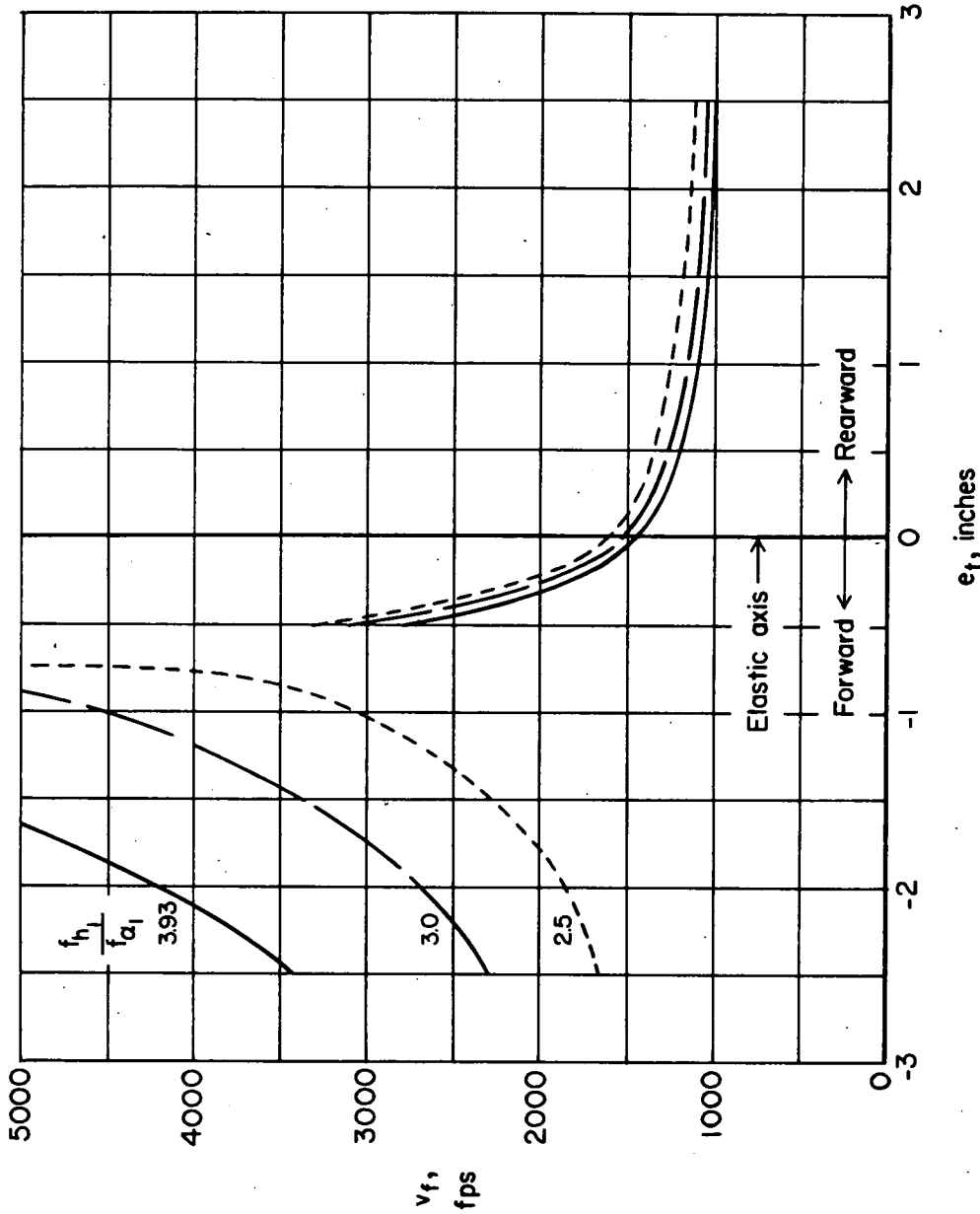


Figure 34.- Calculated antisymmetric flutter velocity (analysis C-1) against tip-tank center of gravity for various values of the frequency ratio. Tank B; $\mu = 1.02$; $I_{f_r} = 0.0605$.

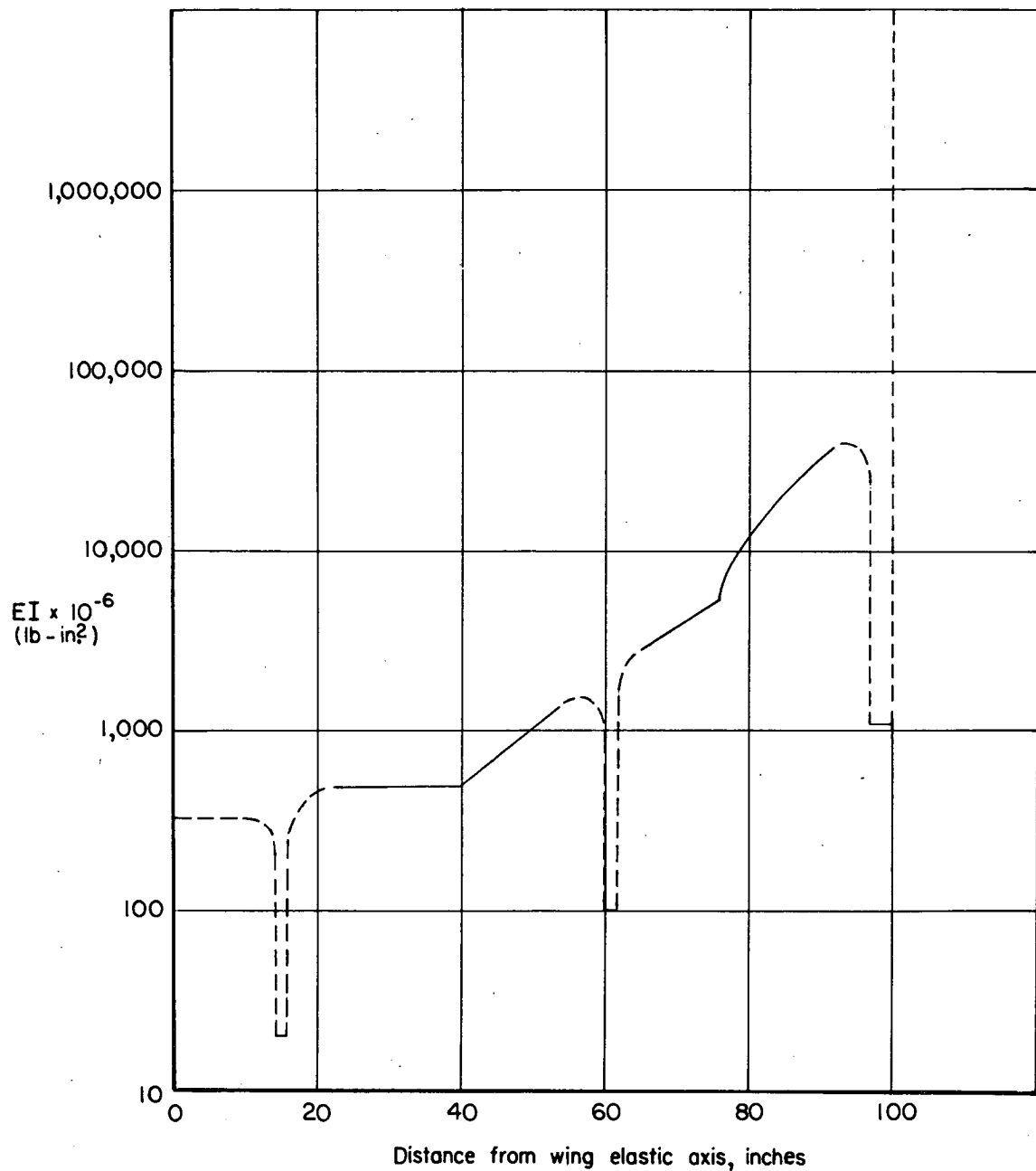


Figure 35.- Sting stiffness distribution.

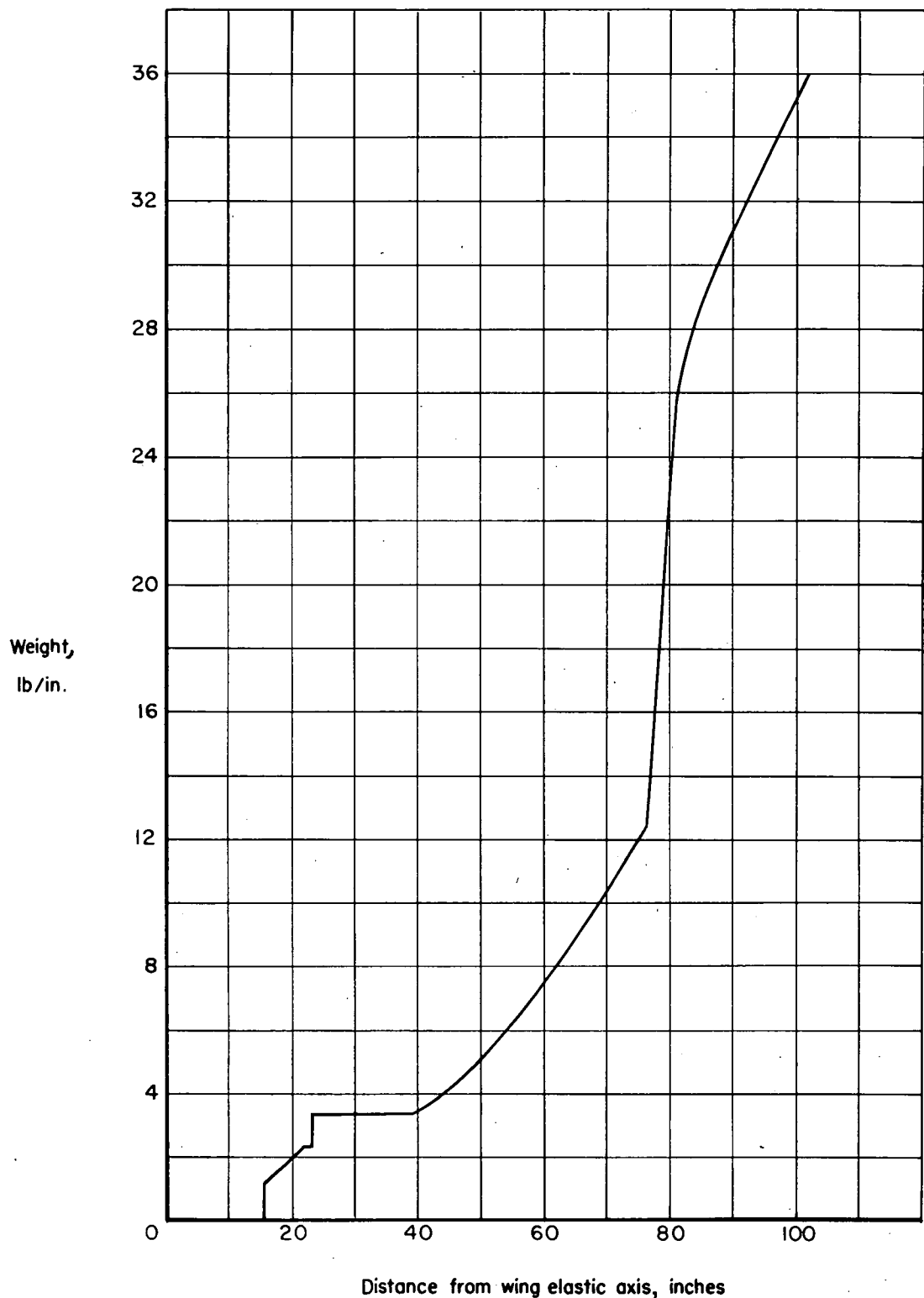


Figure 36.- Calculated sting weight distribution.

UNCLASSIFIED
CONFIDENTIAL

CONFIDENTIAL
UNCLASSIFIED